Master's Theses   Master's Theses and Graduate Research

1996

Effects of surface fluxes and advective tendencies on GCAPE

Gregory Lee Hunt

San Jose State University

Follow this and additional works at: https://scholarworks.sjsu.edu/etd_theses

INFORMATION TO USERS

This manuscript has been reproduced from the microfilm master. UMI films the text directly from the original or copy submitted. Thus, some thesis and dissertation copies are in typewriter face, while others may be from any type of computer printer.

The quality of this reproduction is dependent upon the quality of the copy submitted. Broken or indistinct print, colored or poor quality illustrations and photographs, print bleedthrough, substandard margins, and improper alignment can adversely affect reproduction.

In the unlikely event that the author did not send UMI a complete manuscript and there are missing pages, these will be noted. Also, if unauthorized copyright material had to be removed, a note will indicate the deletion.

Oversize materials (e.g., maps, drawings, charts) are reproduced by sectioning the original, beginning at the upper left-hand corner and continuing from left to right in equal sections with small overlaps. Each original is also photographed in one exposure and is included in reduced form at the back of the book.

Photographs included in the original manuscript have been reproduced xerographically in this copy. Higher quality 6" x 9" black and white photographic prints are available for any photographs or illustrations appearing in this copy for an additional charge. Contact UMI directly to order.

EFFECTS OF SURFACE FLUXES AND ADVECTIVE TENDENCIES ON GCAPE

A Thesis

Presented to

The Faculty of the Department of Meteorology

San Jose State University

In Partial Fulfillment

of the Requirements for the Degree

Master of Science

by

Gregory Lee Hunt

August 1996

UMI Number: 1381422
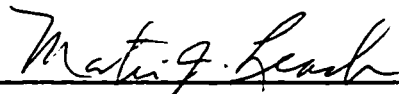
UMI
300 North Zeeb Road
Ann Arbor, MI 48103
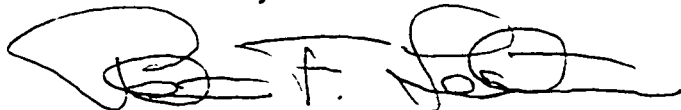
APPROVED FOR THE DEPARTMENT OF METEOROLOGY

_____

Dr. Martin J. Leach

_____

Dr. Peter F. Lester

_____

Dr. Douglas M. Sinton

APPROVED FOR THE UNIVERSITY

_____

ABSTRACT

EFFECTS OF SURFACE FLUXES AND ADVECTIVE TENDENCIES ON GCAPE

by Gregory L. Hunt

Atmospheric convection causes the vertical exchange of heat and moisture on several spatial and temporal scales. Generalized Convective Available Potential Energy (GCAPE) is a quantitative measure of convective potential and is a useful diagnostic and prognostic tool.

This study expands the application of GCAPE to the diagnosis of eleven convective events in the mid-latitudes. In particular, the roles of surface heat and moisture fluxes and of tropospheric temperature and moisture advection were evaluated in the production of GCAPE. Data for this study were collected during the Atmospheric Radiation Measurement program conducted in Oklahoma in 1994 and 1995.

For three of four fall cases, 500 hPa-tropopause cold advection resulted in the greatest GCAPE increases. In the other case surface-500 hPa moisture advection produced the greatest increase. For the seven spring cases, increased low-level moisture, whether by vertical fluxes or by advection, produced the greatest increases.

ACKNOWLEDGMENTS

TABLE OF CONTENTS

LIST OF FIGURES

LIST OF TABLES

List of Symbols

A	amplitude of advection curve
e	vapor pressure
e_s	saturation vapor pressure
h	thermodynamic energy per unit mass
h_G	thermodynamic energy per unit mass of the given state
h_R	thermodynamic energy per unit mass of the reference state
H_L	latent heat flux
H_S	sensible heat flux
L	latent heat of condensation
p	pressure
p_n	new pressure
p_s	saturation pressure
p_{top}	top pressure level
q	specific humidity
s	entropy per unit mass
t	time
T	temperature
T_n	new temperature
T_s	saturation temperature
T_v	virtual temperature
w	water vapor mixing ratio
$\overline{w}$	total water mixing ratio

α specific volume

κ Poisson's constant

ρ air density

θ potential temperature

θ_{top} top potential temperature

ϕ any scalar variable

List of Constants

C specific heat of liquid water = 4170 J kg^{-1} K^{-1}

C_p specific heat of dry air at constant pressure = 1005.7 J kg^{-1} K^{-1}

C_{pw} specific heat of water vapor at constant pressure = 1870 J kg^{-1} K^{-1}

e_0 vapor pressure at 273.15 K = 6.112 hPa

g gravity = 9.8 m s^{-2}

L_0 latent heat of condensation at 273.15 K = 2.501 x 10^6 J kg^{-1}

R_d gas constant for dry air = 287 J kg^{-1} K^{-1}

R_w gas constant for water vapor = 461 J kg^{-1} K^{-1}

ε $\dfrac{R_d}{R_w} = 0.622$

CHAPTER 1 - INTRODUCTION

1.1 Background

Convection encompasses relatively small-scale, thermally direct circulations which result from the action of gravity upon an unstable vertical distribution of mass (Emanuel 1994). In regions which experience deep convection, the convective clouds affect the entire depth of the tropopause to link the boundary layer with the rest of the atmosphere through the vertical transport of heat, moisture, and momentum (Emanuel 1994). Cumulus convection transfers energy to large-scale circulations through latent heat release, resulting in regions that are warmer at a given level than the surroundings, thus generating available potential energy (Raymond 1994). Convection is also an energy source for large scales of motion and plays an important role in large-scale circulations such as the Hadley circulation (Emanuel et al. 1994).

There are several quantitative estimates of the potential for convection including Convective Available Potential Energy (CAPE) and buoyant energy. By vertically integrating the buoyancy from the level of free convection, z_{LFC}, to the level of neutral buoyancy, z_{LNB}, following the motion of a parcel, the expression for CAPE is:

$$CAPE = \int_{z_{LFC}}^{z_{LNB}} g\left(\frac{Tparcel - Tenv}{Tenv}\right) dz. \tag{1.1}$$

1

A typical CAPE value for a sounding representative of severe storm conditions in the Midwest U. S. is 2300 - 3000 J kg^{-1}. Weisman and Klemp (1986) derived an alternate measure of the amount of energy available for convection, i. e., buoyant energy, B,

$$B = g \int \left(\frac{\theta(z)_{parcel} - \theta(z)_{env}}{\theta_{env}(z)} \right) dz,$$

(1.2)

where $\theta(z)$ defines the potential temperature of a representative moist-adiabatically ascending surface parcel, $\bar{\theta}(z)$ defines the environmental potential temperature profile, and the integral is taken over the vertical interval where the lifted parcel is warmer than its environment. They found the buoyant energy can be as large as 4500 J kg^{-1} in the Midwest and generally ranges from 1500-2500 J kg^{-1} for moderately unstable convective days. Buoyant energy and CAPE provide useful measures of instability but neglect the effects of water vapor and liquid water on buoyancy. Thus, they overestimate the amount of energy available for convection.

Lorenz (1978) attempted to overcome these shortcomings with the concept of moist available energy. He defined moist available energy as the amount by which the potential plus internal (including latent) energy of a given atmospheric mass field exceeds that of a hypothetical reference field, which can be constructed from the given field by rearranging the atmospheric mass, under reversible dry- and moist-adiabatic processes. He also presented a graphical procedure for determining moist available energy. Lorenz (1979) extended this work with a numerical procedure for evaluating moist

2

available energy. In this procedure he develops a method to minimize the total thermodynamic energy in an actual sounding. He does this by rearranging parcels within the sounding while conserving both the mass and entropy of each parcel. Once the new sounding is determined, the total minimized thermodynamic energy can be calculated. It can then be subtracted from the total thermodynamic energy of the original sounding; the difference is moist available energy.

Randall and Wang (1992; hereafter RW92) found that Lorenz's method could increase the total thermodynamic energy of the sounding in some cases. They corrected for this by modifying Lorenz's algorithm to choose the parcel arrangement that would result in the minimum total thermodynamic energy of the sounding. RW92 referred to the energy difference between the given sounding and the resulting sounding as the Generalized Convective Available Potential Energy or GCAPE. In contrast, CAPE represents the difference between the temperature of a parcel and the temperature of its surrounding environment.

Wang and Randall (1994) analyzed the GCAPE during the GARP (Global Atmospheric Research Program) Atlantic Tropical Experiment (GATE). They investigated the effects of large-scale, non-convective processes including temperature and moisture advection as well as surface fluxes on the production of GCAPE. Large-scale temperature and moisture was analyzed every 25 hPa and the surface fluxes were assumed to act uniformly on the air between the surface and 950 hPa. They found the following: (1) the

effects of large-scale vertical motion on temperature and moisture were powerful GCAPE producers, (2) surface evaporation was an even more powerful producer of GCAPE, and (3) surface sensible heat flux and radiation were only very minor contributors to the production of GCAPE.

Wang and Randall (1994) also investigated the GCAPE quasi-equilibrium hypothesis (Arakawa and Schubert 1974) which asserts that cumulus convection "consumes" GCAPE as quickly as it is produced by large-scale, non-convective forcing. In this case, the convectively active atmosphere remains close to a state of conditional neutrality. Their results were consistent with this hypothesis.

Cripe (1994) has conducted the only mid-latitude study of GCAPE. He also investigated the validity of the GCAPE quasi-equilibrium hypothesis in a region of stronger baroclinicity. The hypothesis was generally validated for the winter and spring periods. The instances when the hypothesis was not valid were attributed to the neglect of the effects of surface latent and sensible heat fluxes. Cripe (1994) also concluded that GCAPE is somewhat larger under convectively active conditions in the mid-latitudes than it is in the tropics, and the rates of GCAPE production by large-scale forcing appear to be as much as an order of magnitude greater than those calculated by Wang and Randall (1994).

Unlike Wang and Randall (1994), Cripe (1994) did not explicitly investigate the effects of surface latent and sensible heat fluxes and horizontal temperature and moisture advection on the production of GCAPE.

4

1.2 Objective

The objective of this research is to investigate the effects of surface latent and sensible heat fluxes and horizontal temperature and moisture advection on the production of GCAPE for a mid-latitude location. Specifically, two hypotheses will be tested: 1) *low-level moisture creates GCAPE* (Hong et al. 1995); 2) *upper-level cold advection creates GCAPE* (Lorenz 1955).

1.3 Scope

Data from the Atmospheric Radiation Measurement (ARM) program are used to investigate the relative effects of various processes in producing GCAPE. The observation site, data, and methodology are described in Chapter two. Results for fall and spring case study periods are presented in Chapters three and four, respectively. Summary and conclusions are presented in Chapter five.

CHAPTER 2 - METHODOLOGY

This chapter describes the observation site, data, and procedures used to calculate 1) GCAPE, 2) temperature and moisture advection, and 3) surface latent and sensible heat fluxes.

2.1 Observation Site and Data

This study used radiosonde and surface flux data from the Central Facility located within the ARM site in north-central Oklahoma (Fig. 2.1). All figures appear at the end of each chapter. A detailed description of the Central Facility and the ARM program can be found in Stokes and Schwartz (1994). The data covered two three-week Intensive Observation Periods (IOPs) conducted during the fall of 1994 and spring of 1995. The IOPs are described in Chapters three and four.

2.1 GCAPE Algorithm

As discussed in Chapter one and described by RW92, the calculation of GCAPE requires that the sounding must be divided into layers ("parcels") that are, at most, 20 hPa deep. In the current study, the soundings were typically 800 hPa deep and parcels were defined to be 10 hPa deep. Each parcel is then raised to the top pressure level where its virtual temperature is calculated. Subsequently, each parcel is lowered to the bottom pressure level where its

virtual temperature is again calculated. The parcel with the largest virtual temperature when raised to the top (parcel A) and the parcel with the largest virtual temperature when lowered to the bottom (parcel B) are determined. With parcel A at the top, the intervening parcels are lowered one level each, and the total thermodynamic energy of the sounding is calculated. The same procedure is repeated for parcel B. The arrangement that results in the minimum total thermodynamic energy is retained and the height of the sounding is lowered one pressure level. The entire procedure is repeated until all the reference state pressure levels have been determined. The resulting sounding has the smallest possible total thermodynamic energy.

The practical application of this procedure requires nine steps, as follows (Fig. 2.2):

STEP 1: Divide the sounding into 10 hPa parcels (RW92) where each contains a unit mass of dry air, w units of water vapor, and $w - \overline{w}$ units of liquid water.

STEP 2: Calculate the entropy and thermodynamic energy per unit mass [following Lorenz (1979)] of each parcel and the total thermodynamic energy of the sounding. The entropy, s, is calculated using

$$(1 + \overline{w})s =$$
$$(C_p + \overline{w}C_{pw})\ln T - R_d \ln(p-e) - wR_w \ln e - (\overline{w} - w)\frac{L}{T}, \tag{2.1}$$

7

the thermodynamic energy, h, is calculated using

$$(1 + \overline{w})h = (C_p + \overline{w}C_{pw})T - (\overline{w} - w)L,$$ (2.2)

and the total thermodynamic energy, h_{total}, of the sounding is calculated using

$$h_{total} = \frac{1}{N}\sum_{k=1}^{N} h(k).$$ (2.3)

STEP 3: Determine the saturation temperature and pressure of each parcel. The saturation temperature and pressure of each parcel are calculated using an integrated form of the Clausius-Clapeyron equation

$$R_w \ln e_s(T) = -(C - C_{pw})\ln T - \frac{L(T)}{T} + R_w \ln e_0$$ (2.4)

and the latent heat of condensation written as

$$L(T) = -(C - C_{pw})T + L_0.$$ (2.5)

8

The saturation temperature is calculated using

$$(1+\bar{w})s = \left[C_p + \varepsilon(C - C_{pw}) + \bar{w}C\right]\ln T + (\varepsilon + \bar{w})\frac{L_0}{T}$$
$$-R_d \ln\left(\frac{\varepsilon}{\bar{w}}\right) + (\varepsilon + \bar{w})\left[C - C_{pw} + R_w \ln e_0\right] \tag{2.6}$$

and

$$(1+\bar{w})\frac{\partial s}{\partial T} = \frac{\left[C_p + \varepsilon(C - C_{pw}) + \bar{w}C\right]}{T} - (\varepsilon + \bar{w})\frac{L_0}{T^2} \tag{2.7}$$

in the Newton-Raphson iteration scheme

$$T_{s,k+1} = T_{s,k} + \frac{(s - s_k)}{\left(\dfrac{\partial s}{\partial T}\right)_k}, \tag{2.8}$$

where s is calculated using (2.1), s_k calculated from the kth iteration of (2.6), and $\left(\dfrac{\partial s}{\partial T}\right)_k$ is calculated from the kth iteration of (2.7). The saturation vapor pressure is calculated following Bolton (1980)

$$e_s(T) = 6.112\exp\left(\frac{17.67T}{T + 243.5}\right), \tag{2.9}$$

and has an accuracy of 0.1% for -30°C $\le T \le$ -35°C.

9

The saturation pressure is then calculated using

$$p_S = \frac{e_S}{\overline{w}}(\varepsilon + \overline{w}) = e_S\left(\frac{\varepsilon}{\overline{w}} + 1\right). \qquad (2.10)$$

STEP 4: Raise each parcel to the top pressure level and calculate its virtual

temperature. Lower each parcel to the bottom pressure level and calculate its virtual temperature. If the pressure to which the parcel is raised is greater than its saturation pressure, then the new parcel temperature, T_n, is calculated using

$$T_n = T_S\left(\frac{p_n}{p_S}\right)^{\kappa}. \qquad (2.11)$$

In this instance, Poisson's constant

$$\kappa = \frac{\left(R_d + \overline{w}R_w\right)}{\left(C_p + \overline{w}C_{pw}\right)} \qquad (2.12)$$

accounts for the masses of both dry air and moist air in the parcel. If the pressure to which the parcel is raised is less than its saturation pressure, then T_n is calculated as follows. Taking the derivative of (2.1) with respect to temperature gives

$$(1+\overline{w})\frac{\partial s}{\partial T} = \frac{\left[C_p + \overline{w}C - w(C - C_{pw})\right]}{T} + \frac{w(\varepsilon + w)L^2}{RT^3} \qquad (2.13)$$

10

Equations (2.1) and (2.13) are used in (2.8) to obtain T_n. The virtual temperature is then calculated using

$$T_v = T_n \left(1 + \frac{w}{\varepsilon} \right) \left(\frac{1}{1 + \overline{w}} \right).$$

(2.14)

If the pressure the parcel is to be lowered to is greater than its saturation pressure, then the new parcel temperature is calculated using (2.11) and (2.12). However, if the pressure to which the parcel is lowered is less than its saturation pressure, then the new parcel temperature is calculated using (2.1) and (2.13) in (2.8). In either case, virtual temperature is calculated using (2.14). The parcel with the largest virtual temperature when raised to the top is designated parcel A and the parcel with the largest virtual temperature when lowered to the bottom is designated parcel B.

STEP 5: Raise parcel A to the top, lower the intervening parcels one level each, and calculate the total thermodynamic energy of the column. Repeat this procedure for parcel B. A schematic of an intermediate step in the GCAPE calculation is shown in Fig. 2.3, where a buoyant surface parcel is moved to the upper troposphere and the intervening parcels are each lowered one level.

STEP 6: Choose the arrangement that results in the smallest total thermodynamic energy of the column.

STEP 7: Redefine the top pressure level to be the second pressure level from the top.

STEP 8: Iterate steps 4-7 until the reference-state pressures of all the parcels have been determined.

STEP 9: Finally, the GCAPE is calculated using

$$GCAPE = \frac{1}{N} \sum_{k=1}^{N} \left[h_G(k) - h_R(k) \right] \tag{2.15}$$

where $h_G(k)$ and $h_R(k)$ are the thermodynamic energies of the kth parcel in the given and reference states, respectively.

2.2 GCAPE Modifications

The physical processes that affect GCAPE production include surface fluxes of heat and moisture and temperature and moisture advection. RW92 found that surface evaporation is the most powerful producer of GCAPE in the tropics. They also found radiation and surface sensible heat flux were only very minor contributors to GCAPE production. In the current study, the effect of surface sensible heat flux is considered because it can be much larger over land than over water (Arya 1988). The procedures to estimate surface heat and moisture fluxes are described in section 2.2.1. Quantitative estimation of the effects of temperature and moisture advection are described

12

in section 2.2.2. The sensitivity of GCAPE was evaluated by introducing order of magnitude changes of fluxes and advection. These constant values allowed direct comparison of cases. Next, observed values were used to determine actual effects.

2.2.1 Surface Heat and Moisture Fluxes

The effect of an increase in surface sensible heat flux is added to a sounding as follows. First, the vertical difference in dry static energy is integrated upward from the surface until the integrated value reaches 500 W m^{-2}. The corresponding pressure is designated p_{top}. Next, potential temperature at p_{top}, θ_{top}, is calculated using the known temperature from the radiosonde. Holding θ_{top} constant, the new temperature [$T(p)$] profile is calculated from p_{top} down to the surface as:

$$T(p) = \theta_{top}\left(\frac{p}{1000mb}\right)^{\frac{R_d}{C_p}} . \tag{2.16}$$

The resulting potential temperature profile is dry-adiabatic (Fig. 2.4).

The effect of surface latent heat flux is added to the same depth as sensible heat flux so that the comparison of the two effects on GCAPE production is unbiased. Equal moisture amounts are added to each pressure level from the surface to p_{top} so that the added moisture is evenly mixed.

13

The moisture amount added to a given pressure level is determined as follows. The effect of latent heat flux over time can be expressed as

$$\Delta H_L = \int \frac{\partial}{\partial t}(\rho L q)dz .$$ (2.17)

Using the hydrostatic equation, (2.17) can be re-written as

$$\Delta H_L = \frac{L}{g} \int \left(\frac{\partial q}{\partial t}\right)dp .$$ (2.18)

The addition of specific humidity, Δq, can then be approximated as

$$\Delta q = \frac{g}{L}\left(\frac{\Delta H_L \Delta t}{\Delta p}\right).$$ (2.19)

For example, with ΔH_L = 500 W m^{-2}, Δt = 10800 s, and Δp = 10^5 hPa, the moisture amount to be added to each pressure level would be 2.1 g kg^{-1}. An illustration of the given moisture profile and the moisture profile that results when latent heat flux is added is shown in Fig. 2.5.

Latent and sensible heat flux amounts of 100, 200, 300, and 400 W m^{-2} were added to a sounding for various depths of the atmosphere. The intent was to determine the effects of surface latent and sensible heat flux on 1) Lifting Condensation Level (LCL) and 2) on GCAPE production. Fig. 2.6 shows the effects of the surface fluxes on the LCL of the surface air parcel. The

14

LCL lowers for increasing latent heat flux and rises for increasing sensible heat flux. These effects are mitigated as the depth to which latent and sensible heat fluxes are added increases. This means that a parcel will rise through a shallower depth to reach its LCL when the effect of latent heat flux is allowed to act upon it. Thus, the parcel will not cool as much to reach its LCL and will rise moist-adiabatically through a greater depth. Therefore, the parcel will be warmer (more buoyant) and, thus, the atmosphere more unstable, i. e., more GCAPE will be produced. Similarly, the parcel will have a greater virtual temperature when raised to the top of the column and will be a more likely candidate for parcel rearrangement. The implication is that more GCAPE will be produced.

The effect of latent heat flux on GCAPE production is shown in Fig. 2.7. GCAPE increases as latent heat flux increases. GCAPE also increases as the depth through which the fluxes are added decreases. The effect of sensible heat flux on GCAPE production is shown in Fig 2.8. GCAPE increases as sensible heat flux increases and as input depth decreases. However, in general, the GCAPE produced by latent heat flux is more than the GCAPE produced by an equivalent amount of sensible heat flux, in some cases by as much as a factor of three. For example, a latent heat flux of 400 W m^{-2} into 16 hPa produces approximately 340 J kg^{-1} of GCAPE whereas an equivalent amount of sensible heat flux into the same depth produces only approximately 120 J kg^{-1}; that is, increased low-level moisture produces

15

GCAPE most efficiently. This finding is consistent with the results of Segal et al. (1995). They recently showed that deep convection depends significantly on the ratio of sensible to latent heat flux (Bowen ratio); for smaller Bowen ratio the thermodynamic potential for deep convection increases.

2.2.2 Temperature and Moisture Advection

Horizontal temperature and moisture advection was simulated using the following hyperbolic tangent function

$$\Delta\phi(p) = A \tanh\left(\frac{p - 500mb}{P_{tropopause}}\right), \qquad (2.20)$$

where $\Delta\phi(p)$ represents a deviation from either the given moisture or the given temperature sounding as a function of pressure. The deviation of the advection curve was chosen to be zero at 500 hPa, i. e., the level of non-divergence, and the amplitude of the curve, A, was chosen so the resulting temperature and moisture profiles represented of an input of 500 W m^{-2}. The tropopause pressure was kept constant at 175 hPa and moisture advection was confined to the lowest 500 hPa. Examples of temperature and moisture advection profiles due a combination of surface-500 hPa warm advection/500 hPa-tropopause cold advection and surface-500 hPa moisture advection are shown in Figs. 2.9 and 2.10, respectively.

16

The observed horizontal temperature and moisture advection were calculated every three hours as in Wang and Randall (1994). The moisture, temperature, and winds were obtained from radiosondes released every three hours from the Central Facility and four boundary facilities located at Haskell, Hillsboro, Purcell, and Vici (Fig. 2.1). National Weather Service wind profilers collocated with the boundary facilities provided additional wind data. An objective analysis scheme combines the radiosonde and profiler data to provide time sequence estimates of thermodynamic advective tendencies. The scheme is a successive correction scheme based on that originally proposed by Barnes (1964) and utilizes the formulation of Caracena (1987) to calculate derivatives.
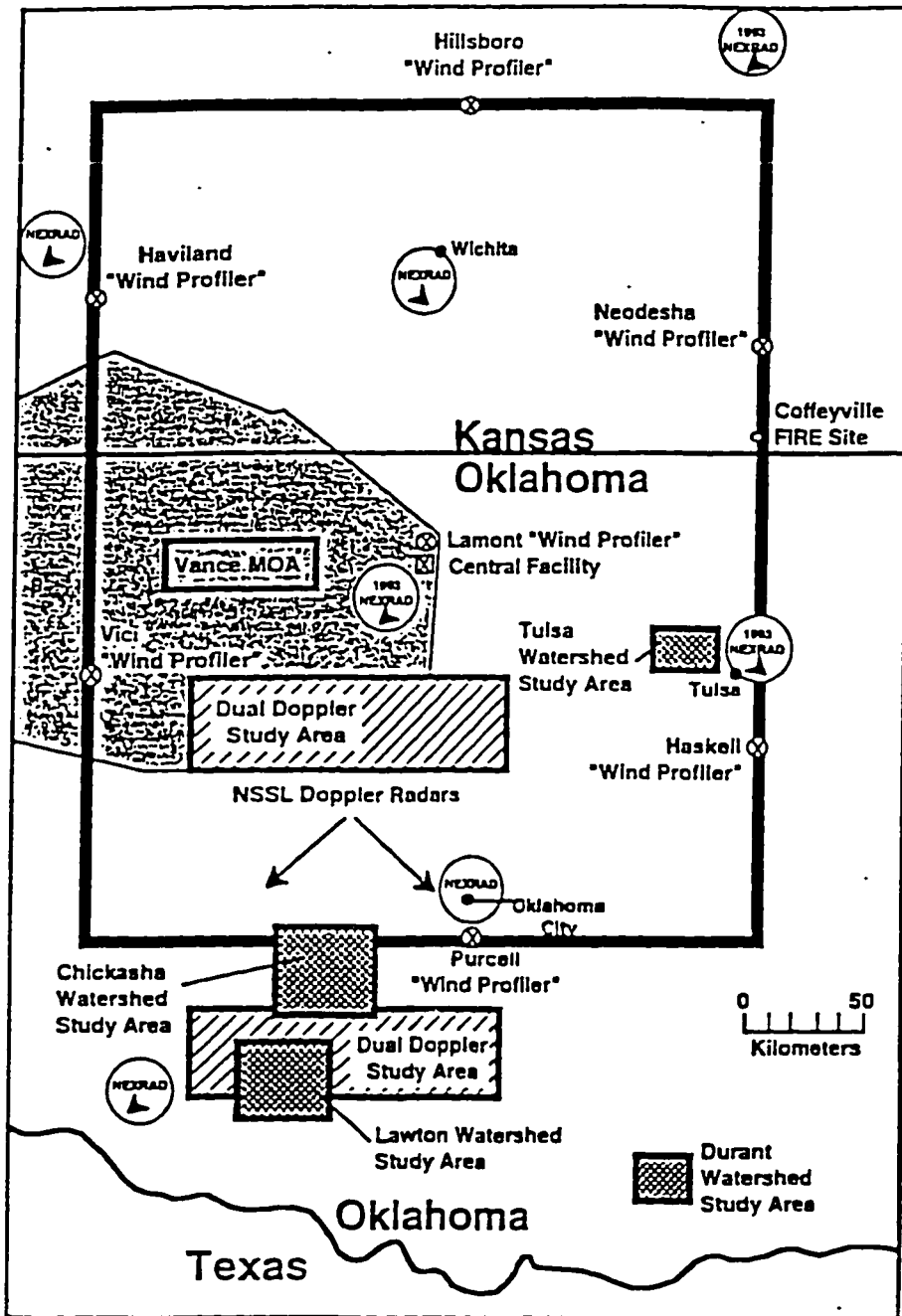
Figure 2.1 - Location of the Central Facility within the ARM site
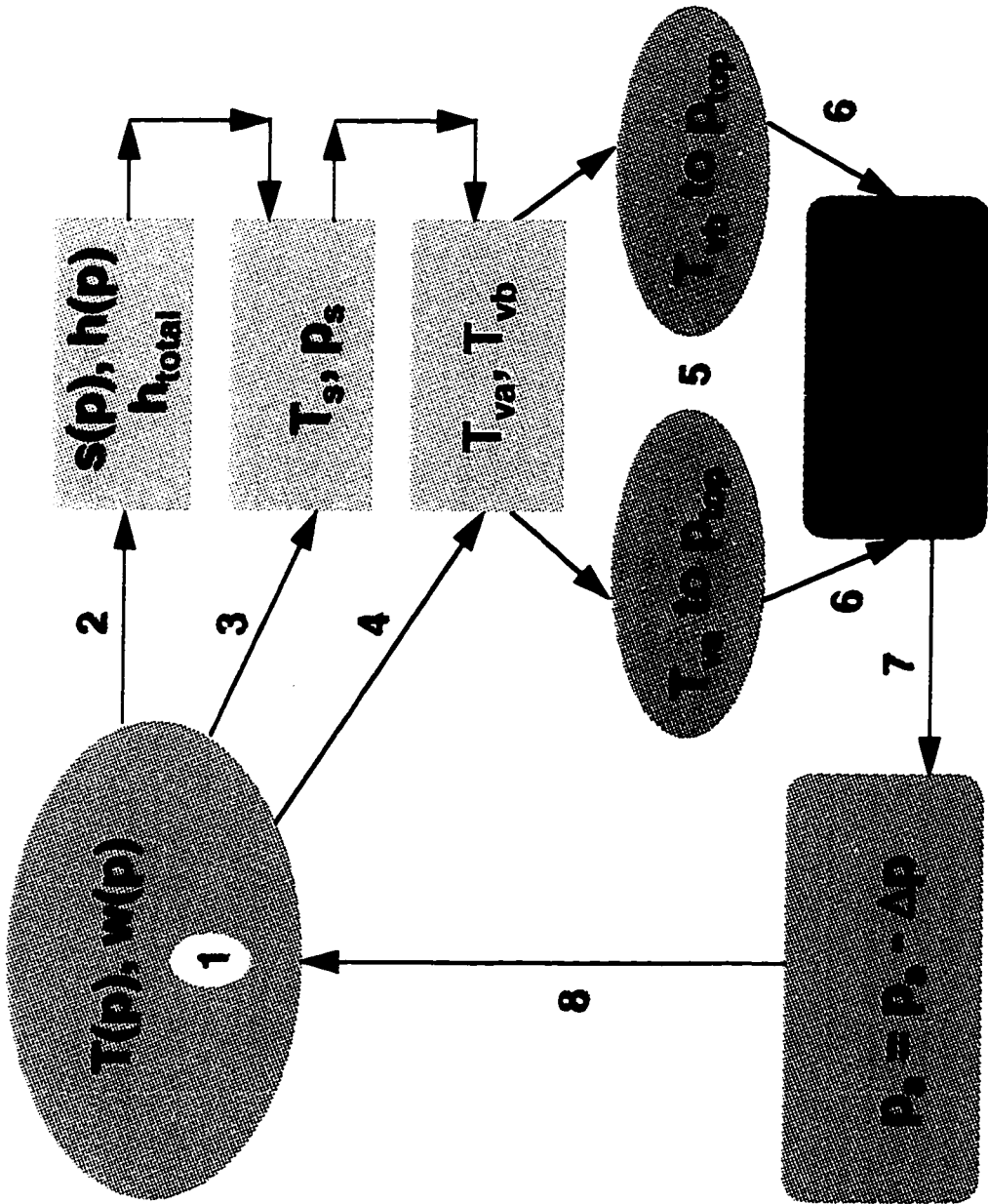
Figure 2.2 - Flow diagram of the GCAPE algorithm

Original
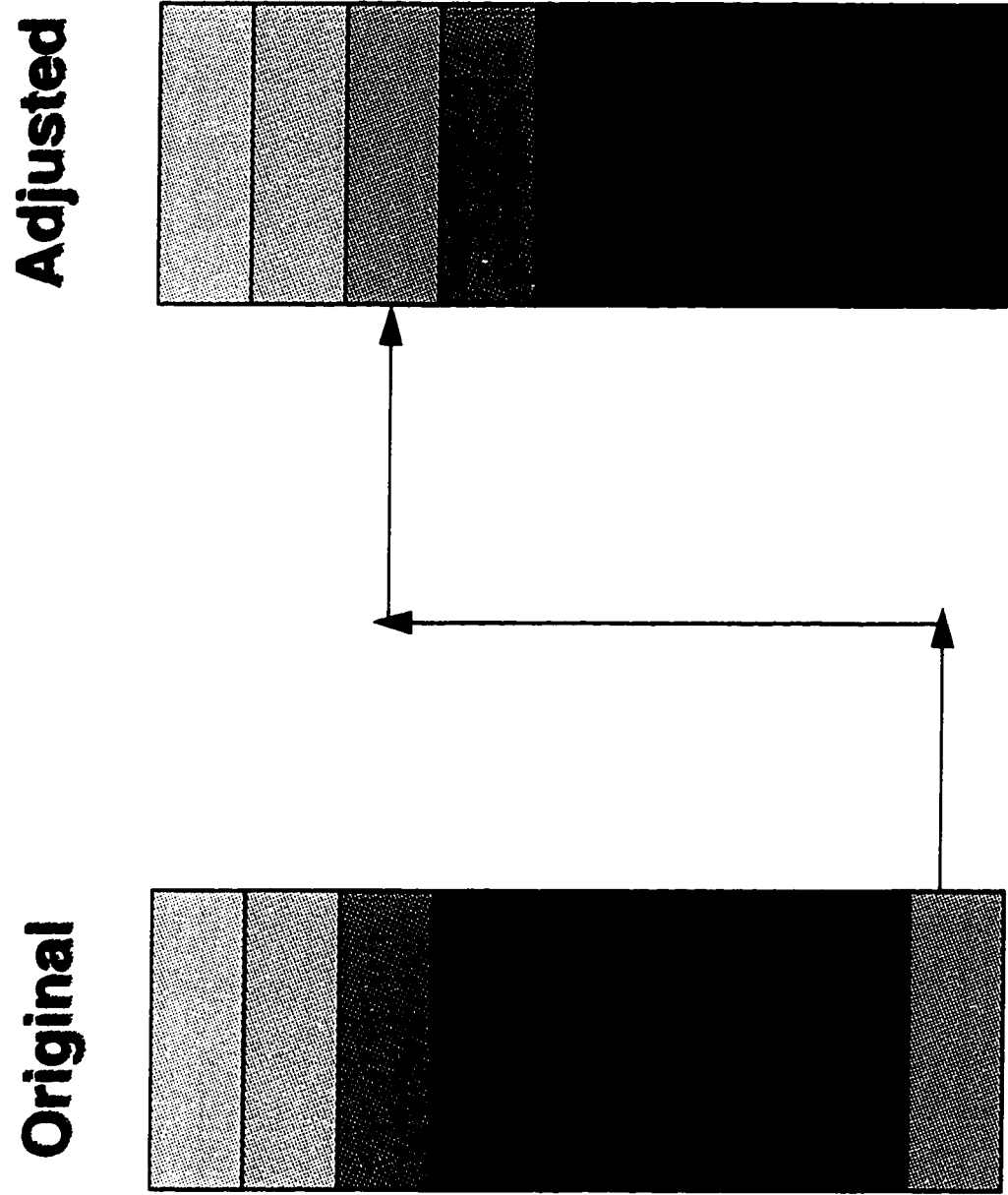
Adjusted

Figure 2.3 - Schematic of an intermediate step in the GCAPE algorithm

20
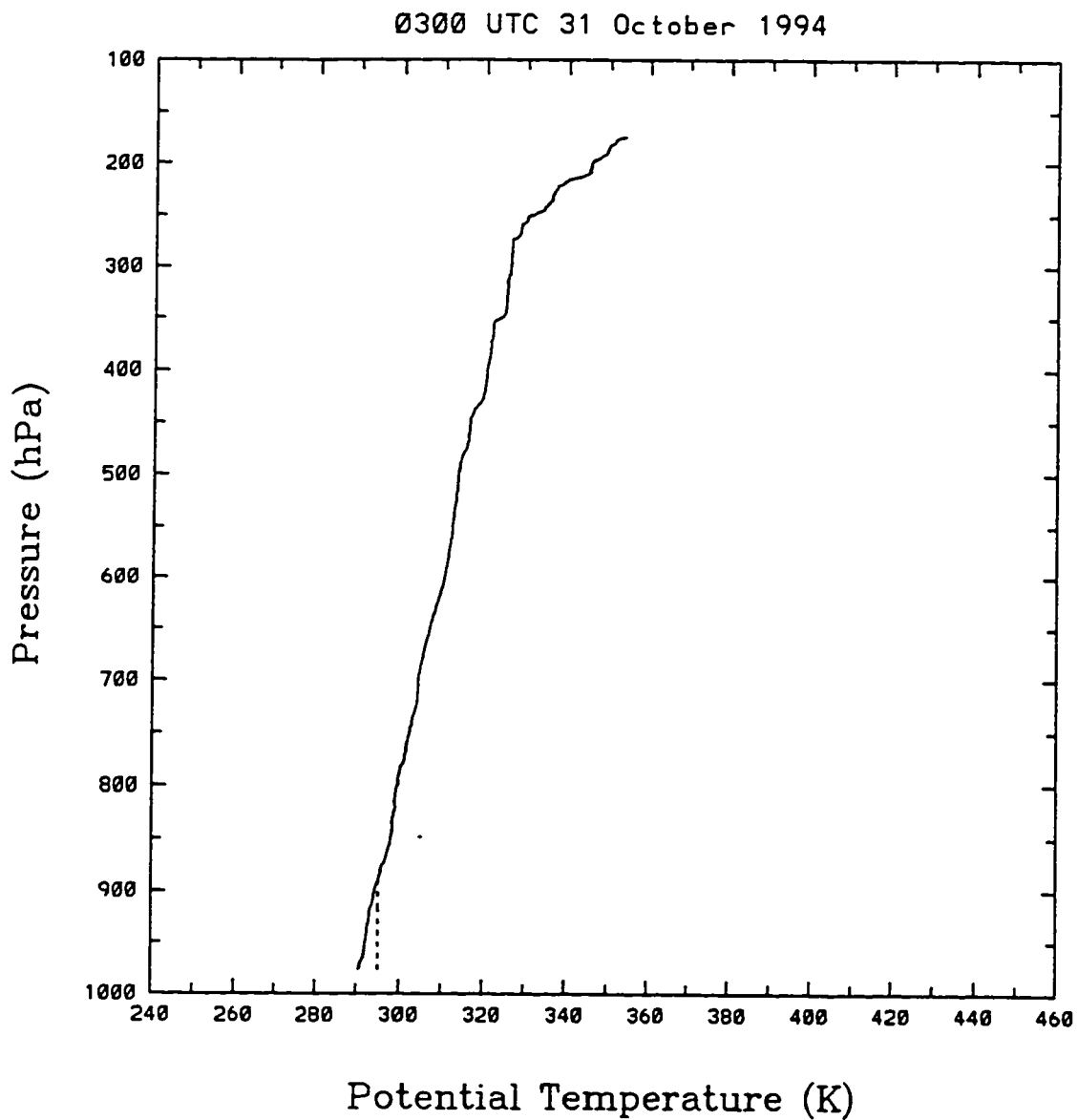
Figure 2.4 - The given potential temperature sounding (solid) and the potential
temperature sounding adjusted for sensible heat flux (dashed)

21

0300 UTC 31 October 1994
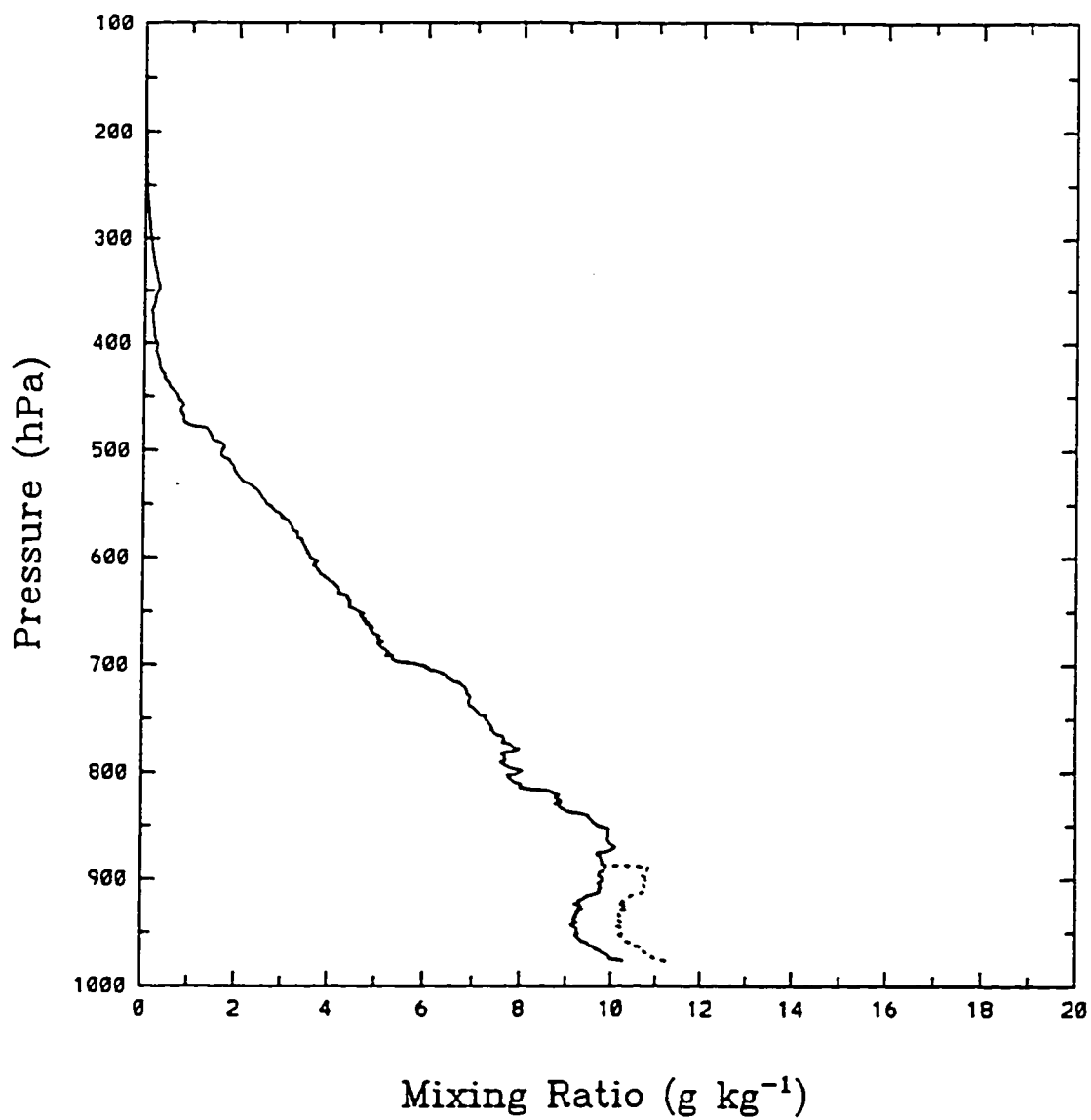
Figure 2.5 - The given mixing ratio sounding (solid) and the mixing ratio

sounding adjusted for latent heat flux (dashed)
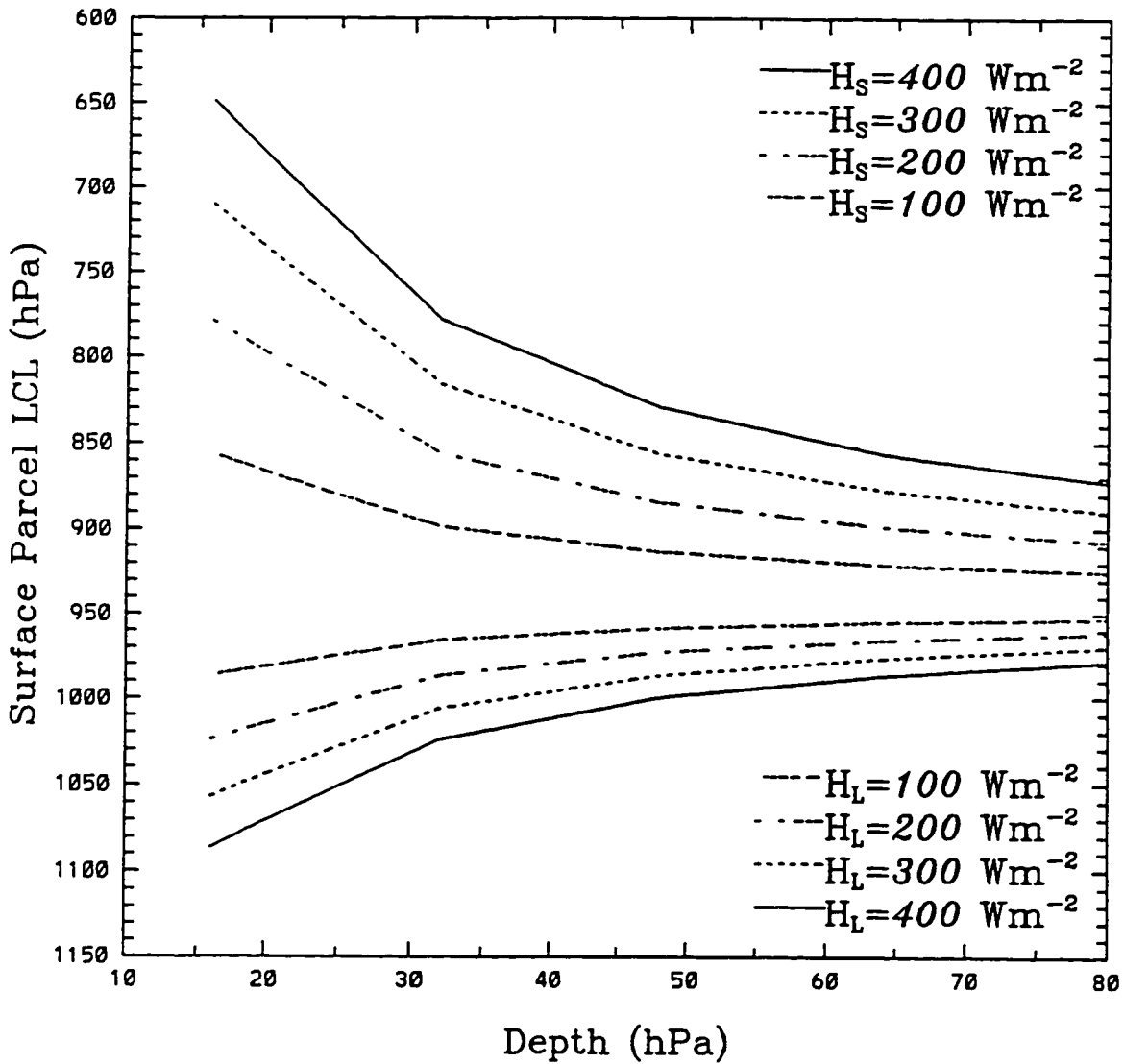
Figure 2.6 - The effects of latent and sensible heat fluxes on surface parcel LCL
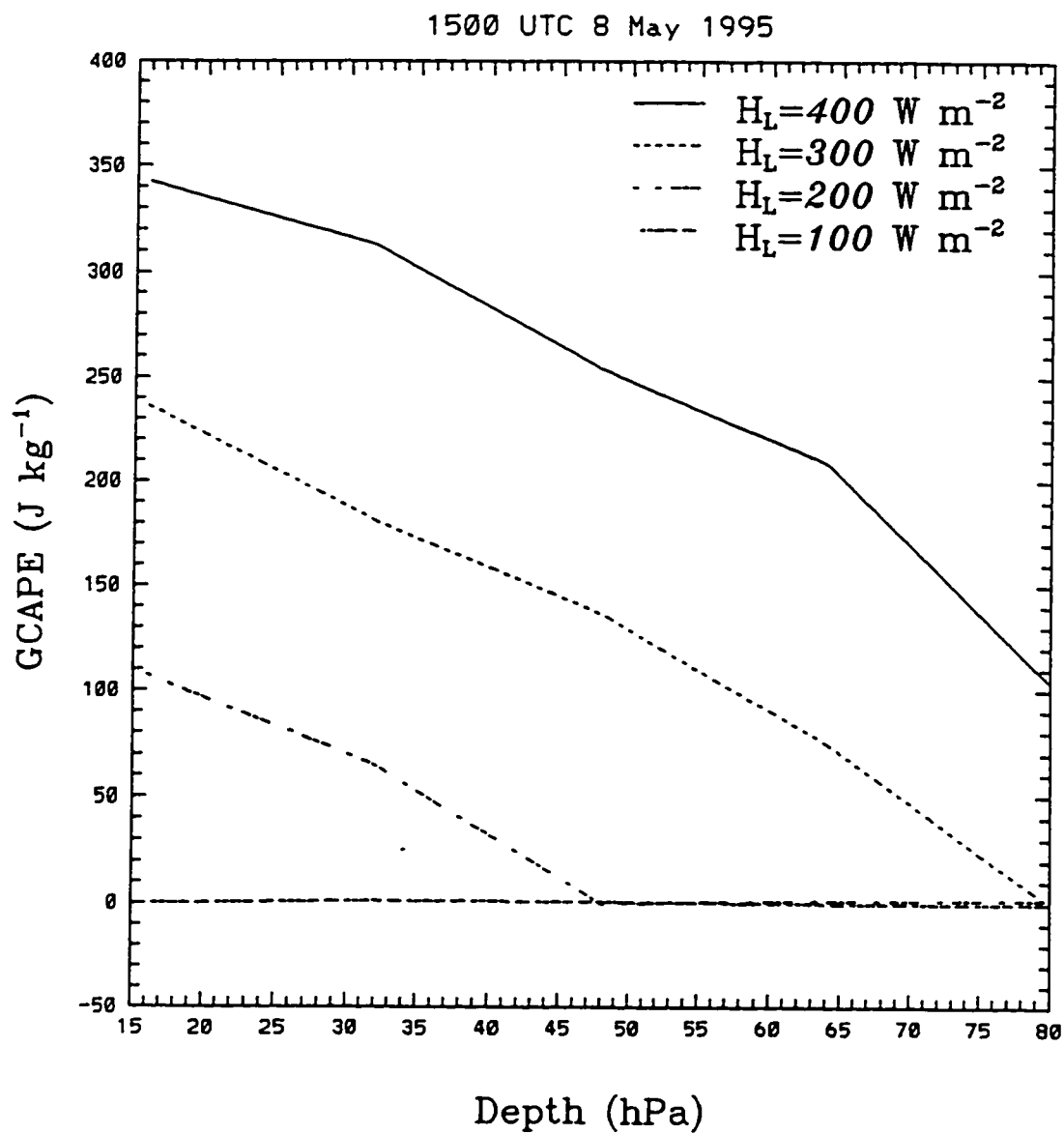
Figure 2.7 - The effect of surface latent heat flux on GCAPE production
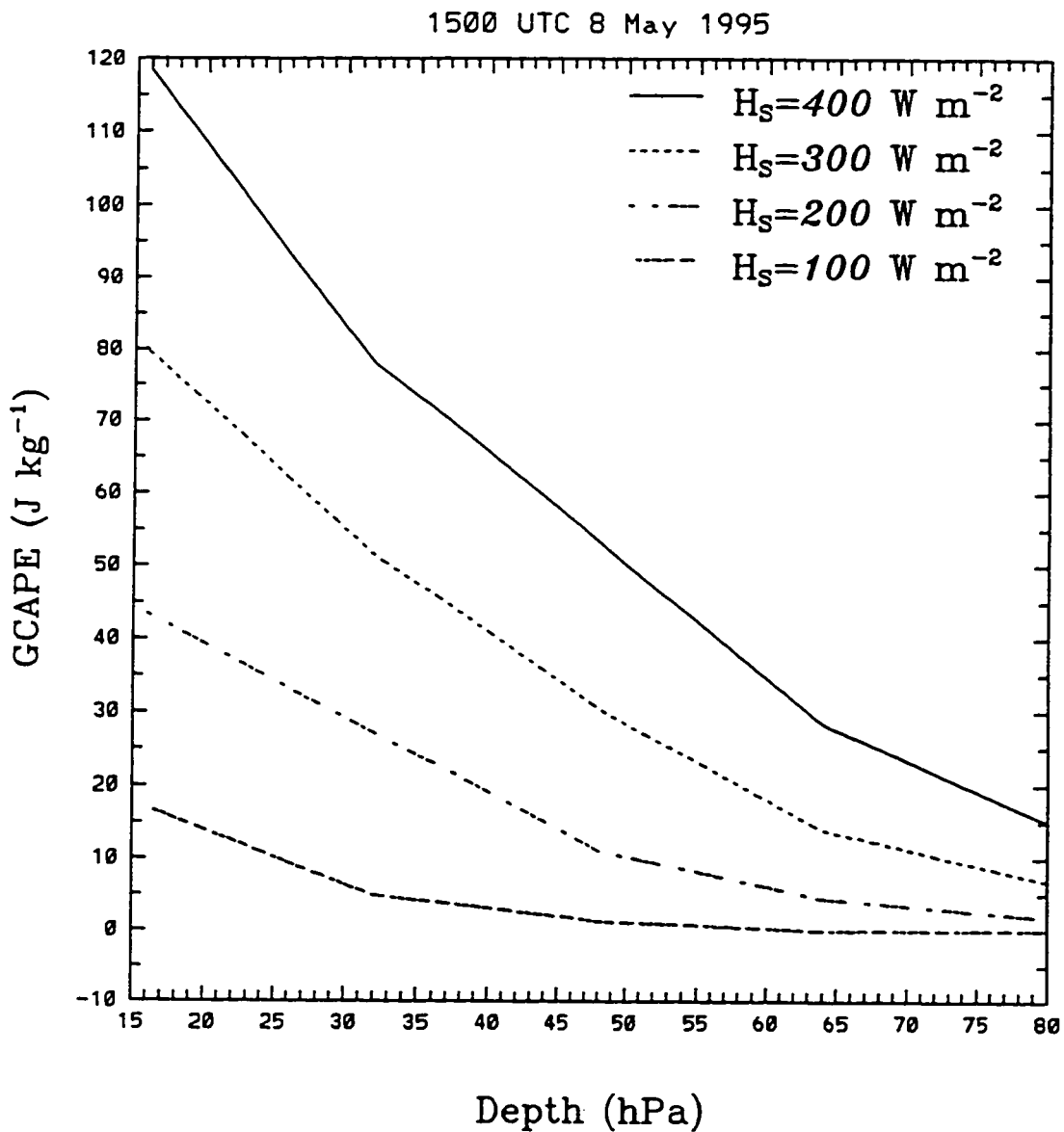
Figure 2.8 - The effect of surface sensible heat flux on GCAPE production

1500 UTC 8 May 1995
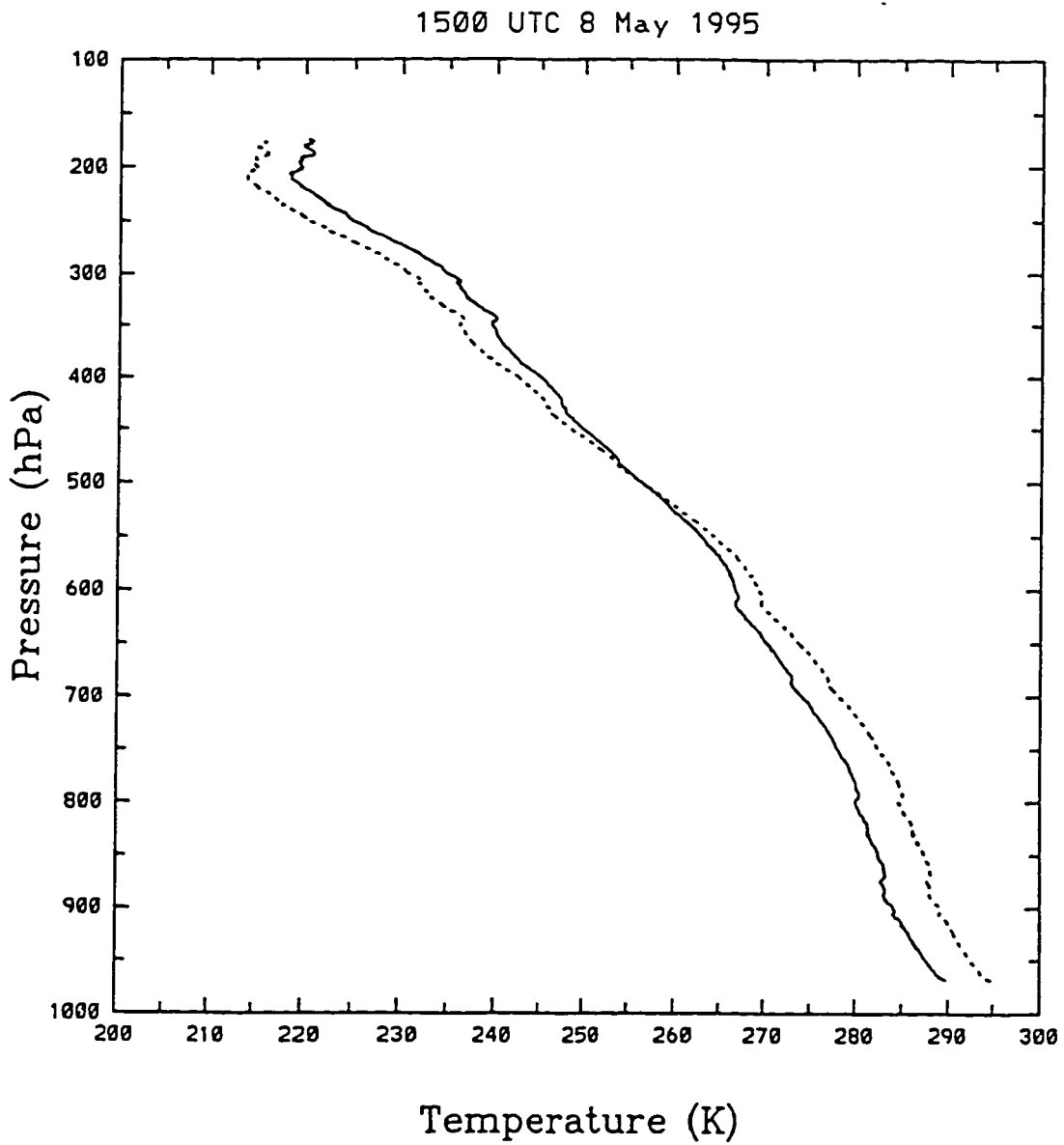
Figure 2.9 - The given temperature sounding (solid) and the temperature

sounding adjusted for temperature advection (dashed)
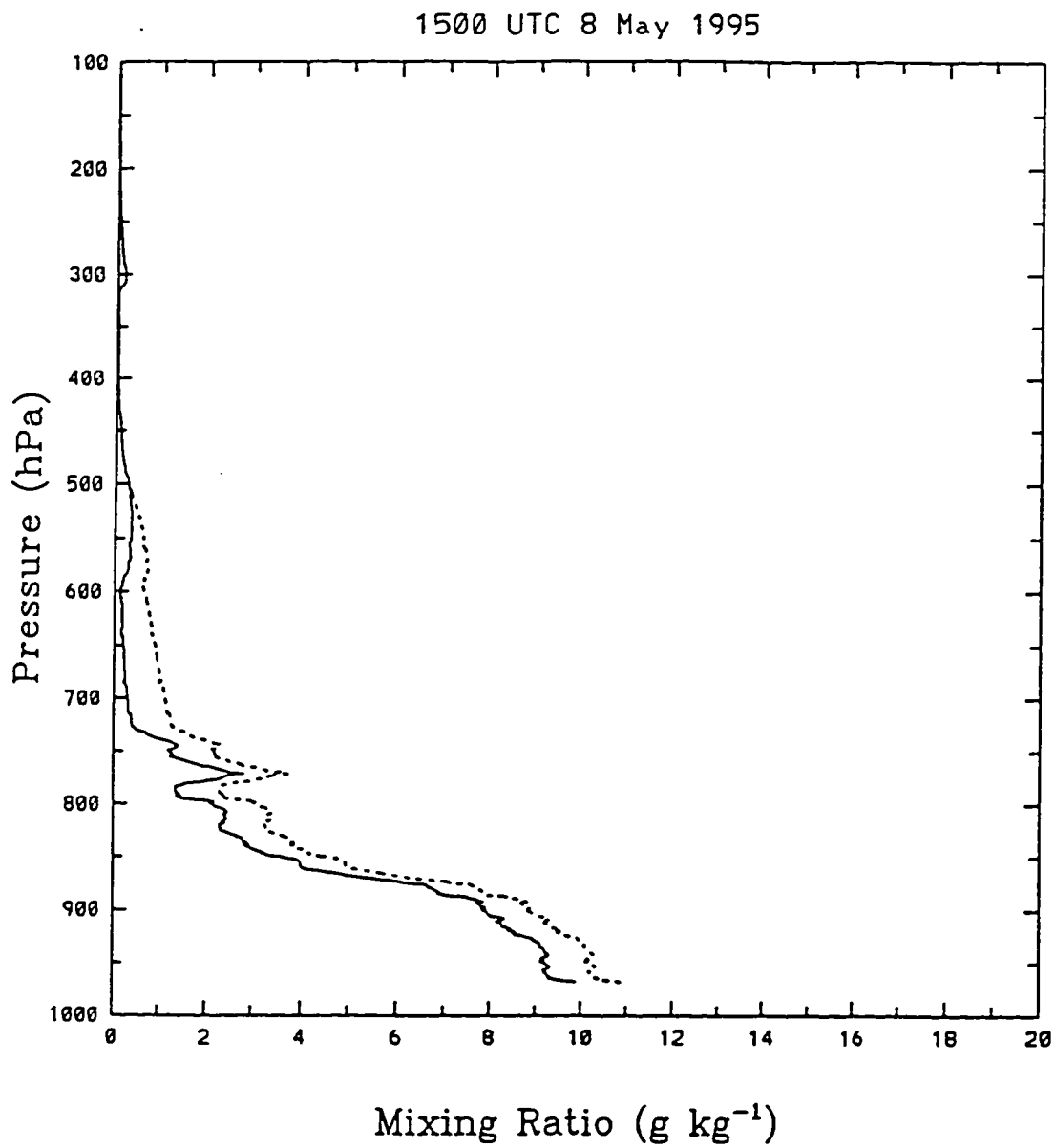
Figure 2.10 - The given mixing ratio sounding (solid) and the mixing ratio sounding adjusted for moisture advection (dashed)

CHAPTER 3 - FALL 1994 IOP

The fall 1994 IOP was conducted from 0000 UTC 24 October to 0000 UTC 15 November 1994. Time series of GCAPE and surface meteorological observations are presented in section 3.1. The effects of surface heat and moisture fluxes and temperature and moisture advection on the production of GCAPE are shown and discussed in section 3.2. Observed surface heat and moisture fluxes, temperature and moisture advection, and the GCAPE produced by them are also shown and discussed in section 3.2. For reference purposes a detailed description of daily meteorological conditions is given in Appendix A. A summary follows in section 3.3.

3.1 Observations

The time series of GCAPE (Fig. 3.1) shows there were three significant GCAPE events during the fall 1994 IOP. These are summarized in Table 3.1.

Table 3.1. Significant GCAPE events during the fall 1994 IOP.

Time and Date	GCAPE ($J\,kg^{-1}$)	Meteorology
1200 UTC 24 October	23.1	Frontal Passage
0600 UTC 31 October	14.3	Cold Front
0600-0900 4 November	36.2 and 39.7	Cold Front

Three hour average surface latent and sensible heat fluxes are plotted in Fig. 3.2 which shows that surface sensible heat flux was greater than surface latent heat flux during the entire fall 1994 IOP. Also evident is the diurnal oscillation of the surface fluxes due to daytime heating and nighttime cooling.

The first significant GCAPE event (24 October, Fig. 3.1) was associated with a frontal passage. The surface latent heat flux was approximately 110 W m^{-2} (Fig. 3.2) and was the second largest surface latent heat flux during the fall 1994 IOP.

The second significant GCAPE event (31 October) when there was a cold front located south of the Central Facility. Three hour average temperature and three hour accumulated precipitation is shown in Fig 3.3. The front produced precipitation at the Central Facility (Fig. 3.3) and cool temperatures as cold air was advected over the Central Facility from the north. The surface fluxes during this time were relatively small compared to the surface fluxes during other convective events (Fig. 3.2).

The third significant GCAPE event (4 November, Fig. 3.1) and was also associated with a cold front. Similar to the previous event, the front produced precipitation at the Central Facility late on the fourth and again on the fifth and cooler air from the north was advected over the Central Facility (Fig. 3.3). The surface fluxes during this time were again small (Fig. 3.2).

29

3.2 GCAPE Sensitivity Experiments

The variability of GCAPE production was examined as a function of each of the following processes: (1) surface latent heat flux, (2) surface sensible heat flux, (3) a combination of surface-500 hPa warm advection and 500 hPa-tropopause cold advection (total temperature advection), (4) surface-500 hPa warm advection (low-level warm advection), (5) 500 hPa-tropopause cold advection (upper-level cold advection), and (6) surface-500 hPa moisture advection (low-level moisture advection). Soundings chosen from the ARM data occurred one observation time (three hours) prior to times when the most GCAPE was observed. An experimental constant energy flux of 500 W m^{-2} was added to the soundings to represent the GCAPE produced by each process. This energy flux value was chosen to represent the upper limit of forcing by the observed processes. Sometimes the observed forcing exceeded this value and other times it did not.

For the first significant GCAPE event (0300 UTC 31 October) experimental low-level moisture advection produced the most GCAPE for an energy flux of 500 W m^{-2} (Fig. 3.4). Surface latent heat flux produced the second largest amount. The observed energy flux magnitudes are shown in Table 3.2.

30

Table 3.2. GCAPE and observed energy fluxes for 0300 UTC 31 October.

Process	Observed Energy Flux (W m^{-2})	GCAPE$_{before}$ (J kg^{-1})	GCAPE$_{after}$ (J kg^{-1})	ΔGCAPE (J kg^{-1})
H$_l$	5.5	4.8	4.8	0
H$_s$	0.5	4.8	4.8	0
$-V \bullet \nabla T_{total}$	1427.9	4.8	0	-4.8
$-V \bullet \nabla T_{lower}$	637.5	4.8	0	-4.8
$-V \bullet \nabla T_{upper}$	790.4	4.8	2.8	-2.0
$-V \bullet \nabla q_{lower}$	7.0	4.8	4.2	-0.8

Total temperature advection constituted most of the observed energy flux and surface sensible heat flux constituted the least.

The resulting vertical temperature and mixing ratio profiles due to observed temperature and moisture advection are shown in Figs. 3.5 and 3.6. Temperature decreased in the lower and upper levels but increased in the middle levels. Moisture decreased in the lower levels and increased in the middle levels. As shown in Table 3.2, GCAPE remained unchanged due to the surface fluxes because they were small. Both total temperature advection and low-level temperature advection reduced the GCAPE because they resulted in more stable vertical temperature profiles. Upper-level temperature advection did not reduce the GCAPE as much as the other two temperature advection processes because it did not stabilize the atmosphere as much. Low-level moisture advection reduced

31

the GCAPE only slightly due to decreased moisture in the lower levels. The observed GCAPE was 4.8 J kg^{-1} and increased to 14.3 J kg^{-1} approximately three hours later which suggests processes other than low-level moisture advection and upper-level temperature advection created GCAPE.

For the second significant GCAPE event (0000 UTC 4 November) experimental surface latent heat flux produced the largest amount of GCAPE and upper-level cold advection produced the second largest amount of GCAPE (Fig. 3.7). Total temperature advection accounted for most of the observed energy flux and surface heat and moisture fluxes accounted for the least (Table 3.3).

Table 3.3. GCAPE and observed energy fluxes for 0000 UTC 4 November.

Process	Observed Energy Flux (W m^{-2})	GCAPE$_{before}$ (J kg^{-1})	GCAPE$_{after}$ (J kg^{-1})	ΔGCAPE (J kg^{-1})
H$_l$	1.8	3.9	3.9	0
H$_s$	19.1	3.9	3.9	0
$-V \bullet \nabla T_{total}$	235.8	3.9	2.8	-1.1
$-V \bullet \nabla T_{lower}$	157.1	3.9	2.7	-1.2
$-V \bullet \nabla T_{upper}$	78.7	3.9	4.2	0.3
$-V \bullet \nabla q_{lower}$	26.9	3.9	3.4	-0.5

The resulting temperature and mixing ratio profiles due to observed temperature and moisture advection are shown in Figs. 3.8 and 3.9, respectively. In general,

32

temperature decreased throughout the troposphere due to cold advection although there was a slight increase from 500-450 hPa due to warm advection. Moisture decreased in the lower levels due to dry advection and increased in the middle levels due to moist advection. It could be expected that because upper-level cold advection produced GCAPE efficiently, and because it was greater than surface latent heat flux, upper-level temperature advection would also produce the majority of observed GCAPE. This is shown in Table 3.3. This also is in agreement with Lorenz (1955) in which he states "...removal of energy is sometimes as effective as addition of energy in making more energy available...," because, "...cooling removes total potential energy from the system, but it still disturbs the density stratification, thus creating horizontal pressure forces which may convert total potential energy into kinetic energy." Again, neither surface flux produced GCAPE because each was small. Total temperature advection and low-level temperature advection reduced the GCAPE because they cooled and stabilized the atmosphere. Upper-level temperature advection produced GCAPE because it de-stabilized the atmosphere. Low-level moisture advection reduced the GCAPE because of dry advection in the lower levels. The GCAPE increased to 7.7 J kg^{-1} which suggests upper-level cold advection was the primary GCAPE producer.

Experimental upper-level cold advection would be the most effective GCAPE producer and surface sensible heat flux would be the least effective GCAPE producer three hours later for 0300 UTC 4 November (Fig. 3.10). Low-level moisture advection constituted most of the observed energy flux and upper-level temperature advection constituted the least (Table 3.4).

Table 3.4. GCAPE and observed energy fluxes for 0300 UTC 4 November.

Process	Observed Energy Flux $(W\,m^{-2})$	$GCAPE_{before}$ $(J\,kg^{-1})$	$GCAPE_{after}$ $(J\,kg^{-1})$	$\Delta GCAPE$ $(J\,kg^{-1})$
H_l	0.1	5.4	5.4	0
H_s	11.2	5.4	5.4	0
$-V \cdot \nabla T_{total}$	74.6	5.4	4.1	-1.3
$-V \cdot \nabla T_{lower}$	39.2	5.4	4.4	-1.0
$-V \cdot \nabla T_{upper}$	35.4	5.4	5.2	-0.2
$-V \cdot \nabla q_{lower}$	123.2	5.4	4.0	-1.4

Moisture decreased in the lower and middle levels due to dry advection but increased from 750-650 hPa due to moist advection (Fig. 3.11). Temperature decreased in the lower and upper levels due to cold advection and increased in the middle levels due to warm advection (Fig. 3.12). Upper-level temperature advection generated the most GCAPE but the amount generated was actually less than that calculated for the given sounding (Table 3.4). Total temperature advection and upper-level temperature advection reduced the GCAPE because they resulted in more stable vertical temperature profiles. Low-level temperature advection reduced the GCAPE because it cooled the lower troposphere and reduced parcel buoyancy. Negative low-level moisture advection reduced the GCAPE because it reduced low-level moisture also resulting in reduced parcel buoyancy.

For 0600 UTC 4 November, upper-level cold advection would produce the most GCAPE followed by low-level moisture advection (Fig. 3.13). Temperature decreased in the lower and upper levels due to cold advection and increased in the middle levels due to warm advection (Fig. 3.14). Moisture decreased from the surface to 800 hPa and from 620-510 hPa due to dry advection whereas it increased from 800-620 hPa due to moist advection (Fig. 3.15). Low-level moisture advection constituted most of the observed energy flux and upper-level temperature advection constituted the least (Table 3.5).

Table 3.5. GCAPE and observed energy fluxes for 0600 UTC 4 November.

Process	Observed Energy Flux (W m^{-2})	GCAPE$_{before}$ (J kg^{-1})	GCAPE$_{after}$ (J kg^{-1})	ΔGCAPE (J kg^{-1})
H$_l$	13.1	41.7	41.7	0
H$_s$	5.3	41.7	41.7	0
$-V \cdot \nabla T_{total}$	85.8	41.7	40.3	-1.4
$-V \cdot \nabla T_{lower}$	69.6	41.7	20.8	-20.9
$-V \cdot \nabla T_{upper}$	16.3	41.7	43.1	1.4
$-V \cdot \nabla q_{lower}$	162.4	41.7	18.4	-23.3

Upper-level temperature advection generated GCAPE (Table 3.5). Temperature increased from 425-375 hPa due to warm advection but decreased from 375-335 hPa and again from 315-200 hPa due to cold advection (Fig. 3.14). This

35

differential advection appears to have caused the increase in GCAPE because the upper-level temperature structure was made more unstable. Low-level temperature advection reduced the GCAPE because it cooled the lower troposphere and reduced parcel buoyancy. Negative low-level moisture advection reduced the GCAPE by even more because it dried the lower troposphere resulting in an even greater reduction in parcel buoyancy. The GCAPE increased to 39.7 J kg^{-1} three hours later apparently due to upper-level temperature advection.

3.3 Summary

For the fall 1994 IOP, some simple experiments designed to change the initial GCAPE by introducing constant forcing via surface fluxes and advection have show that low-level moisture advection and upper-level cold advection produce the most GCAPE. There is an apparent positive correlation between the process that produced the most GCAPE in the experiments and the process that produced the most GCAPE in reality. In one case experimental low-level moisture advection generated the most GCAPE by reducing the height of the LCL, thereby increasing parcel buoyancy. In the remaining three cases experimental upper-level cold advection produced the most GCAPE and the observed upper-level temperature advection produced the most GCAPE. Observed upper-level temperature advection produced the most GCAPE by disturbing the vertical temperature structure such that the atmosphere was made unstable. These results confirm the hypotheses stated in Chapter two and the results of Lorenz (1955).

0000 UTC 24 Oct – 0000 UTC 15 Nov 1994
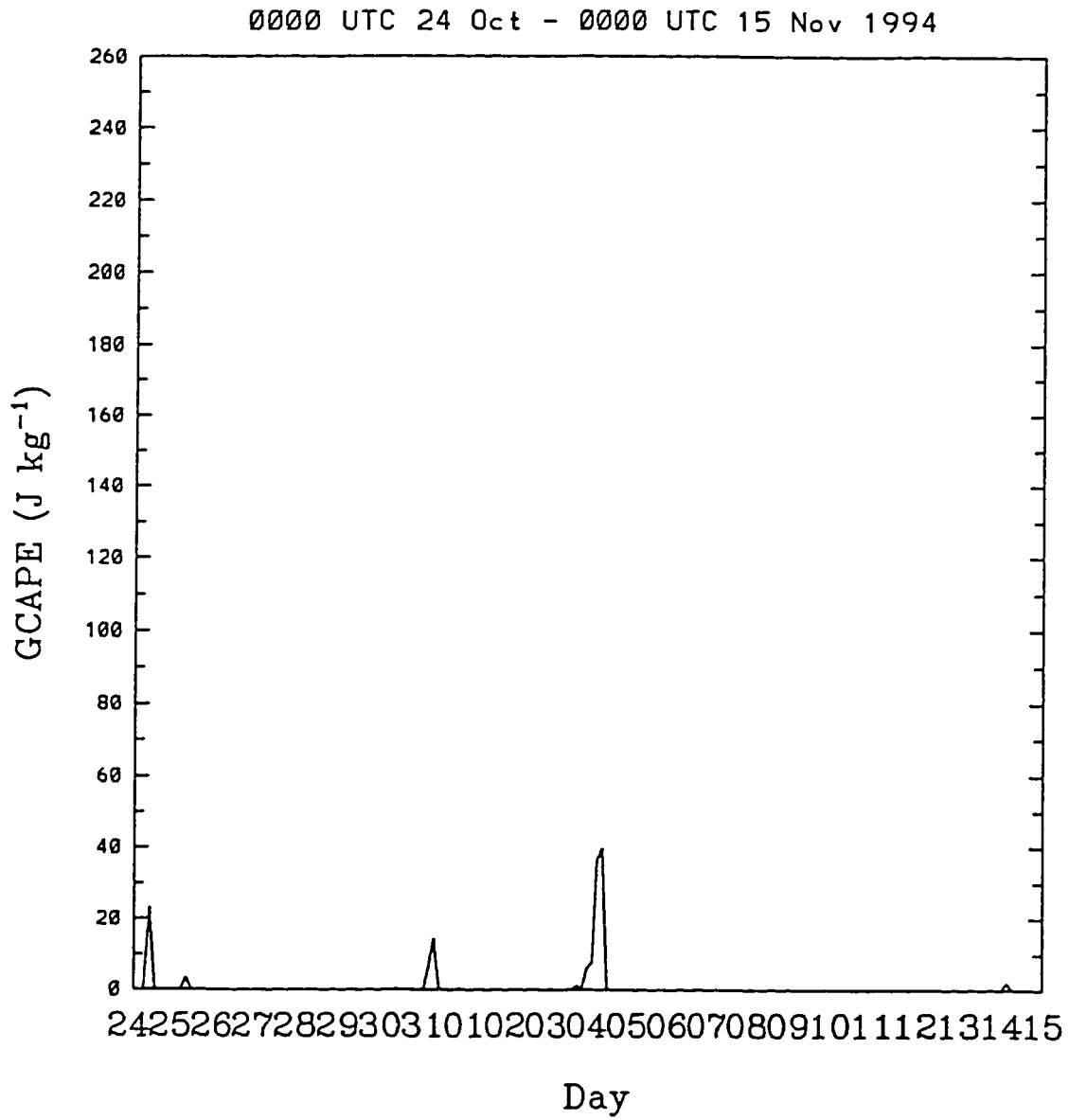
Figure 3.1 - GCAPE time series for the fall 1994 IOP
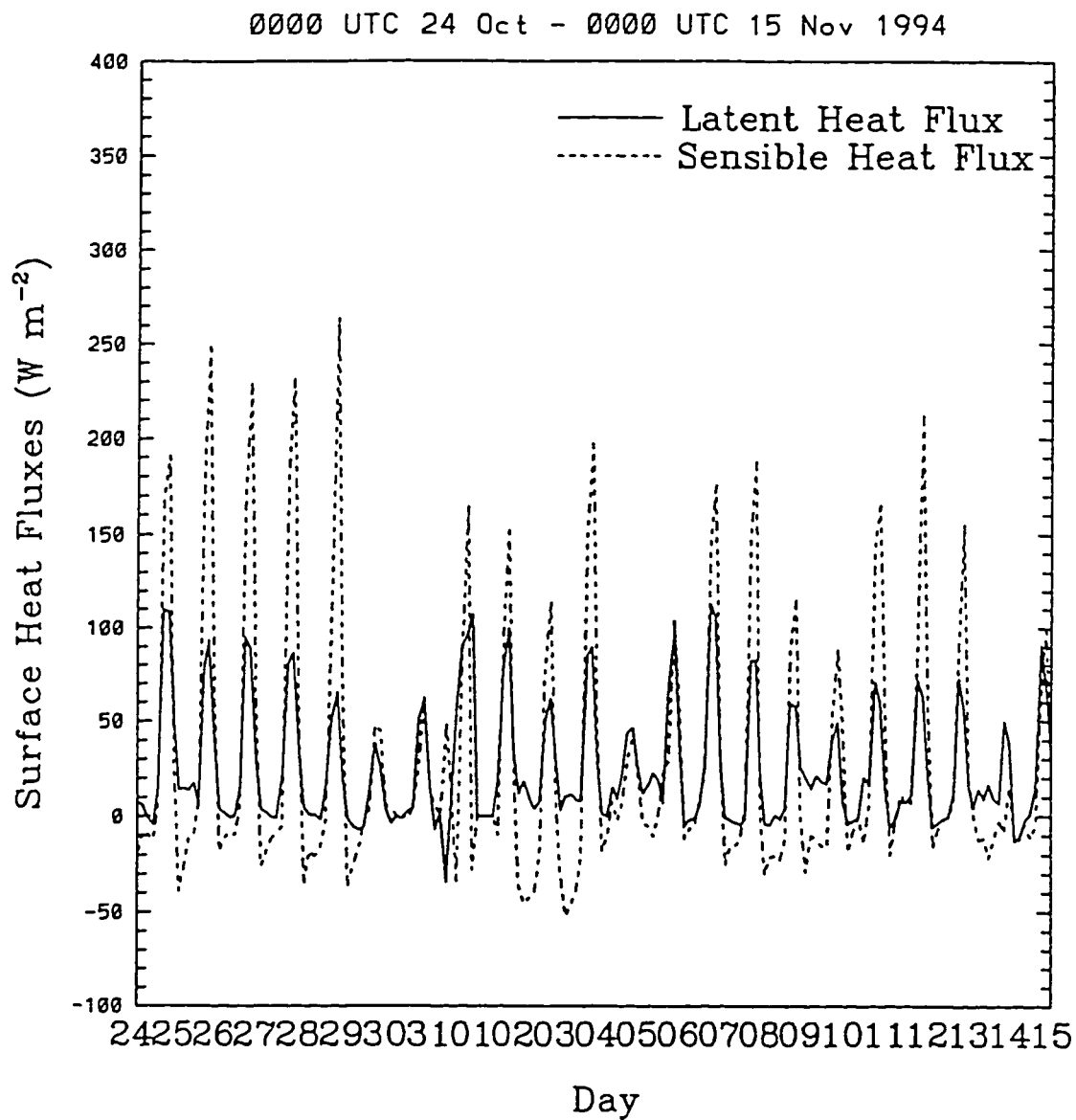
Figure 3.2 - Time series of latent and sensible heat fluxes for the fall 1994 IOP
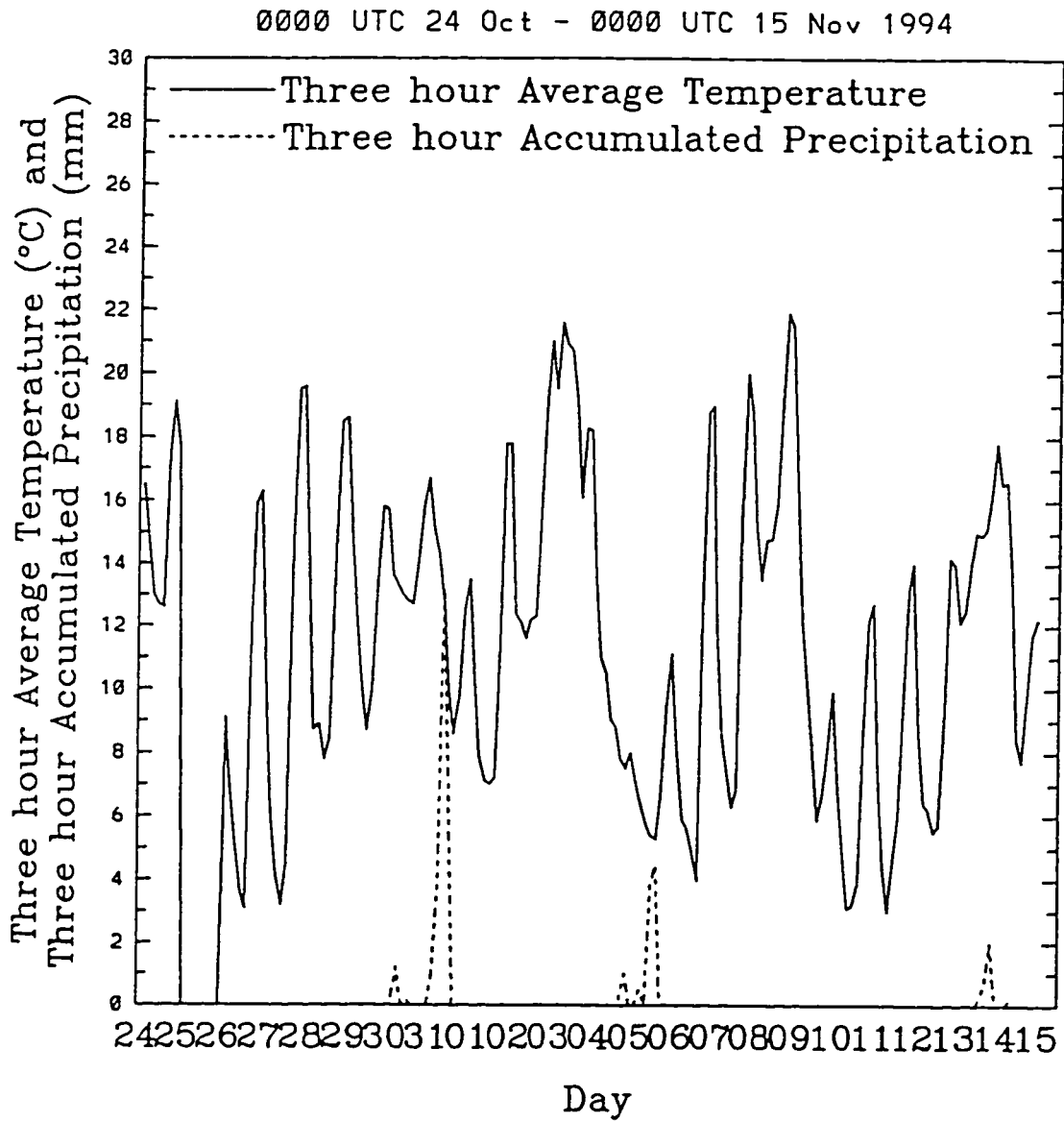
Figure 3.3 - Time series of three hour average temperature and three hour accumulated precipitation for the fall 1994 IOP

0300 UTC 31 Oct 1994
INPUT = 500 W m^{-2}
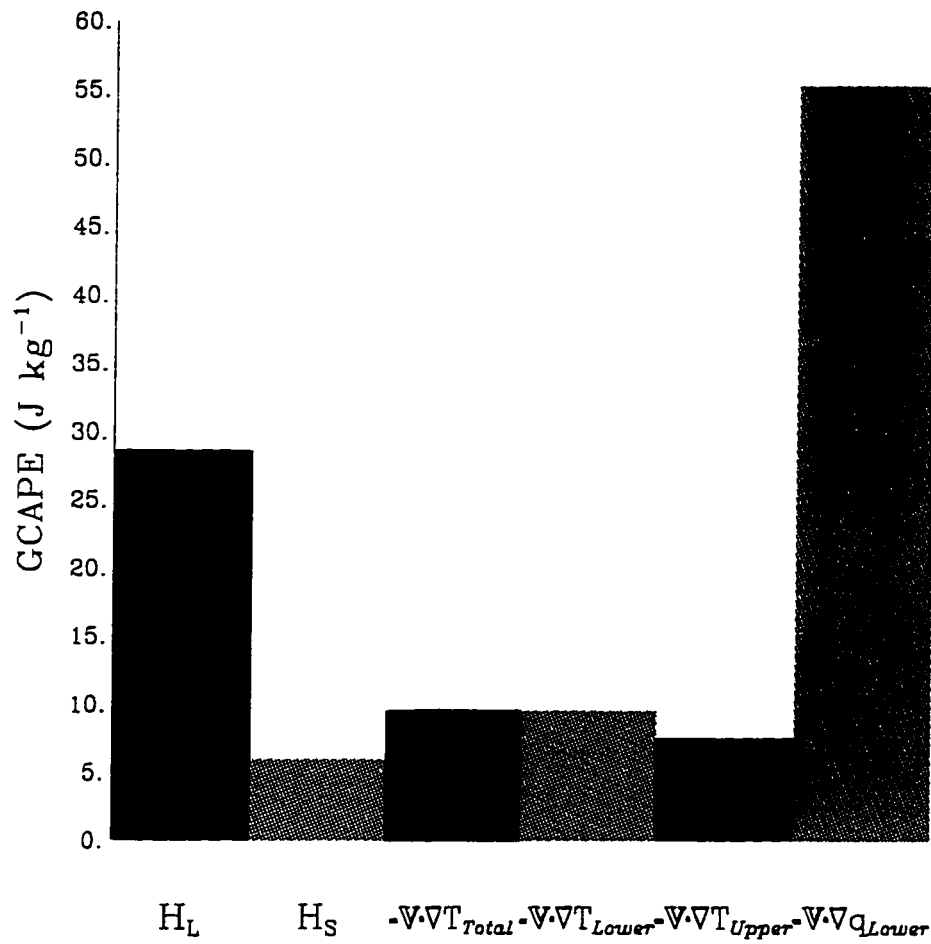
Figure 3.4 - Hypothetical GCAPE production for 0300 UTC 31 October 1994
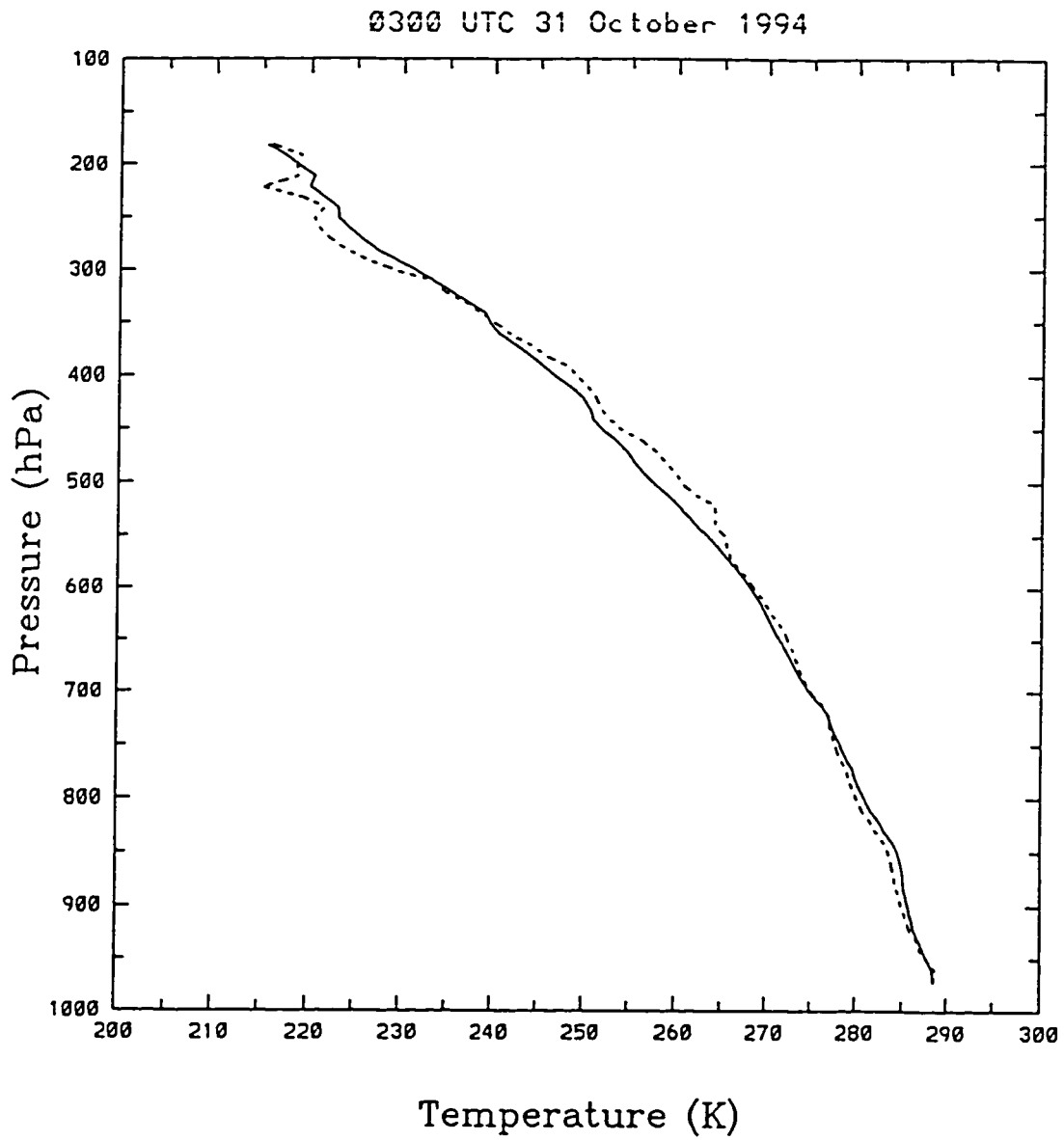
Figure 3.5 - Temperature advection for 0300 UTC 31 October 1994
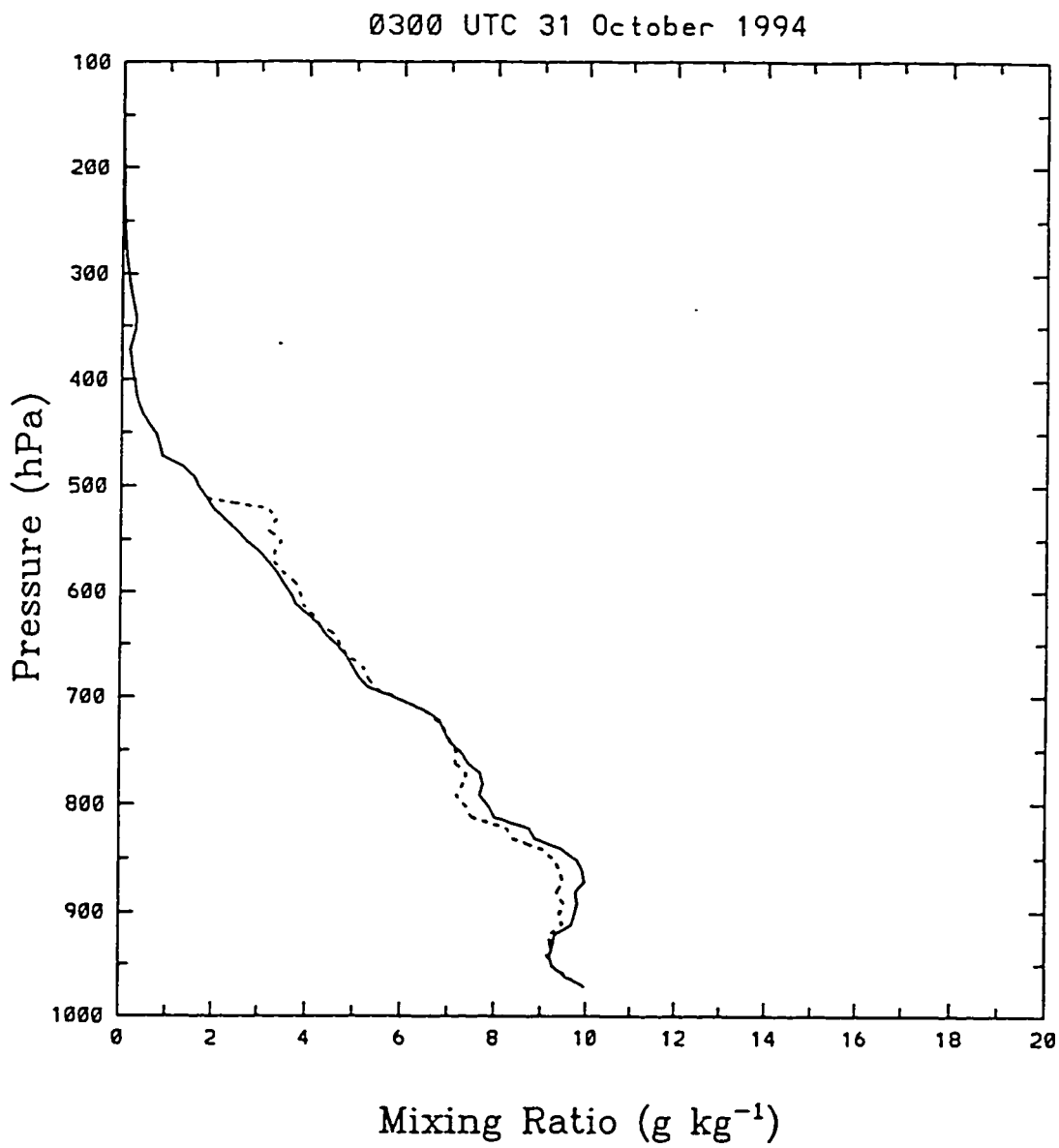
Figure 3.6 - Moisture advection for 0300 UTC 31 October 1994

0000 UTC 4 Nov 1994
INPUT = 500 W m^{-2}

GCAPE (J kg^{-1})

H_L H_S $-\mathbb{V}{\cdot}\nabla T_{Total}$ $-\mathbb{V}{\cdot}\nabla T_{Lower}$ $-\mathbb{V}{\cdot}\nabla T_{Upper}$ $-\mathbb{V}{\cdot}\nabla q_{Lower}$
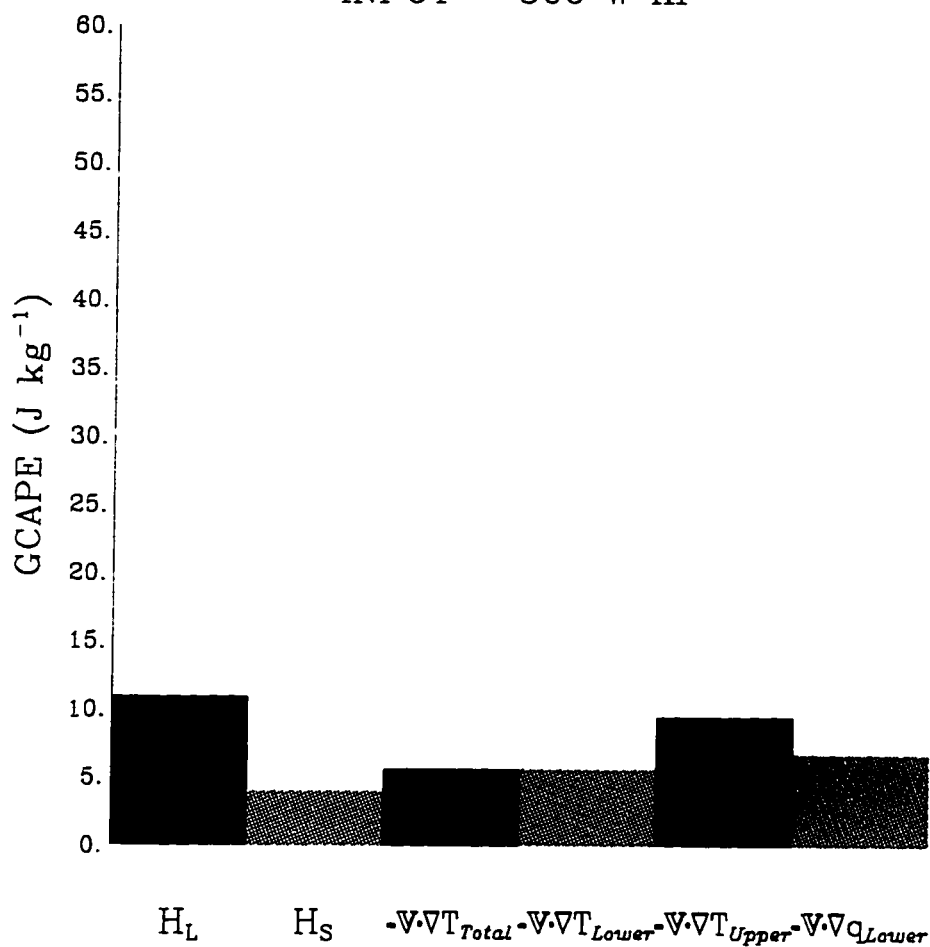
Figure 3.7 - Hypothetical GCAPE production for 0000 UTC 4 November 1994

0000 UTC 4 November 1994
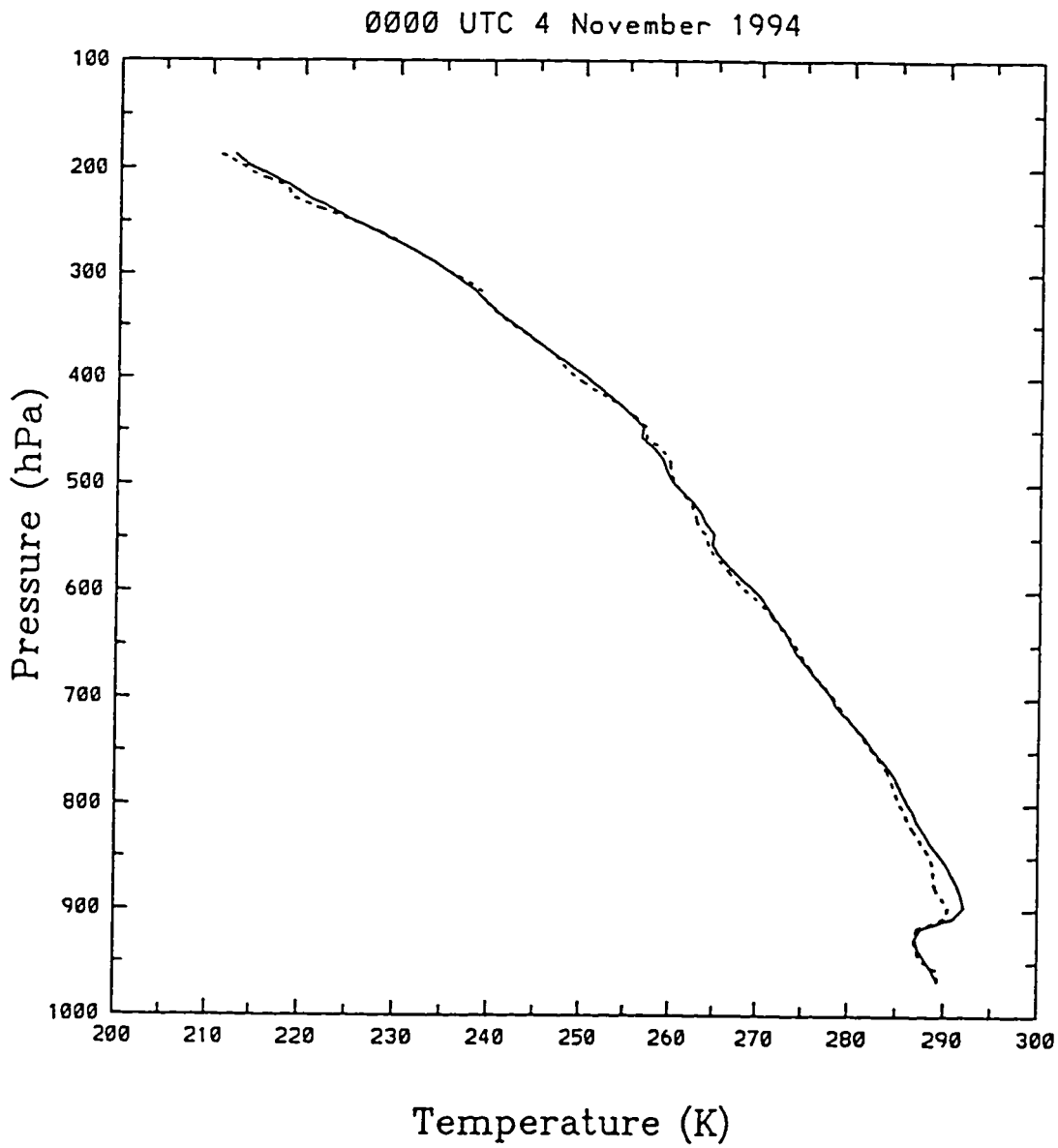
Figure 3.8 - Temperature advection for 0000 UTC 4 November 1994

44
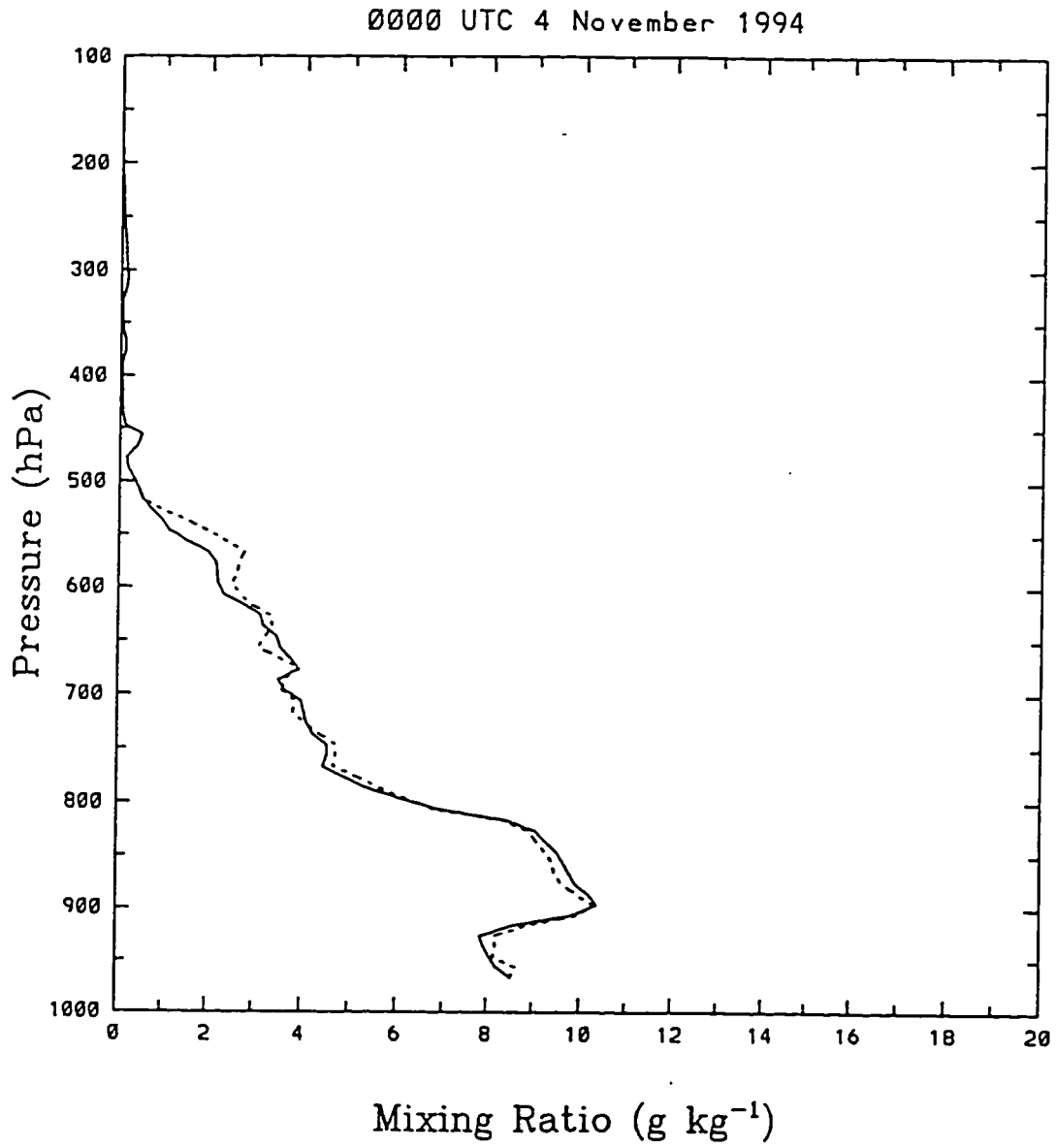
Figure 3.9 - Moisture advection for 0000 UTC 4 November 1994

45

Figure 3.10 - Hypothetical GCAPE production for 0300 UTC 4 November 1994

0300 UTC 4 November 1994
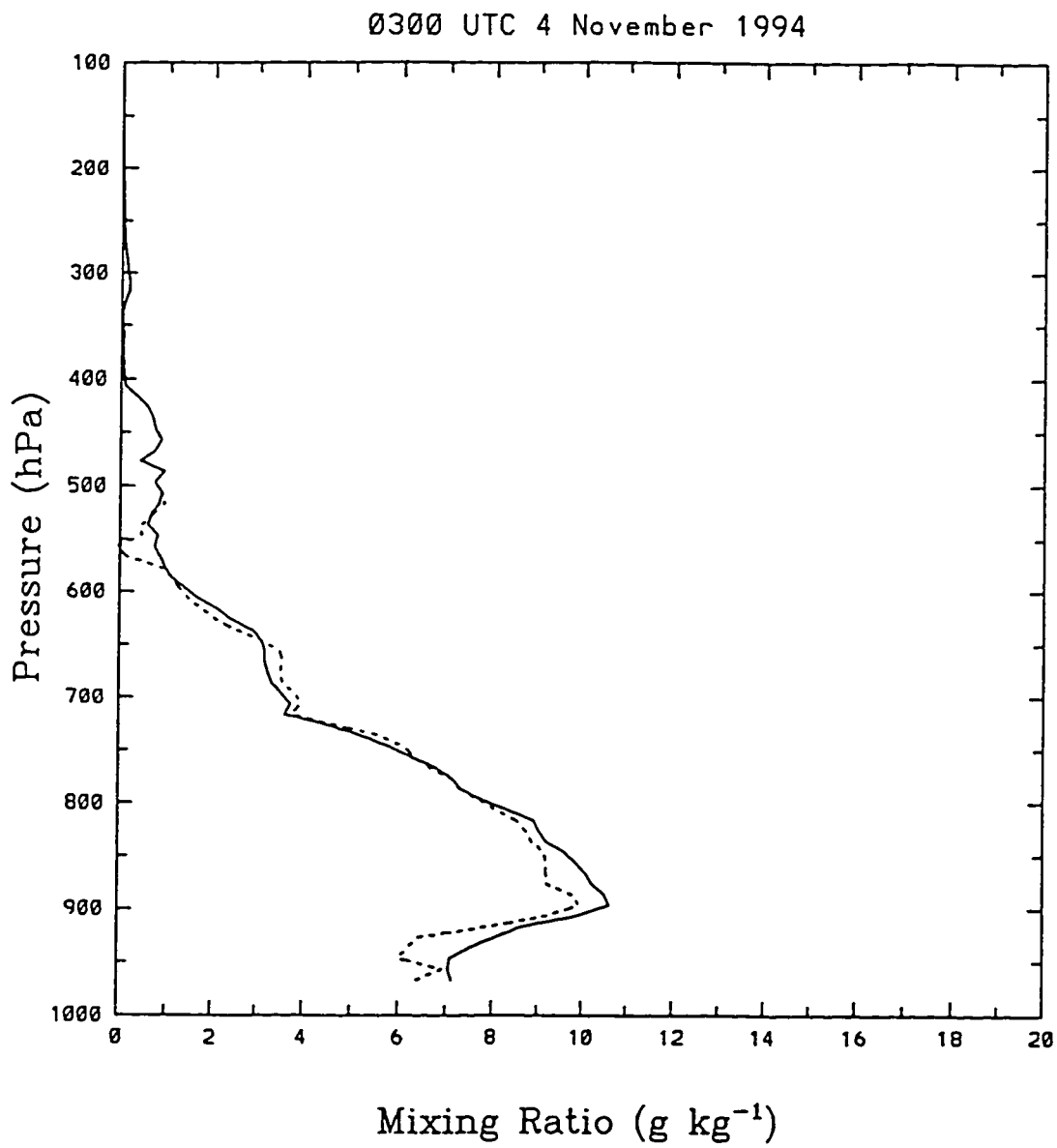
Figure 3.11 - Moisture advection for 0300 UTC 4 November 1994

47

0300 UTC 4 November 1994
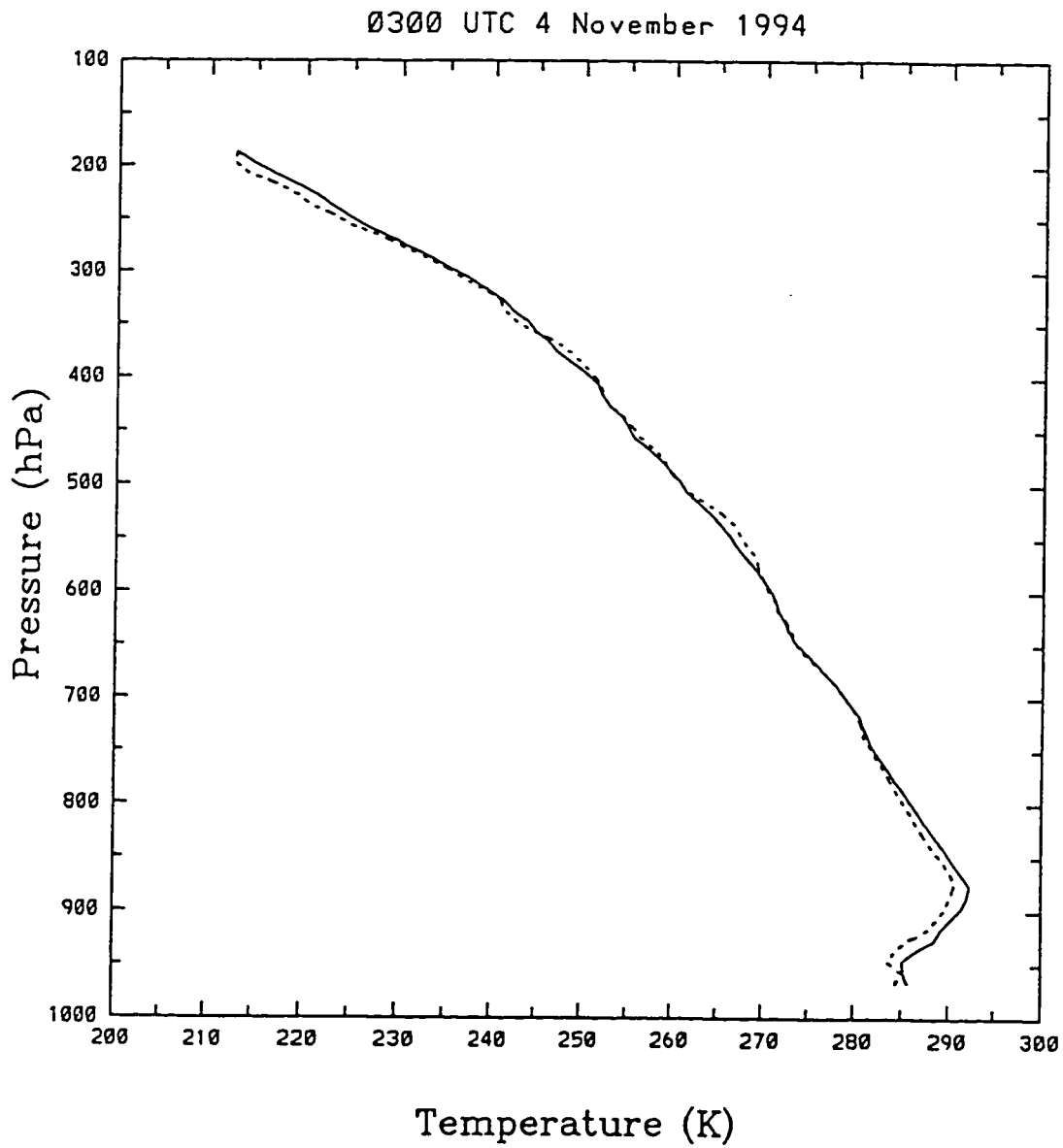
Figure 3.12 - Temperature advection for 0300 UTC 4 November 1994

48

0600 UTC 4 Nov 1994

INPUT = 500 W m^{-2}

GCAPE (J kg^{-1})

H_L H_S $-V \cdot \nabla T_{Total}$ $-V \cdot \nabla T_{Lower}$ $-V \cdot \nabla T_{Upper}$ $-V \cdot \nabla q_{Lower}$
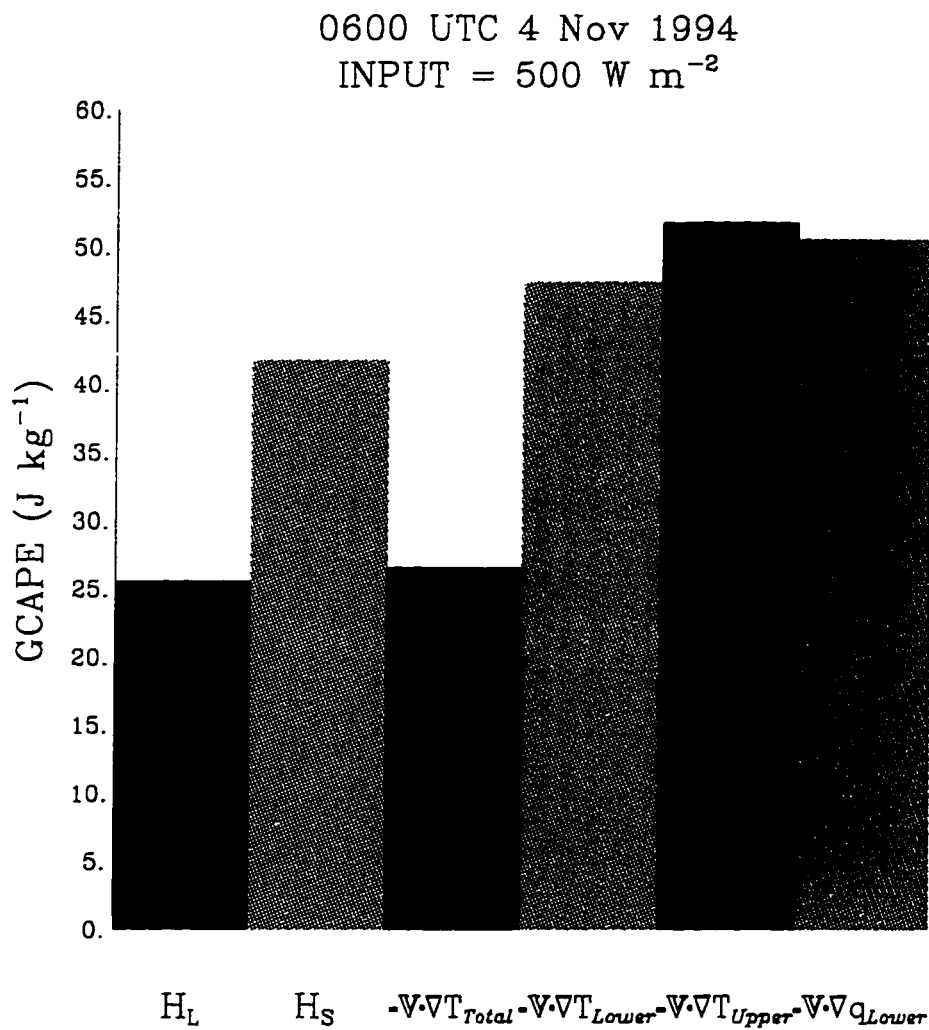
Figure 3.13 - Hypothetical GCAPE production for 0600 UTC 4 November 1994

49

0600 UTC 4 November 1994

Pressure (hPa)
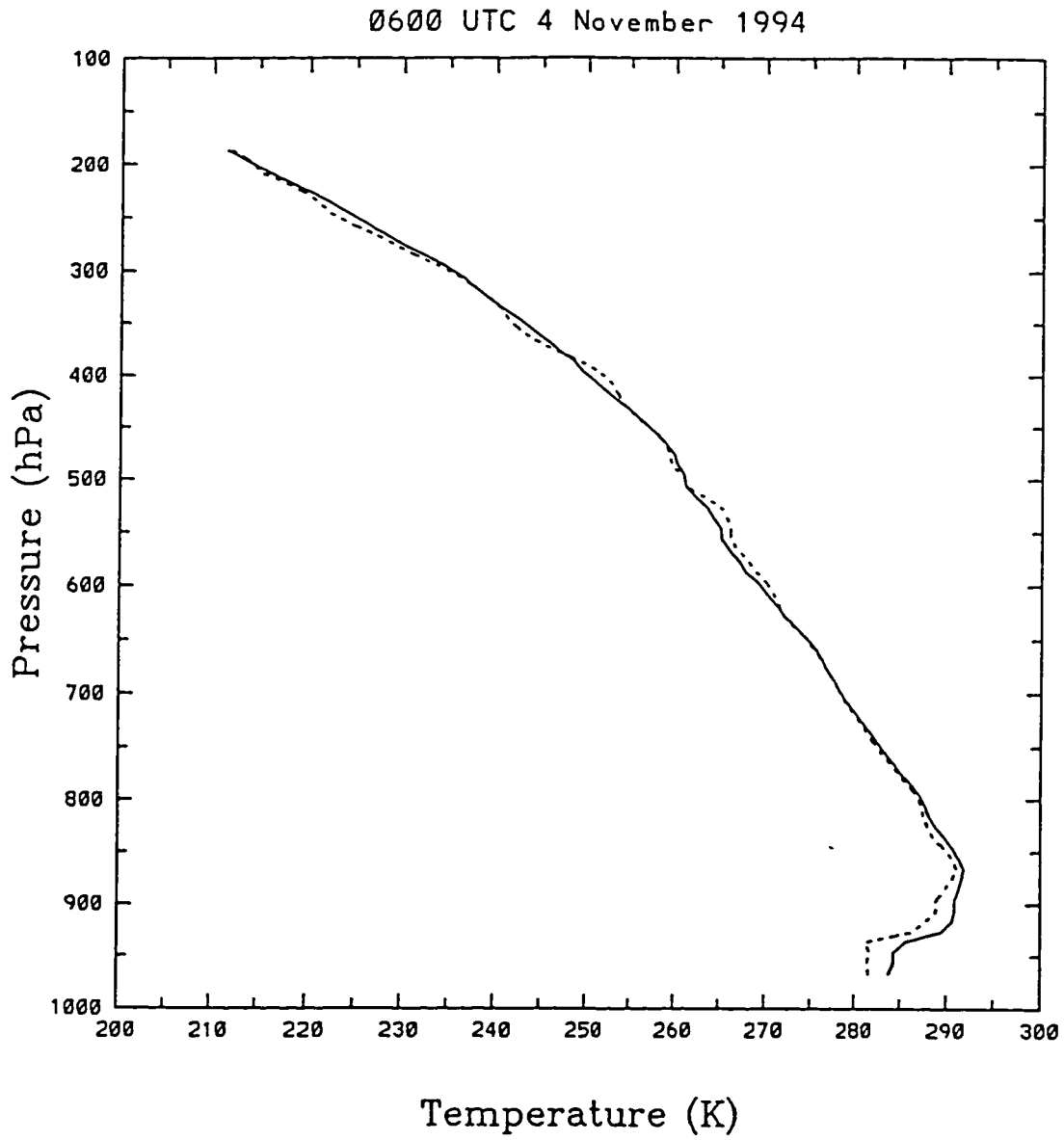
Temperature (K)

Figure 3.14 - Temperature advection for 0600 UTC 4 November 1994

50

0600 UTC 4 November 1994
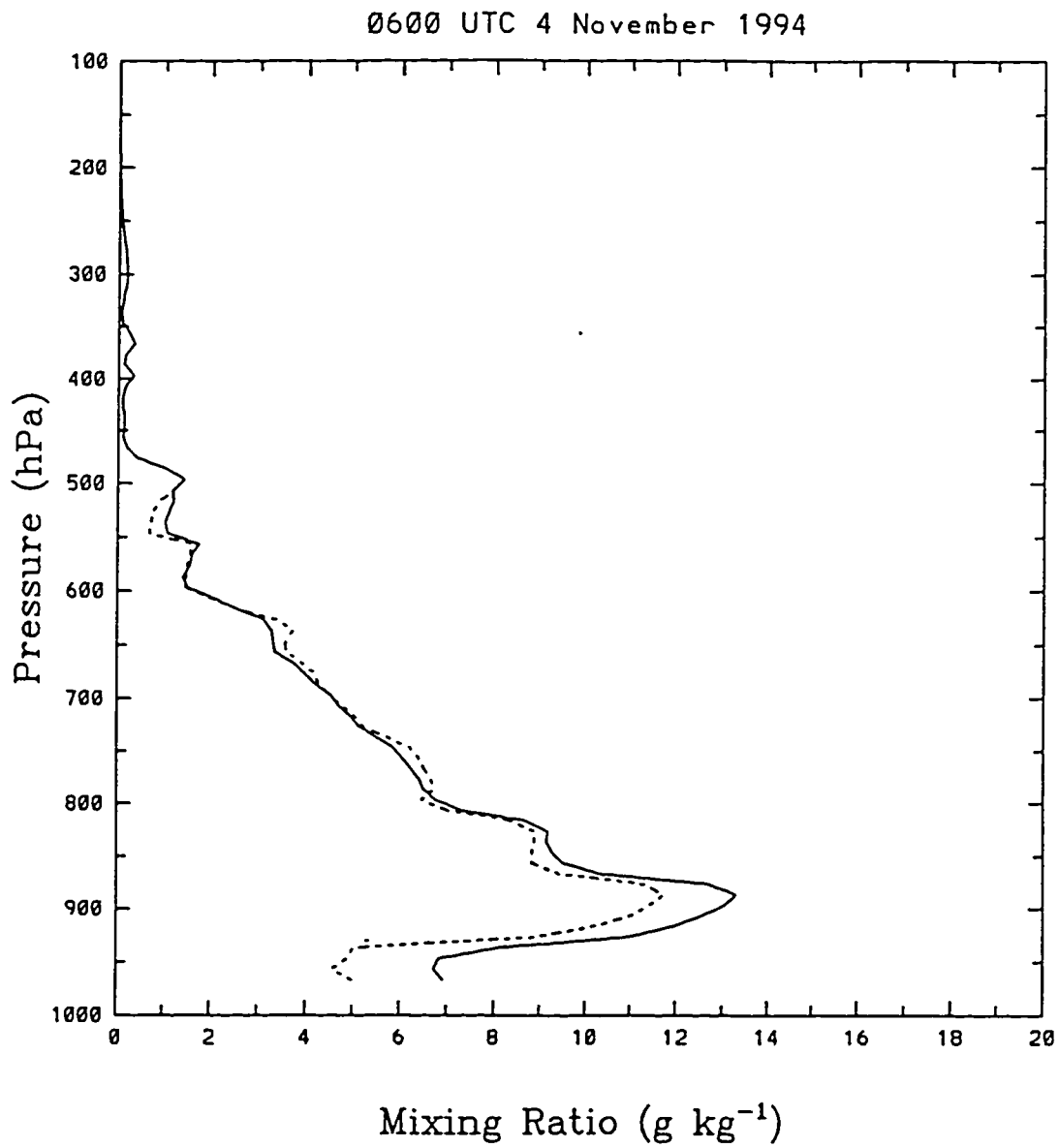
Figure 3.15 - Moisture advection for 0600 UTC 4 November 1994

51

CHAPTER 4 - SPRING 1995 IOP

The spring 1995 IOP was conducted from 0000 UTC 17 April to 0000 UTC 8 May 1995. Time series of GCAPE and surface meteorological observations are presented in section 4.1. The effects of surface heat and moisture fluxes and temperature and moisture advection on the production of GCAPE are shown and discussed in section 4.2. Observed surface heat and moisture fluxes, temperature and moisture advection, and the GCAPE produced by them are also shown and discussed in section 4.2. A summary follows in section 4.3. The daily meteorological conditions are described in Appendix B.

4.1 Observations

The time series of GCAPE for the spring 1995 IOP (Fig. 4.1) shows the significant GCAPE events. A summary of significant GCAPE events is shown in Table 4.1.

Table 4.1. Significant GCAPE events during the spring 1995 IOP.

Time and Date	GCAPE (J kg^{-1})	Meteorology
2100 UTC 24 April	35.5	Cold Front
2100 UTC 28 April - 1200 UTC 29 April	9.6, 20.8, 44.4, 12.3, and 10.6	Warm Front
2100 UTC 30 April - 0000 UTC 1 May	28.8 and 44.4	Frontal Boundary
1200 UTC 6 May	79.8	Frontal Boundary
2100 UTC 6 May - 1500 UTC 7 May	33.7, 40.9, 56.7, 64.2, 238.2, 31.3, and 29.5	Upward vertical motion & Warm Front

Three hour average surface latent and sensible heat fluxes are plotted in Fig. 4.2 which shows surface latent heat flux was greater than surface sensible heat flux during the spring 1995 IOP. This is in contrast to what was observed during the fall 1994 IOP and is one reason why more GCAPE was produced during the spring 1995 IOP than during the fall 1994 IOP. (It was shown in Chapter 2 that surface latent heat flux can produce more GCAPE than surface sensible heat flux). In several cases, large surface latent heat fluxes followed periods of precipitation. Three hour average temperature and three hour accumulated precipitation are shown in Fig. 4.3.

The first significant GCAPE event occurred late on 24 April and was associated with a cold front. The front produced precipitation at the Central Facility (Fig. 4.3) that resulted in a large surface latent heat flux value of approximately 225 W m^{-2} (Fig. 4.2).

The second GCAPE event occurred during 28-29 April and was associated with a warm front. The warm front produced precipitation at the Central Facility late on the 29th and also resulted in warmer temperatures (Fig. 4.3) as warmer air replaced cooler air over the Central Facility. The surface fluxes on the 28th were small due to clouds but the maximum surface latent heat flux on the 29th was approximately 230 W m^{-2} (Fig. 4.2).

The third significant GCAPE event occurred during 30 April-1 May in which a frontal boundary affected the Central Facility. More precipitation fell at the Central Facility (Fig. 4.3) and the surface fluxes were small due to clouds (Fig. 4.2).

The fourth GCAPE event occurred on 6 May and was associated with another frontal boundary which produced additional precipitation at the Central Facility (Fig. 4.3). The maximum surface latent heat flux was approximately 200 W m^{-2} (Fig. 4.2). The 850 hPa analysis showed a southerly 22.5 m s^{-1} LLJ had formed to the south at Dallas and was advecting moisture into Oklahoma from the Gulf Mexico. This influx of moisture along with the relatively large surface latent heat flux served to lower the height of the LCL, increase parcel buoyancy, and de-stabilize the atmosphere.

The fifth and most significant GCAPE event occurred during 7 May due to a warm front which produced more precipitation at the Central Facility (Fig. 4.3). The largest GCAPE value occurred during this time and was six times greater than the largest GCAPE value observed during the fall 1994 IOP. The 1200 UTC 850 hPa analysis showed a strong (25 m s^{-1}) southerly LLJ at Oklahoma City. In addition, temperature over the Central Facility increased as warmer air replaced cooler air (Fig. 4.3) but the surface fluxes were small due to clouds (Fig. 4.2). Therefore, it appears that increased low-level moisture due to the strong LLJ was the primary cause of instability during this period. An intense squall line developed in response to deep convection initiated by these unstable conditions (Fig. 4.4).

Small amounts of GCAPE were produced more frequently during the spring IOP than during the fall IOP. For the spring IOP there were 24 times when the GCAPE ranged from 1-10 J kg^{-1}, five times when it ranged from 10 - 20 J kg^{-1}, three times when it ranged from 20 -30 J kg^{-1}, and three more times when

it ranged from 30–40 J kg^{-1} (Fig. 4.5). In contrast, there were just four instances during the fall IOP when the GCAPE was greater than 10 J kg^{-1} but less than 40 J kg^{-1} (Fig. 4.6). It has been shown that increased low-level produces GCAPE most efficiently. More GCAPE was produced during the spring IOP than during the fall IOP because of the presence of more low-level moisture during the spring IOP.

4.2 GCAPE Sensitivity Experiments

For 0000 UTC 29 April, experimental surface latent heat flux produced the most GCAPE followed by low-level moisture advection (Fig. 4.7). Total temperature advection constituted most of the observed energy flux followed by low-level temperature advection (Table 4.2).

Table 4.2. GCAPE and observed energy fluxes for 0000 UTC 29 April.

Process	Observed Energy Flux (W m^{-2})	GCAPE$_{before}$ (J kg^{-1})	GCAPE$_{after}$ (J kg^{-1})	ΔGCAPE (J kg^{-1})
H_l	9.5	9.6	9.6	0
H_s	9.1	9.6	9.6	0
$-V \cdot \nabla T_{total}$	575.4	9.6	9.5	-0.1
$-V \cdot \nabla T_{lower}$	337.3	9.6	9.5	-0.1
$-V \cdot \nabla T_{upper}$	238.1	9.6	9.5	-0.1
$-V \cdot \nabla q_{lower}$	0	9.6	9.6	0

55

Temperature decreased throughout most of the troposphere due to cold advection except for the layer from 450-360 hPa where temperature increased due to warm advection (Fig. 4.8). Low-level moisture advection was not calculated due to missing moisture data. A summary of the GCAPE produced by the observed energy fluxes is shown in Table 4.2. The GCAPE due to surface latent and sensible heat fluxes remained constant because they were small. The GCAPE was reduced by the temperature advection processes because they cooled the troposphere and reduced parcel buoyancy. The GCAPE calculated three hours later for 0300 UTC 29 April was 20.8 J kg^{-1}.

One reason for the difference that exists between the GCAPE calculated when the observed energy fluxes are added to the sounding and the GCAPE that is calculated at the next observation time is the continuous process of GCAPE production is being approximated with discrete observations. The spatial and temporal resolution of the radiosonde and wind profiler data may be too coarse to resolve the advective quantities in the objective analysis scheme accurately. Another reason is the depth through which the surface fluxes are added may be such that GCAPE production due to surface fluxes is greatly reduced. RW92 assumed surface fluxes acted uniformly on the air between the surface and 950 hPa, i. e., approximately the lowest 60-70 hPa. In this study surface flux effects have been confined to the lowest 100-140 hPa in most cases. GCAPE production is very sensitive and inversely proportional to the depth through which surface fluxes are added (Fig. 4.9). For example, the GCAPE produced when a latent heat flux of 500 W m^{-2} is added to the lowest 85 hPa is 225 J kg^{-1} whereas only 80

J kg^{-1} is produced when the latent heat flux is added through the lowest 115 hPa. The GCAPE is reduced 145 J kg^{-1} for an increase of just 20 hPa in input depth. Thus, the GCAPE produced when the observed surface fluxes were added was less than what would have been produced if the depth through which the surface fluxes were added was reduced.

For 1800 UTC 30 April experimental low-level moisture advection produced the most GCAPE followed by total temperature advection (Fig. 4.10). Most of the observed energy flux consisted of total temperature advection followed by low-level temperature advection (Table 4.3).

Table 4.3. GCAPE and observed energy fluxes for 1800 UTC 30 April.

Process	Observed Energy Flux (W m^{-2})	GCAPE$_{before}$ (J kg^{-1})	GCAPE$_{after}$ (J kg^{-1})	ΔGCAPE (J kg^{-1})
H$_l$	88.4	3.1	29.1	26
H$_s$	42.6	3.1	3.1	0
$-V \bullet \nabla T_{total}$	1528.6	3.1	3.1	0
$-V \bullet \nabla T_{lower}$	376.0	3.1	3.1	0
$-V \bullet \nabla T_{upper}$	1153.0	3.1	3.1	0
$-V \bullet \nabla q_{lower}$	0	3.1	3.1	0

Temperature cooled in portions of the lower, middle, and upper troposphere due to cold advection (Fig. 4.11). Surface latent heat flux generated the most GCAPE

57

whereas the other processes did not generate any GCAPE (Table 4.3). This is the best example of when the observed surface latent heat flux produced an amount of GCAPE (29.1 J kg^{-1}) that was essentially equal to the GCAPE calculated at the next observation time (28.8 J kg^{-1}).

For 2100 UTC 30 April experimental low-level moisture advection produced the most GCAPE (Fig. 4.12). Total temperature advection produced the second largest GCAPE amount. Most of the observed energy flux was comprised of total temperature advection followed by low-level temperature advection (Table 4.4).

Table 4.4. GCAPE and observed energy fluxes for 2100 UTC 30 April.

Process	Observed Energy Flux (W m^{-2})	GCAPE$_{before}$ (J kg^{-1})	GCAPE$_{after}$ (J kg^{-1})	ΔGCAPE (J kg^{-1})
H$_l$	53.5	28.8	28.8	0
H$_s$	25.8	28.8	28.8	0
$-V \bullet \nabla T_{total}$	931.2	28.8	28.1	-0.7
$-V \bullet \nabla T_{lower}$	578.8	28.8	28.1	-0.7
$-V \bullet \nabla T_{upper}$	352.4	28.8	28.1	-0.7
$-V \bullet \nabla q_{lower}$	0	28.8	28.8	0

Temperature advection cooled portions of the lower, middle, and upper troposphere (Fig. 4.13). Therefore, it could be expected that the temperature

58

advection processes would reduce the GCAPE. A summary of GCAPE produced by the observed energy fluxes is shown in Table 4.4. The temperature advection processes reduced the GCAPE by cooling the troposphere, thereby reducing parcel buoyancy. The GCAPE due to the observed surface fluxes remained unchanged because the surface fluxes were small. The GCAPE increased 15.6 J kg^{-1} to 44.4 J kg^{-1} by the next observation time. This increase in GCAPE could have been the result of increased low-level moisture due to low-level moisture advection but because of missing moisture data it is impossible to determine if this was the case.

The most convincing example of when increased low-level moisture generated the most GCAPE is for 2100 UTC 6 May. Experimental surface latent heat flux produced the most GCAPE followed closely by low-level moisture advection (Fig. 4.14). The temperature advection processes were among the least efficient at generating GCAPE. However, total temperature advection contributed most of the forcing and was slightly greater than the observed surface latent heat flux (Table 4.5).

Table 4.5. GCAPE and observed energy fluxes for 2100 UTC 6 May.

Process	Observed Energy Flux (W m^{-2})	GCAPE$_{before}$ (J kg^{-1})	GCAPE$_{after}$ (J kg^{-1})	ΔGCAPE (J kg^{-1})
H$_l$	152.2	33.7	133.8	100.1
H$_s$	67.1	33.7	33.7	0
$-V \bullet \nabla T_{total}$	156.8	33.7	32.8	-0.9
$-V \bullet \nabla T_{lower}$	99.6	33.7	32.8	-0.9
$-V \bullet \nabla T_{upper}$	57.3	33.7	32.8	-0.9
$-V \bullet \nabla q_{lower}$	0	33.7	33.7	0

The GCAPE generated by the observed surface latent heat flux was four times greater than the GCAPE generated by any other process (Table 4.5). This also represents the largest amount of GCAPE produced by an observed process during both the fall and spring IOPs. Surface latent heat flux produced the most GCAPE by increasing low-level moisture, thus increasing parcel buoyancy. Temperature advection cooled the lower and middle troposphere but warmed the upper troposphere (Fig. 4.16). This resulted a more stable vertical temperature structure in which the GCAPE was reduced by reducing parcel buoyancy. Surface sensible heat flux did not generate any additional GCAPE because it was relatively small. This example clearly shows the strong positive correlation between the efficiency in which GCAPE is produced by surface latent

heat flux and the GCAPE produced by the observed surface latent heat flux. It is also another example in which the hypothesis regarding increased low-level moisture was validated. The GCAPE increased 7.2 J kg^{-1} to 40.9 J kg^{-1} three hours later, primarily due to latent heat flux.

For 0000 UTC 7 May experimental surface latent heat flux produced the most GCAPE followed by low-level moisture advection (Fig. 4.16). The temperature advection processes produced the least amount of GCAPE. The observed energy fluxes were small (Table 4.6).

Table 4.6. GCAPE and observed energy fluxes for 0000 UTC 7 May.

Process	Observed Energy Flux (W m^{-2})	GCAPE$_{before}$ (J kg^{-1})	GCAPE$_{after}$ (J kg^{-1})	ΔGCAPE (J kg^{-1})
H_l	14.1	40.9	40.9	0
H_s	16.0	40.9	40.9	0
$-V \cdot \nabla T_{total}$	145.4	40.9	39.9	-1
$-V \cdot \nabla T_{lower}$	27.3	40.9	39.9	-1
$-V \cdot \nabla T_{upper}$	118.0	40.9	39.9	-1
$-V \cdot \nabla q_{lower}$	0	40.9	39.9	0

Temperature advection cooled the lower levels and warmed the upper levels (Fig. 4.17). Thus, it could be expected that the temperature advection processes would reduce the GCAPE. The observed temperature advection processes

61

reduced the GCAPE whereas the GCAPE due to the observed surface fluxes remained unchanged because they were small (Table 4.6). Once again, the GCAPE was reduced by the temperature advection processes because they resulted in more stable vertical temperature profiles. The GCAPE increased 15.8 J kg^{-1} to 56.7 J kg^{-1} by the next observation time. This increase may have been due to low-level moisture advection.

The next case is for 0300 UTC 7 May. Experimental surface latent heat flux produced the most GCAPE (Fig. 4.18). Experimental surface sensible heat flux produced the second largest amount of GCAPE followed by low-level moisture advection. Observed energy fluxes continued to be small (Table 4.7).

Table 4.7. GCAPE and observed energy fluxes for 0300 UTC 7 May.

Process	Observed Energy Flux (W m^{-2})	GCAPE$_{before}$ (J kg^{-1})	GCAPE$_{after}$ (J kg^{-1})	ΔGCAPE (J kg^{-1})
H$_l$	41.3	56.7	56.7	0
H$_s$	14.7	56.7	56.7	0
$-V \cdot \nabla T_{total}$	140.4	56.7	56.0	-0.7
$-V \cdot \nabla T_{lower}$	118.3	56.7	56.0	-0.7
$-V \cdot \nabla T_{upper}$	22.1	56.7	56.0	-0.7
$-V \cdot \nabla q_{lower}$	0	56.7	56.7	0

The GCAPE remained unchanged by the surface fluxes because they were small,

however, the temperature advection processes reduced the GCAPE (Table 4.7). The resulting vertical temperature profile due to the observed temperature advection is shown in Fig. 4.19. Total temperature advection and low-level temperature advection reduced the GCAPE by resulting in more stable vertical temperature profiles. However, upper-level temperature advection resulted in a more unstable vertical temperature profile in the upper troposphere. Nevertheless, the cooling near 200 hPa was enough to offset the warming below and reduce the GCAPE by reducing parcel buoyancy. The GCAPE increased 7.5 J kg^{-1} to 64.2 J kg^{-1} three hours later.

Finally, the last case is for 0600 UTC 7 May. Experimental surface latent heat flux produced the most GCAPE (Fig. 4.20). As in the previous case, experimental surface sensible heat flux produced the second largest amount of GCAPE. Total temperature advection contributed the largest observed energy flux and upper-level temperature advection contributed the least (Table 4.8).

Table 4.8. GCAPE and observed energy fluxes for 0600 UTC 7 May.

Process	Observed Energy Flux (W m^{-2})	GCAPE$_{before}$ (J kg^{-1})	GCAPE$_{after}$ (J kg^{-1})	ΔGCAPE (J kg^{-1})
H_l	0.1	64.2	64.2	0
H_s	16.0	64.2	64.2	0
$-V \bullet \nabla T_{total}$	57.0	64.2	62.6	-1.6
$-V \bullet \nabla T_{lower}$	42.2	64.2	62.6	-1.6
$-V \bullet \nabla T_{upper}$	14.8	64.2	62.6	-1.6
$-V \bullet \nabla q_{lower}$	0	64.2	64.2	0

Temperature advection had very little effect on the tropospheric temperature profile (Fig. 4.21). The only effect it did have was to cool the layer adjacent to the surface and a layer in the upper troposphere. The temperature advection processes reduced the GCAPE whereas the observed surface fluxes had no effect (Table 4.8). Once again, the temperature advection processes reduced the GCAPE by reducing parcel buoyancy through cooling of the troposphere and the GCAPE due to the surface fluxes remained unchanged because they were small. The largest GCAPE amount was generated at the next observation time when it increased by 174.1 J kg^{-1} from 64.2 J kg^{-1} to 238.3 J kg^{-1}. Despite the absence of moisture data, it does appear that low-level moisture advection was largely responsible for this large GCAPE increase. This is based on the fact that a strong (25.7 m s^{-1}) LLJ developed over Oklahoma just six hours later which advected

moist air northward from the Gulf of Mexico over the Central Facility. Furthermore, surface winds at 0600 UTC 7 May were southeasterly over Oklahoma and Texas and dew point temperatures were in the 60s and low 70s, respectively. Thus, it appears low-level moisture advection was largely responsible for the large increase in GCAPE.

4.3 Summary

Theoretical surface latent heat flux would produce the most GCAPE in five of the seven cases and theoretical low-level moisture advection would produce the most GCAPE in the remaining two cases. These results confirm the hypothesis: *increased low-level moisture creates GCAPE.* The observed surface latent heat flux for 1800 UTC 30 April produced essentially the same GCAPE amount as the one calculated three hours later. This is one example where the method in which the effect of observed surface latent heat flux is accounted for closely simulated reality and suggests that this method was sound. It also represents one example in which the averaging of surface latent heat flux observations sufficiently accounted for what happened in reality. The observed surface latent heat flux for 2100 UTC 6 May produced more GCAPE than any other process at any other time and also validates the above hypothesis. Increased low-level moisture creates GCAPE by lowering the height of the LCL, thus increasing parcel buoyancy. In most cases the observed temperature advection processes resulted in a slight reduction in GCAPE because they

stabilized the atmosphere by cooling the troposphere and reducing parcel buoyancy. Furthermore, on just two occasions did the GCAPE generated by the observed energy fluxes equal or exceed the GCAPE calculated at the subsequent observation time. This was probably due to the rapidity with which GCAPE was consumed.
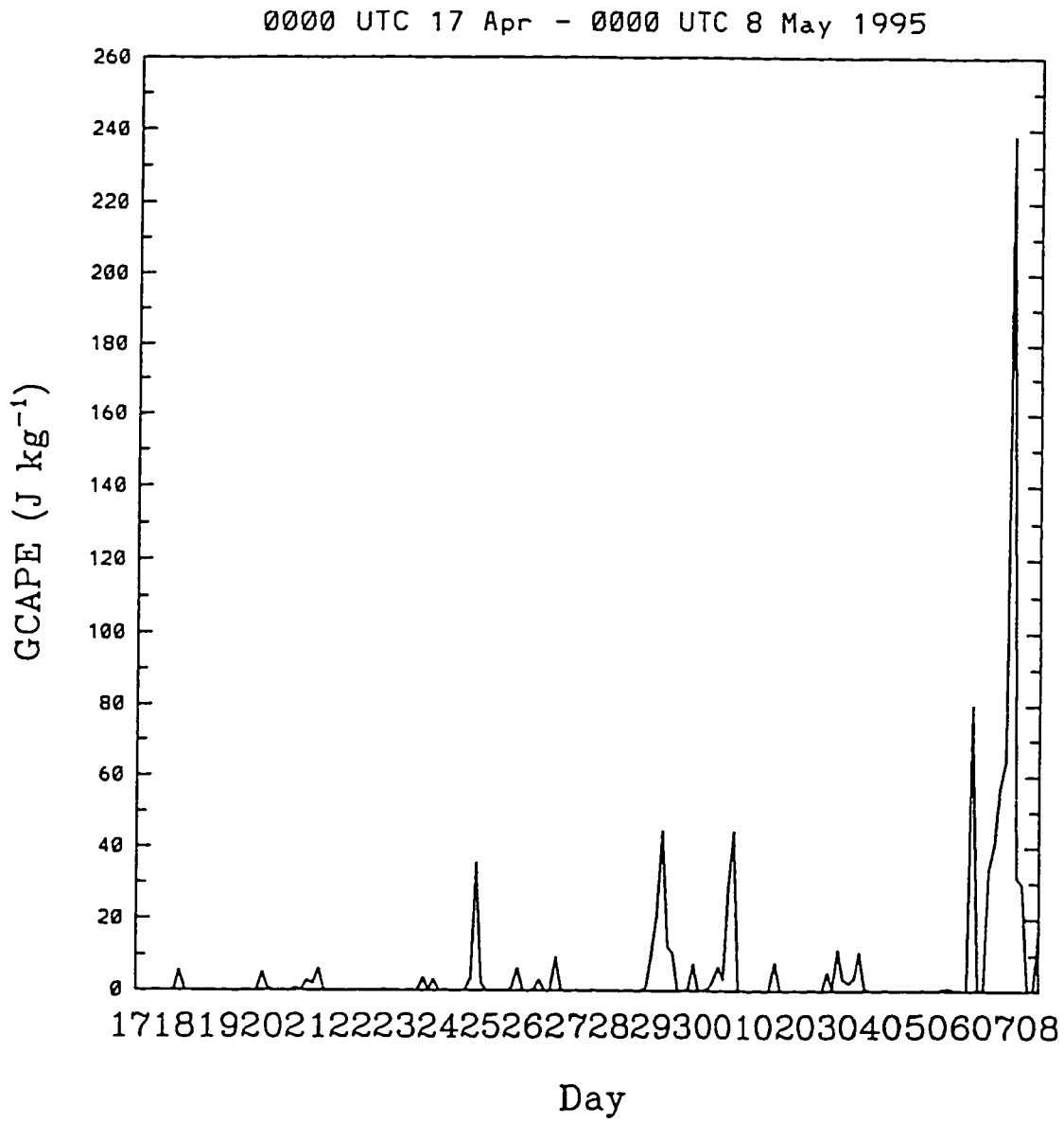
Figure 4.1 - GCAPE time series for the spring 1995 IOP
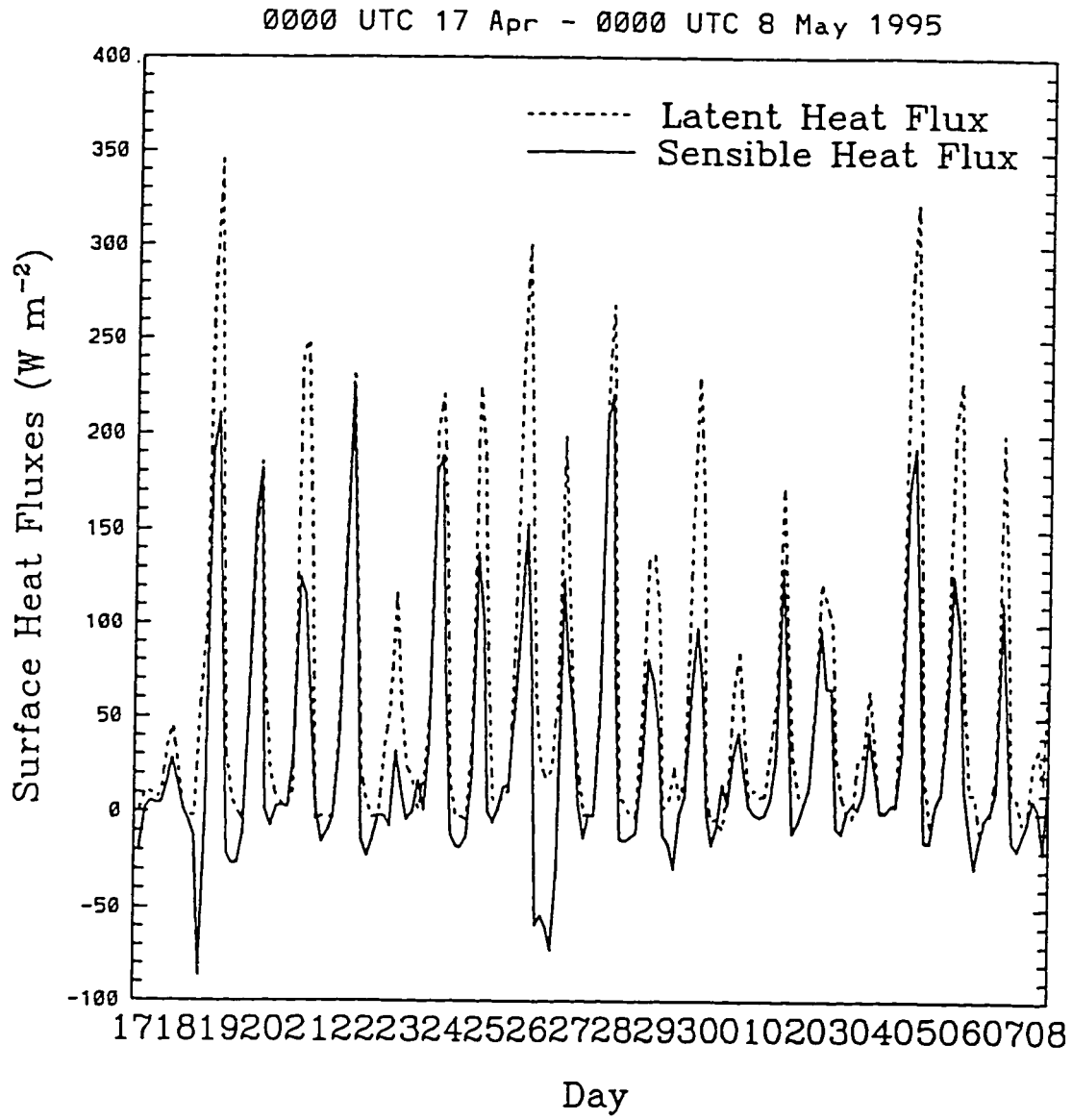
Figure 4.2 - Time series of latent and sensible heat fluxes for the spring 1995 IOP

0000 UTC 17 Apr - 0000 UTC 8 May 1995
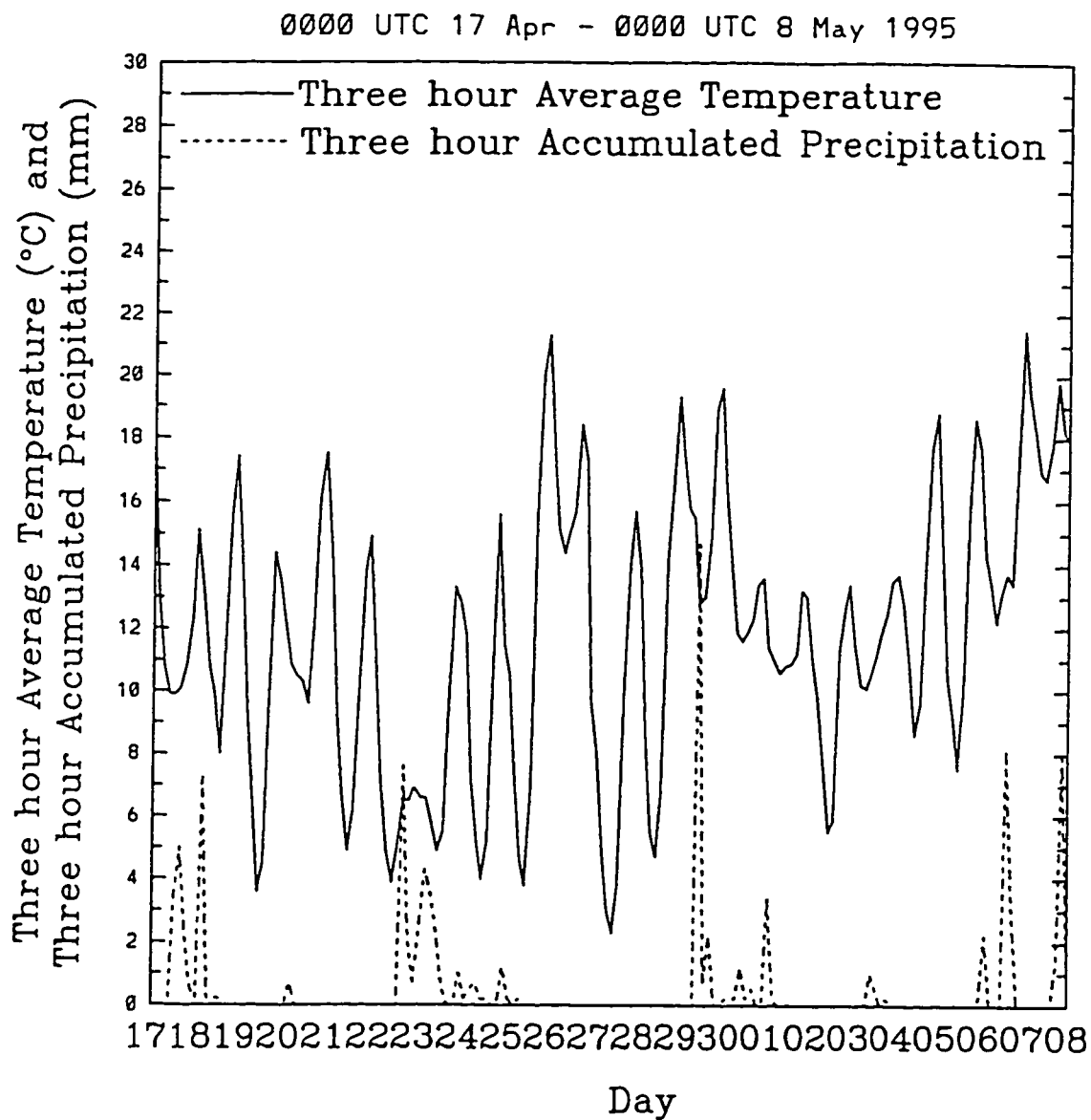
Figure 4.3 - Time series of three hour average temperature and three hour

accumulated precipitation for the spring 1995 IOP
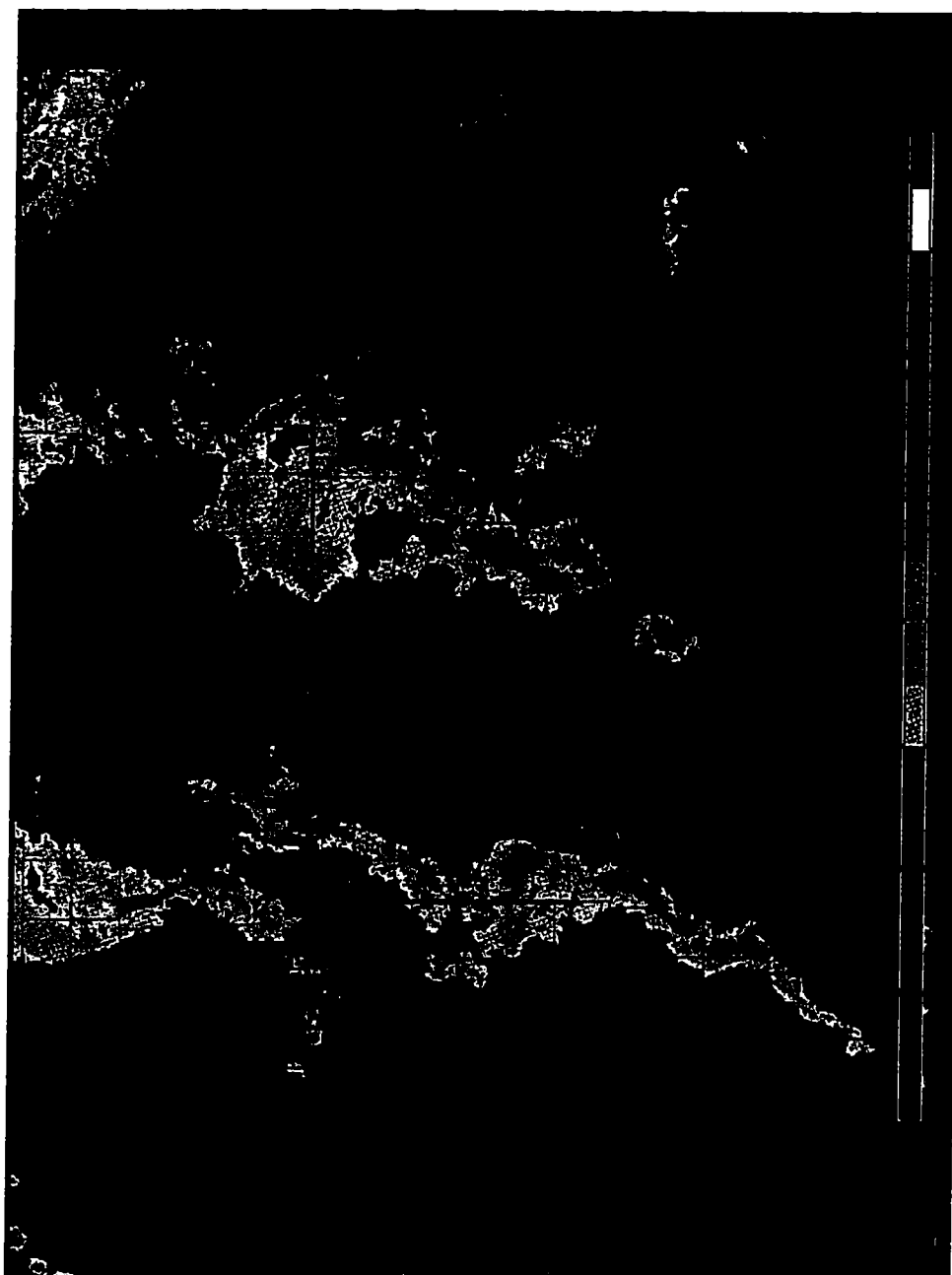
Figure 4.4 - Southern Great Plains radar plot for 2115 UTC 7 May 1995

0000 UTC 17 April — 0000 UTC 8 May 1995
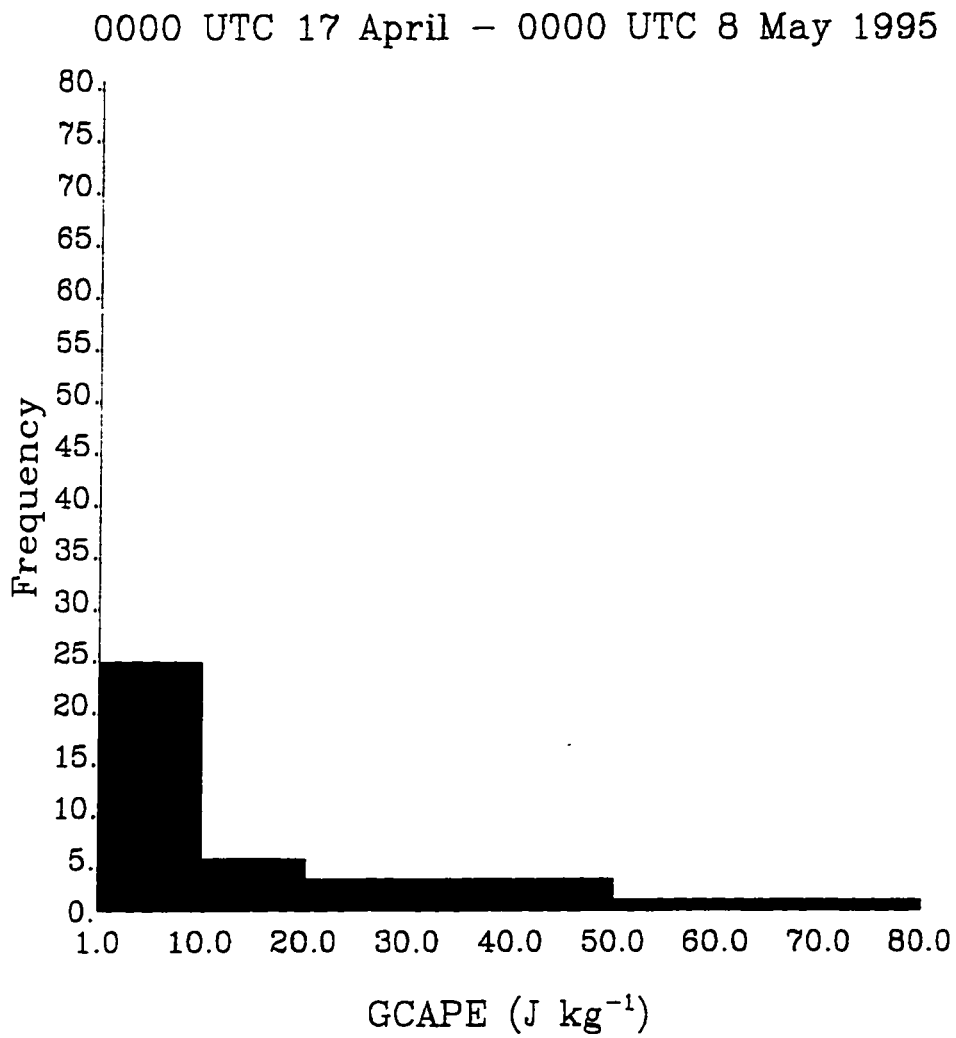
Figure 4.5 - GCAPE histogram for the spring 1995 IOP

71

0000 UTC 24 Oct — 0000 UTC 15 Nov 1994

GCAPE (J kg^{-1})
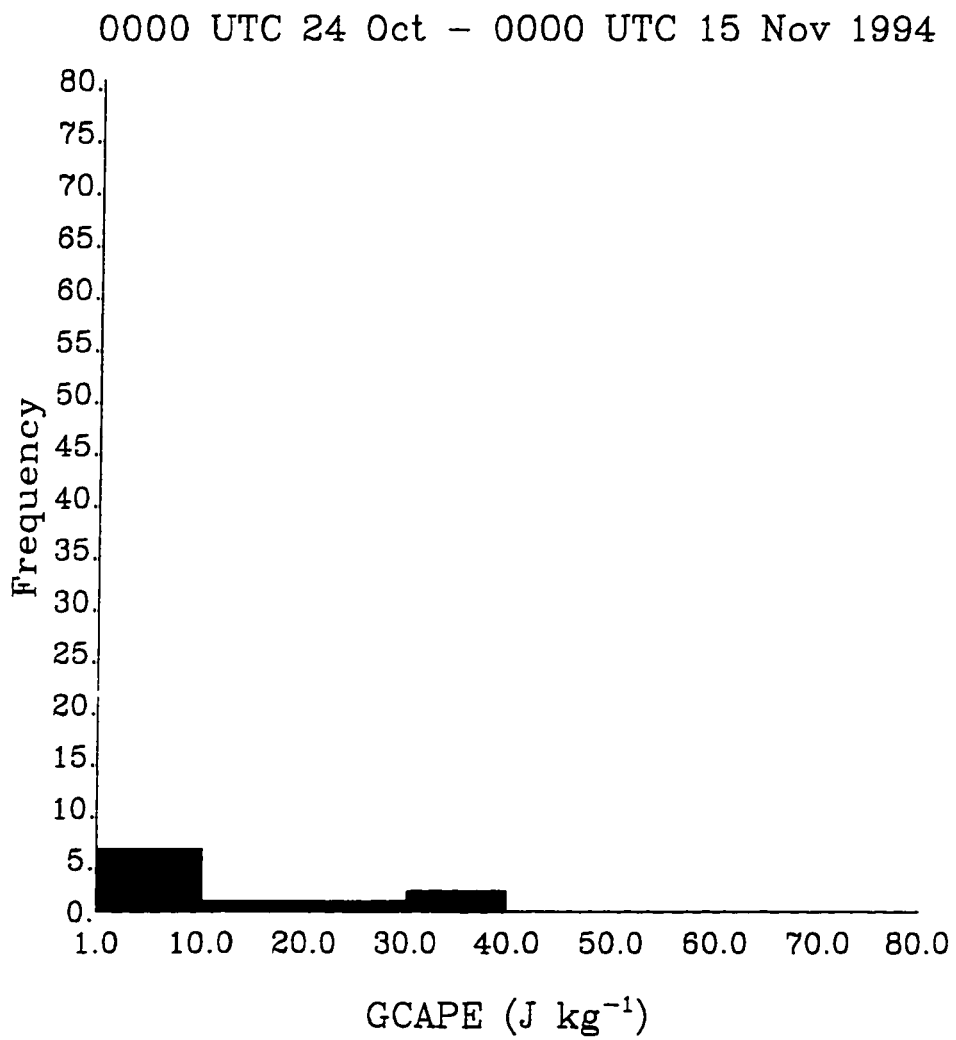
Figure 4.6 - GCAPE histogram for the fall 1994 IOP

0000 UTC 29 April 1995
INPUT = 500 W m^{-2}
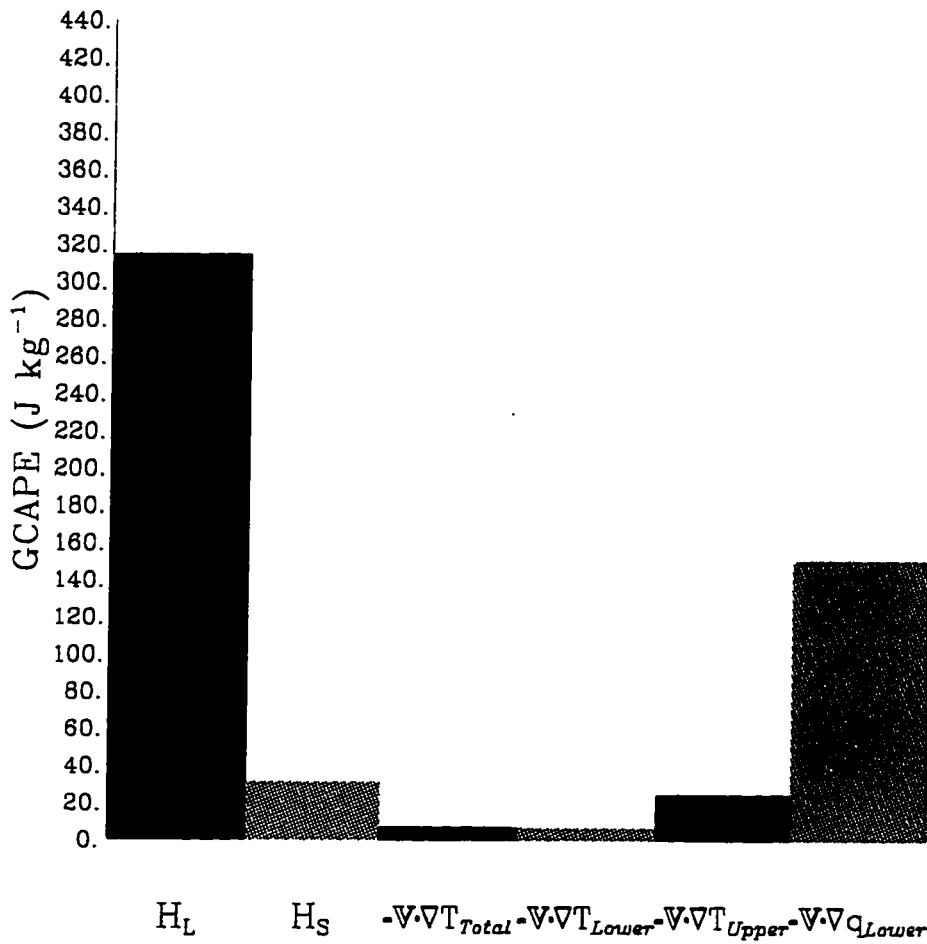
Figure 4.7 - Hypothetical GCAPE production for 0000 UTC 29 April 1995
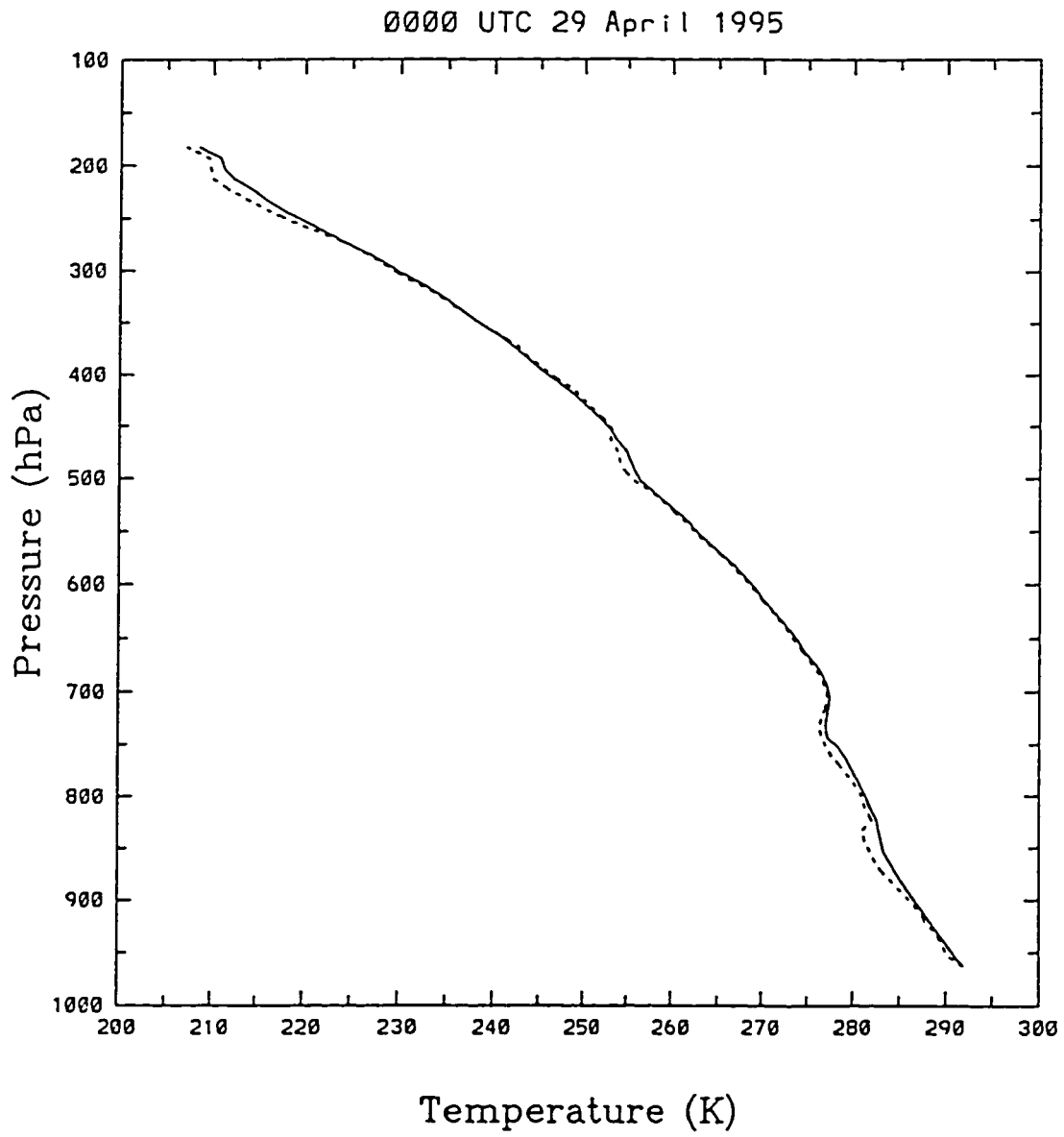
Figure 4.8 - Temperature advection for 0000 UTC 29 April 1995

74
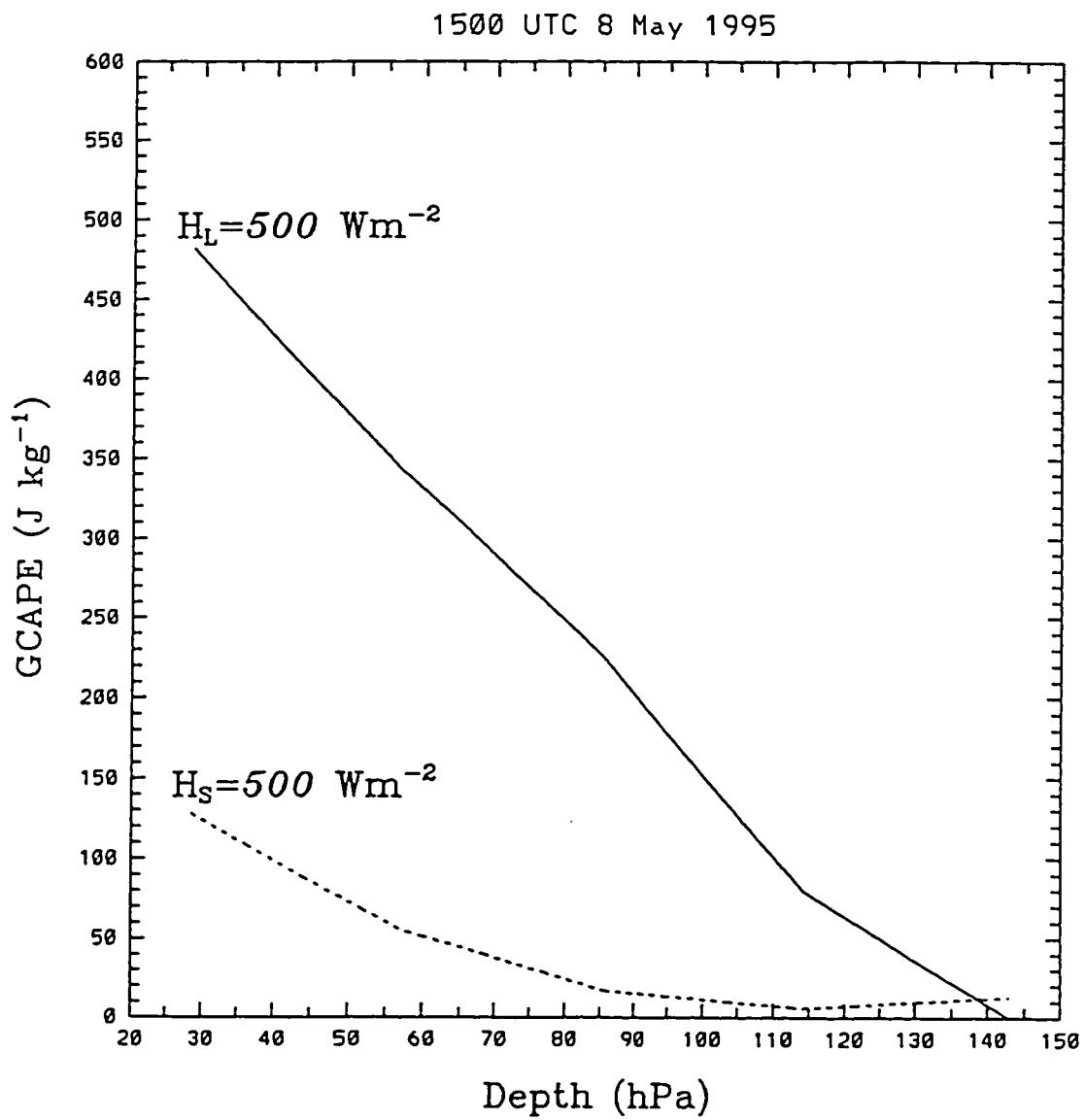
Figure 4.9 - GCAPE production as a function of the depth through which

surface heat and moisture fluxes are added

1800 UTC 30 April 1995
INPUT = 500 W m^{-2}

GCAPE (J kg^{-1})

440.
420.
400.
380.
360.
340.
320.
300.
280.
260.
240.
220.
200.
180.
160.
140.
120.
100.
80.
60.
40.
20.
0.

H_L H_S $-V \cdot \nabla T_{Total}$ $-V \cdot \nabla T_{Lower}$ $-V \cdot \nabla T_{Upper}$ $-V \cdot \nabla q_{Lower}$
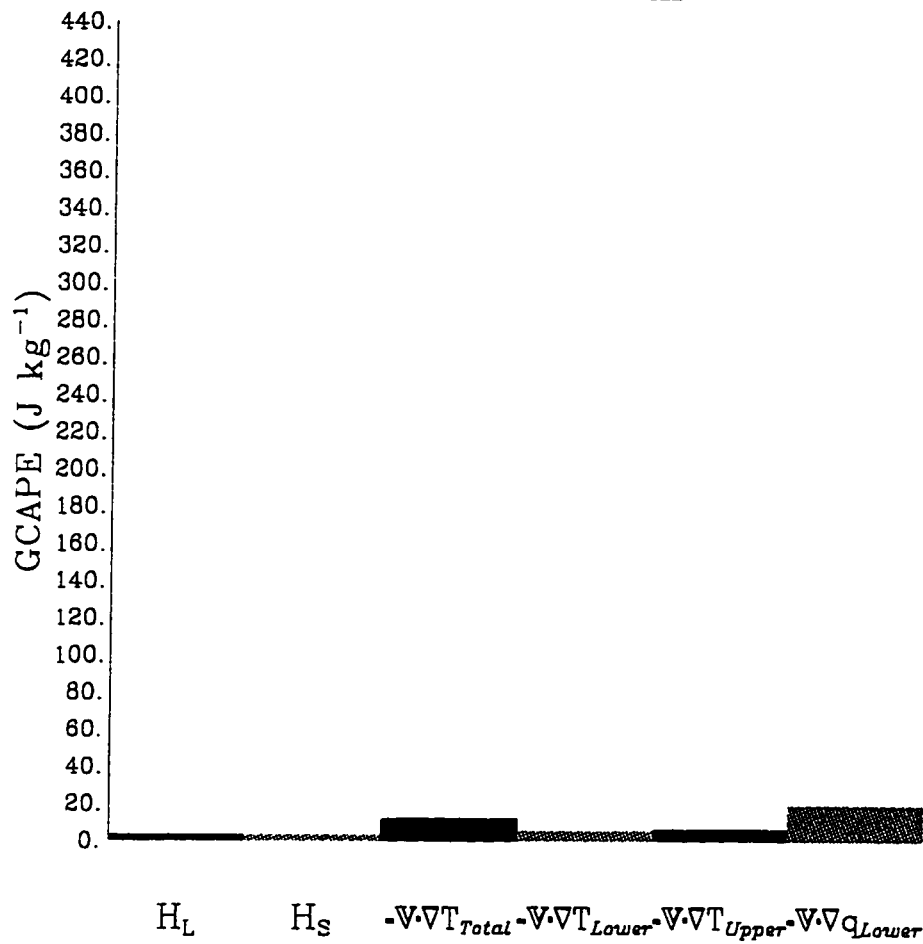
Figure 4.10 - Hypothetical GCAPE production for 1800 UTC 30 April 1995

76

1800 UTC 30 April 1995
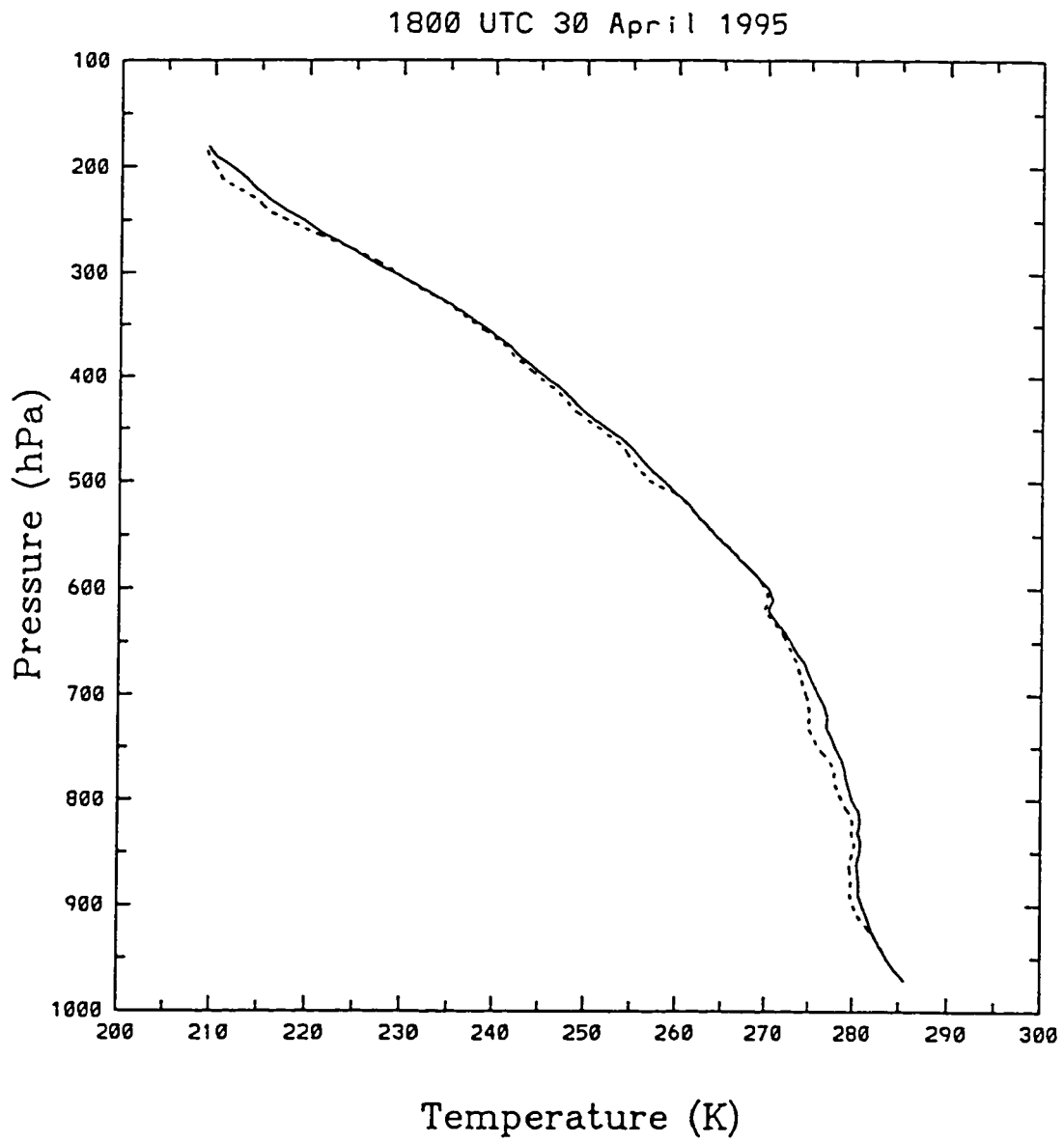
Figure 4.11 - Temperature advection for 1800 UTC 30 April 1995

2100 UTC 30 April 1995
INPUT = 500 W m^{-2}

GCAPE (J kg^{-1})

440.
420.
400.
380.
360.
340.
320.
300.
280.
260.
240.
220.
200.
180.
160.
140.
120.
100.
80.
60.
40.
20.
0.

H$_L$ H$_S$ $-\mathbf{V}\cdot\nabla T_{Total}$ $-\mathbf{V}\cdot\nabla T_{Lower}$ $-\mathbf{V}\cdot\nabla T_{Upper}$ $-\mathbf{V}\cdot\nabla q_{Lower}$
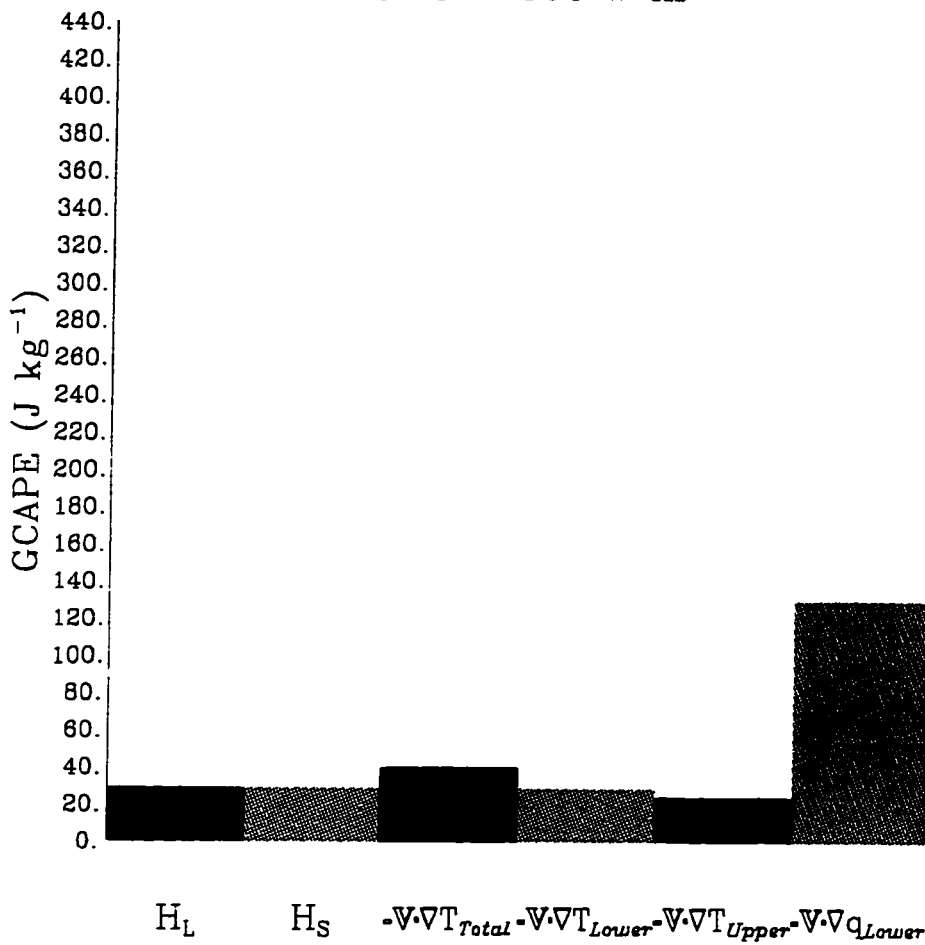
Figure 4.12 - Hypothetical GCAPE production for 2100 UTC 30 April 1995

2100 UTC 30 April 1995

Pressure (hPa) vs Temperature (K)
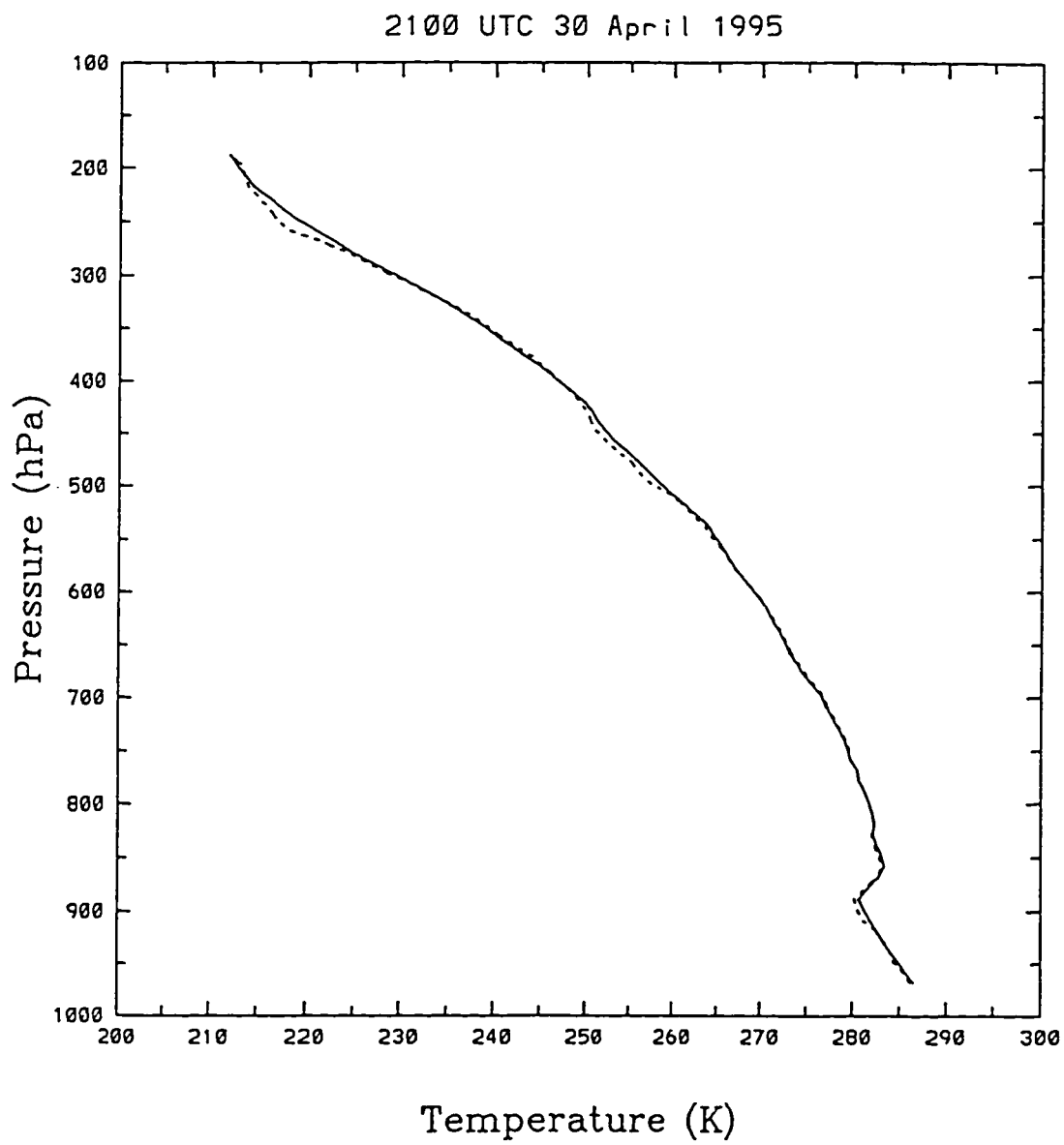
Figure 4.13 - Temperature advection for 2100 UTC 30 April 1995

2100 UTC 6 May 1995
INPUT = 500 W m^{-2}

GCAPE (J kg^{-1})

H_L H_S $-\mathbb{V}\cdot\nabla T_{Total}$ $-\mathbb{V}\cdot\nabla T_{Lower}$ $-\mathbb{V}\cdot\nabla T_{Upper}$ $-\mathbb{V}\cdot\nabla q_{Lower}$
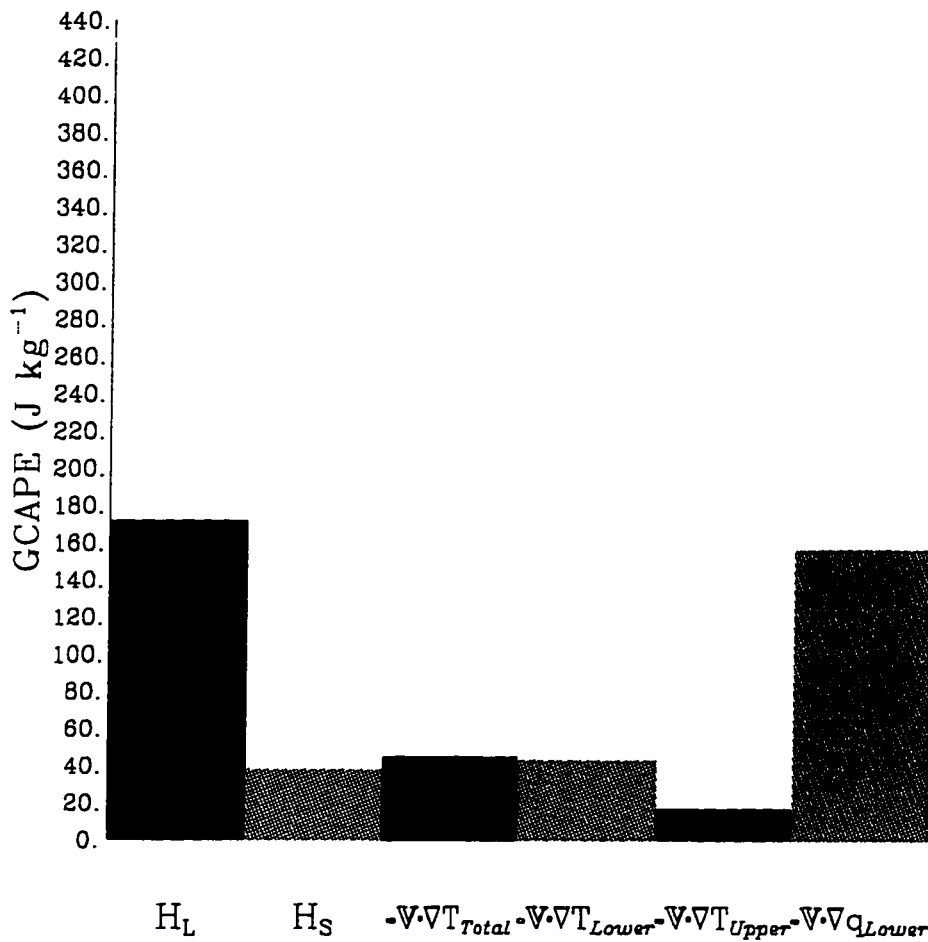
Figure 4.14 - Hypothetical GCAPE production for 2100 UTC 6 May 1995

2100 UTC 6 May 1995
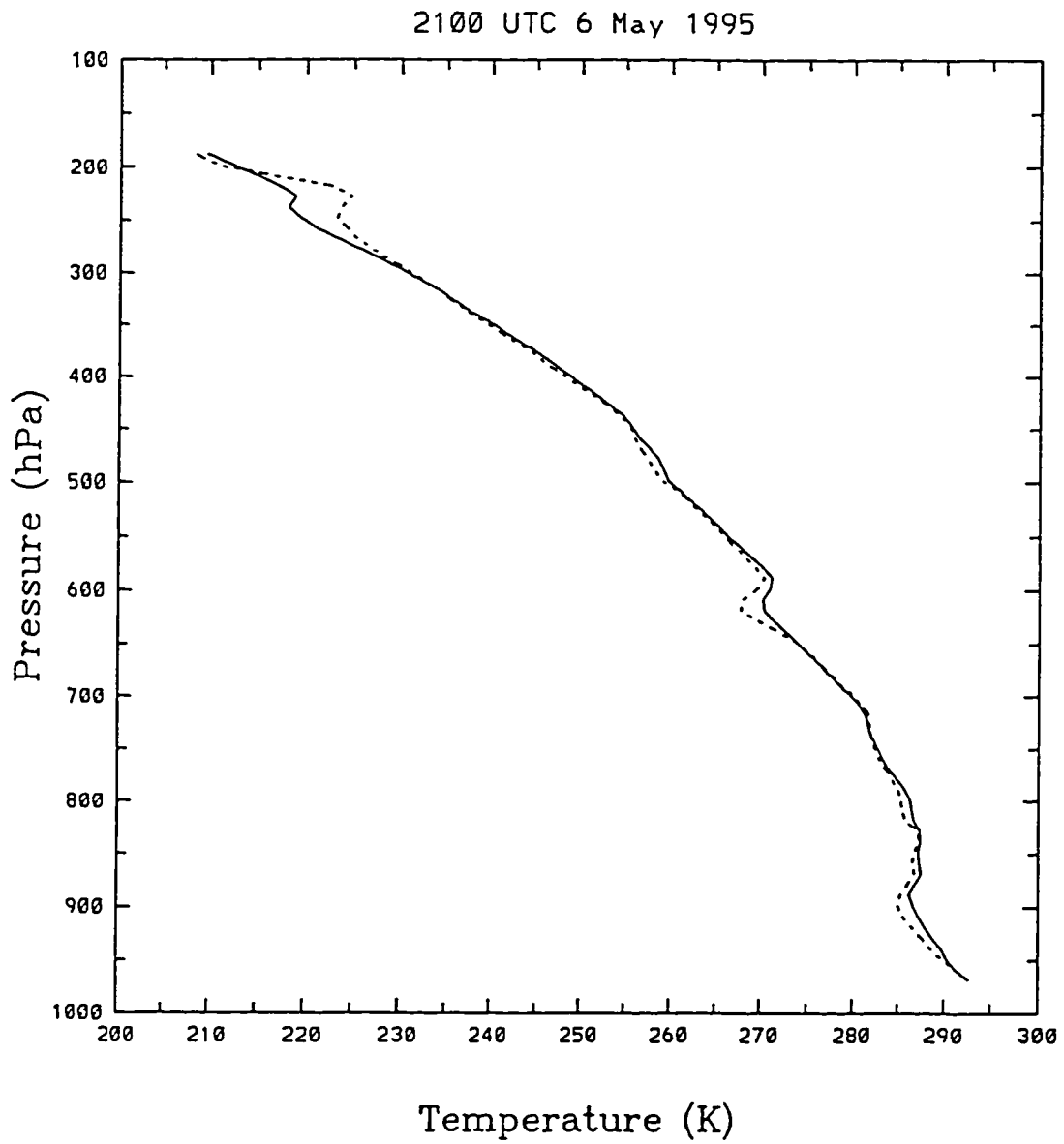
Temperature (K)

Figure 4.15 - Temperature advection for 2100 UTC 6 May 1995

81

0000 UTC 7 May 1995
INPUT = 500 W m^{-2}

GCAPE (J kg^{-1})

440.
420.
400.
380.
360.
340.
320.
300.
280.
260.
240.
220.
200.
180.
160.
140.
120.
100.
80.
60.
40.
20.
0.

H_L H_S $-V \cdot \nabla T_{Total}$ $-V \cdot \nabla T_{Lower}$ $-V \cdot \nabla T_{Upper}$ $-V \cdot \nabla q_{Lower}$
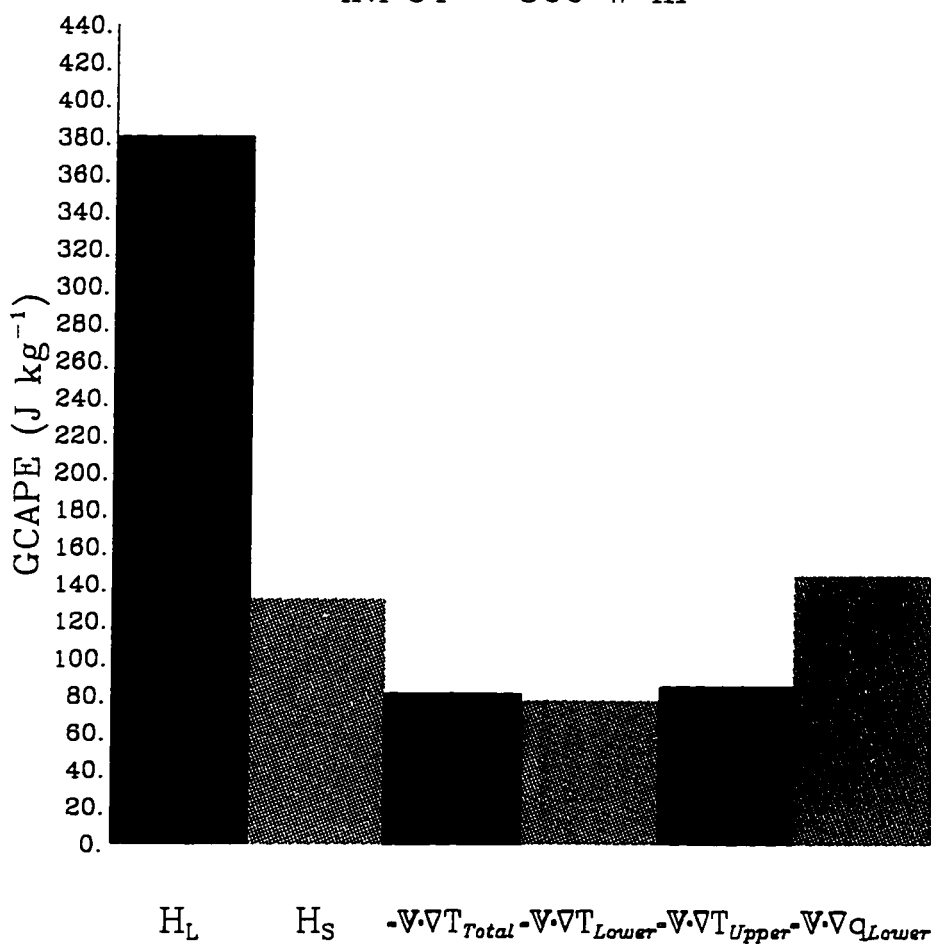
Figure 4.16 - Hypothetical GCAPE production for 0000 UTC 7 May 1995
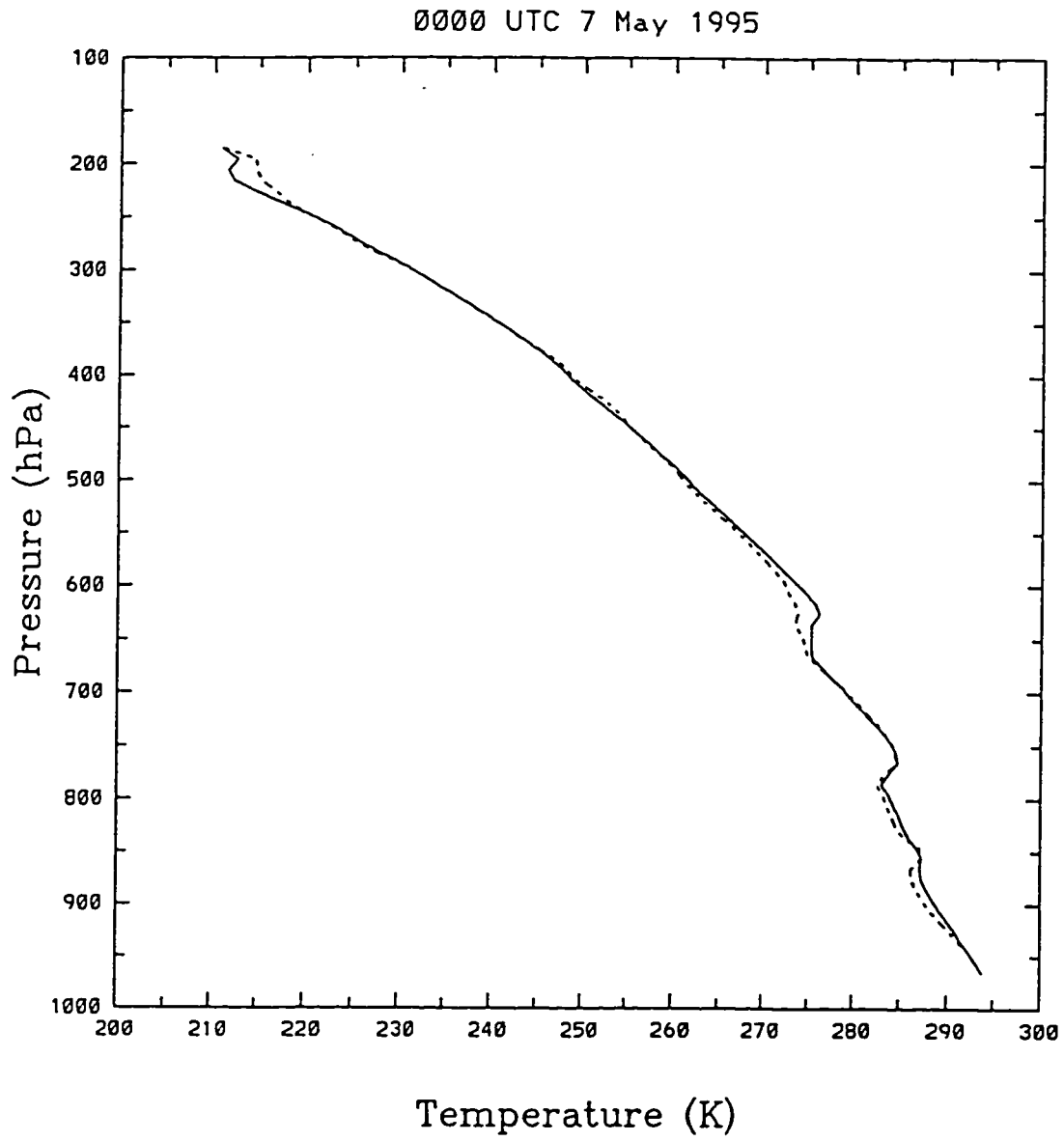
Figure 4.17 - Temperature advection for 0000 UTC 7 May 1995

Figure 4.18 - Hypothetical GCAPE production for 0300 UTC 7 May 1995
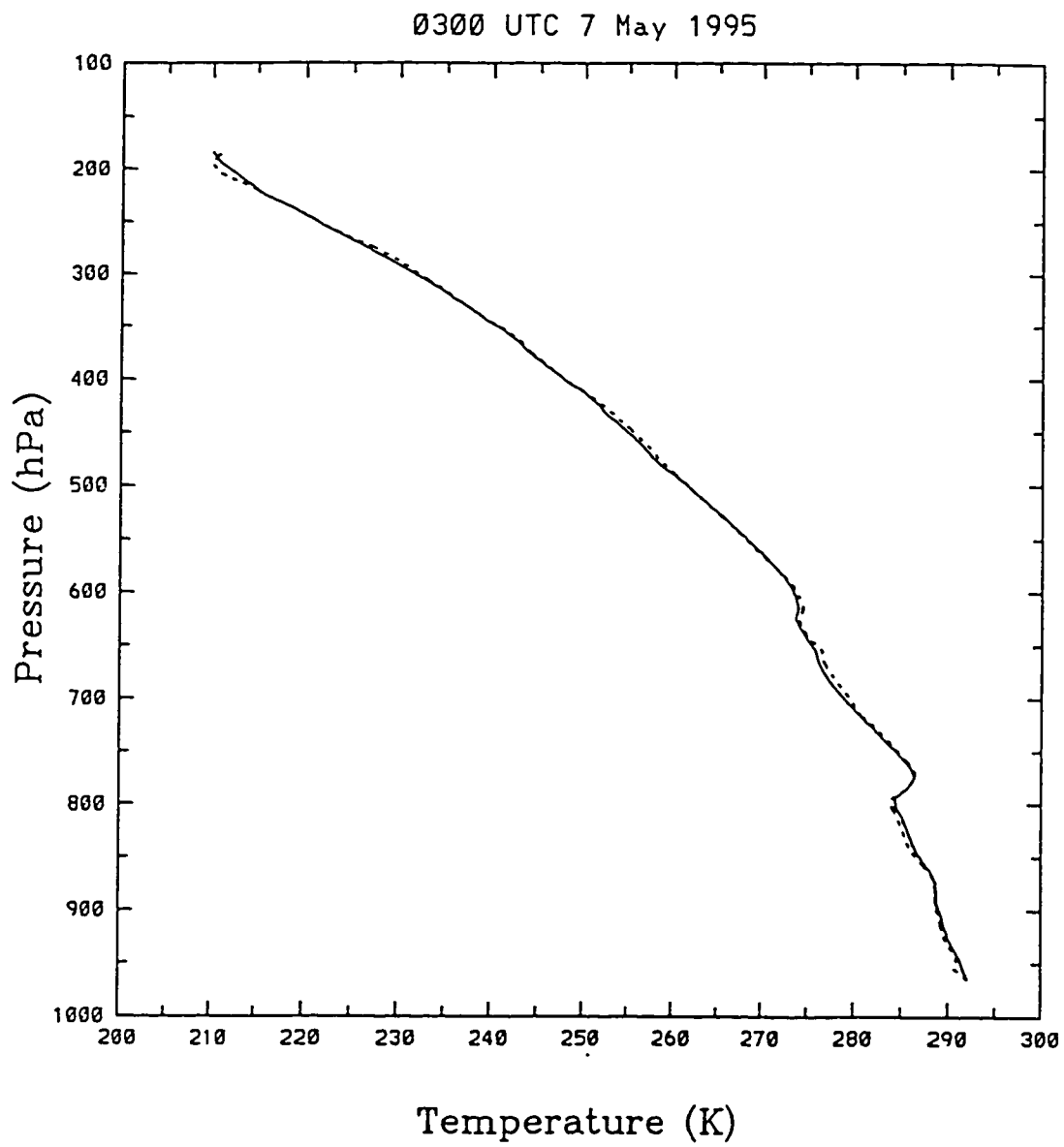
0300 UTC 7 May 1995

Figure 4.19 - Temperature advection for 0300 UTC 7 May 1995

0600 UTC 7 May 1995
INPUT = 500 W m^{-2}
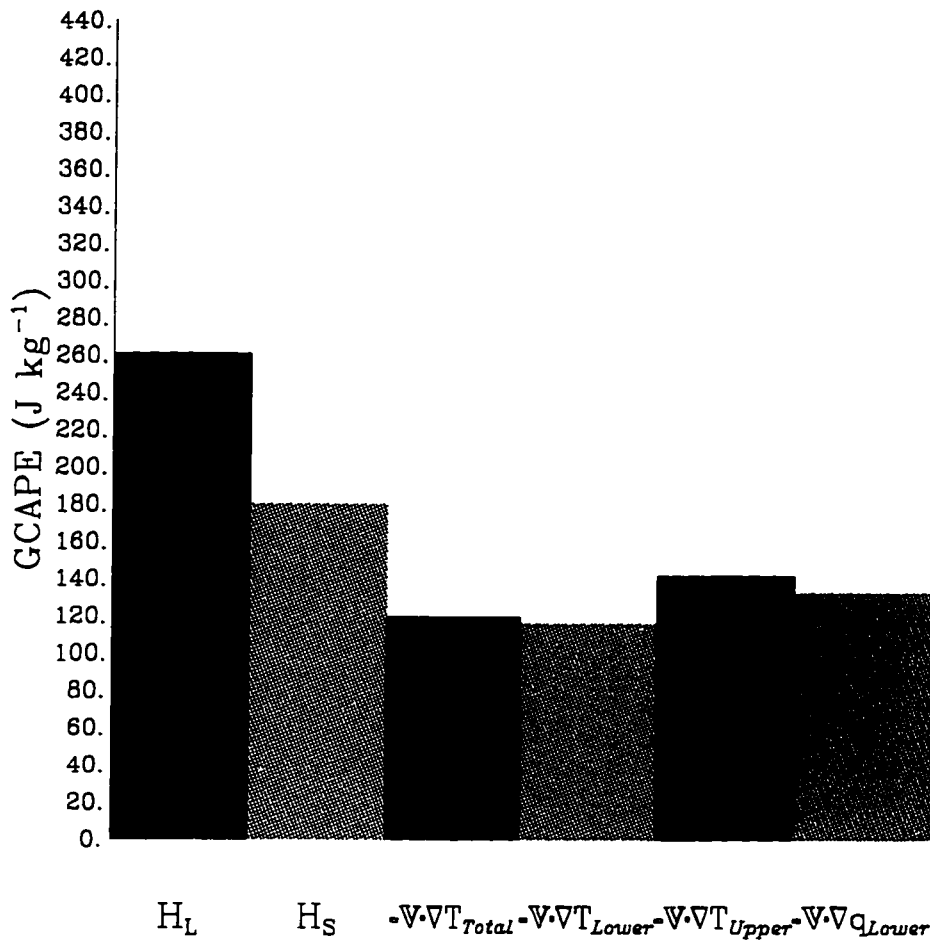
Figure 4.20 - Hypothetical GCAPE production for 0600 UTC 7 May 1995

86
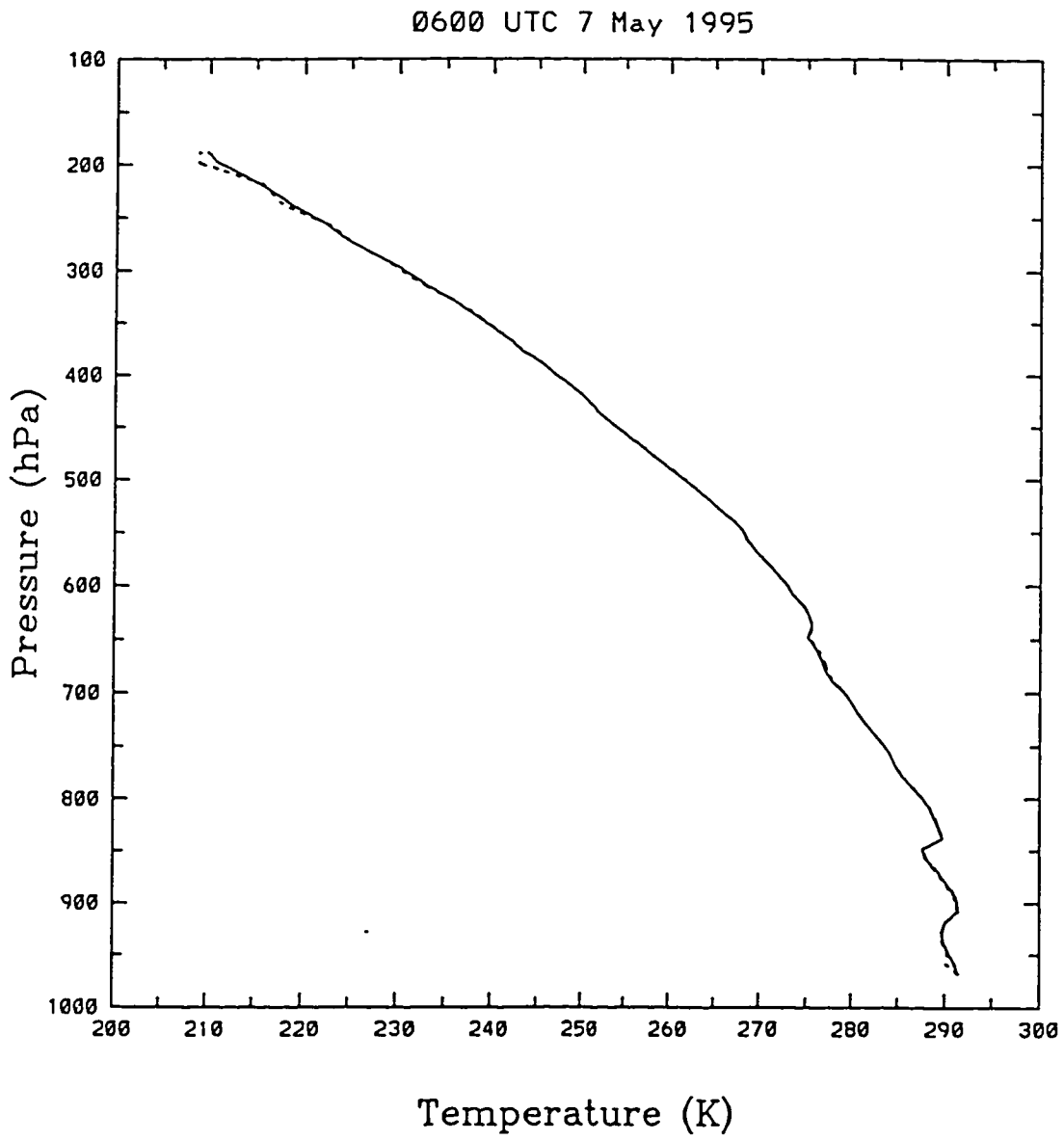
0600 UTC 7 May 1995

Figure 4.21 - Temperature advection for 0600 UTC 7 May 1995

87

CHAPTER 5 - CONCLUSIONS

5.1 Discussion

Data from the from the fall 1994 and spring 1995 IOPs conducted at the ARM Central Facility in north-central Oklahoma have been analyzed to determine the effects of surface heat and moisture fluxes and temperature and moisture advection on the production of GCAPE. Hypothetical and observed inputs of 1) surface latent heat flux, 2) surface sensible heat flux, 3) low-level warm advection/upper-level cold advection, 4) low-level warm advection, 5) upper-level cold advection, and 6) low-level moisture advection were used to test the hypotheses: one, *increased low-level moisture creates GCAPE,* and two, *upper-level cold advection creates GCAPE* .

It has been shown that increased low-level moisture creates GCAPE by reducing the height of the LCL, i. e., by increasing parcel buoyancy. This result is consistent with Crook (1996), Hong et al. (1995), and Segal et al. (1995). Removal of energy from the upper troposphere in the form of upper-level cold advection also creates GCAPE. This is accomplished by disturbing the horizontal density stratification such that horizontal pressure forces are created which convert total potential energy into convective kinetic energy (Lorenz 1955).

Low-level moisture advection and upper-level cold advection created the most GCAPE during the fall 1994 IOP. There is an apparent positive correlation between the process that produced the most GCAPE in the experiments and the

88

process that produced the most GCAPE in reality. In three of four cases analyzed experimental upper-level cold advection generated the most GCAPE and the observed upper-level temperature advection generated the most GCAPE. In the remaining case experimental low-level moisture advection generated the most GCAPE. These results validate the hypotheses stated above.

Experimental surface latent heat flux produced the most GCAPE in five of seven cases analyzed during the spring 1995 IOP. Experimental low-level moisture advection produced the most GCAPE in the remaining two cases. These results validate the hypothesis: *increased low-level moisture creates GCAPE*. Surface latent heat flux was greater during the spring IOP than during the fall IOP and more GCAPE was produced in the spring than in the fall. More precipitation was also produced in the spring IOP which suggest a positive correlation between GCAPE production and precipitation (Wang and Randall 1994).

In most cases the observed temperature advection processes slightly reduced the GCAPE because they stabilized the atmosphere. On two occasions the GCAPE generated by the observed energy fluxes equaled or exceeded the observed GCAPE. The GCAPE generated by the observed energy fluxes was less than the observed GCAPE for the remaining five cases. This was probably due to the rapidity with which GCAPE was produced and consumed. That is, in these cases, the continuous process of GCAPE production was poorly approximated with available discrete observations.

GCAPE was developed out of the necessity to determine the potential energy

available for cumulus convection without the restrictions found in other conditional instability measures (RW92). Tests of a cumulus parameterization scheme in which the reference state associated with the GCAPE is chosen as the end-state of the convective adjustment have recently been conducted (Wang and Randall 1996). Their results were in fair agreement with the observations taken

during GATE. However, this scheme has yet to be tested for a mid-latitude setting. The results of this research regarding the effects of small-scale processes such as latent and sensible heat fluxes and large-scale processes such as temperature and moisture advection on GCAPE production could be very useful in adapting this promising new cumulus parameterization scheme for use in numerical models used to simulate mid-latitude atmospheric processes.

Appendix A. Fall 1994 IOP Meteorology

The daily surface meteorological conditions at the Central Facility and adjacent areas were as follows:

- 24 October

A weak quasi-stationary front was located over eastern Oklahoma at 0000 UTC and moved northward into southern Kansas by 0600 UTC in response to southeasterly flow. Lightning was reported to the southeast and southwest of the Central Facility at 1100 UTC. By 1200 UTC the front had strengthened and moved southward into northern Oklahoma due to colder air moving southward in response to building high pressure over eastern Montana. At 1500 UTC the front had moved into central Oklahoma, where it would remain quasi-stationary. Thunderstorms were reported in southwest Oklahoma. The minimum temperature at the Central Facility was 12.1 °C at 1200 UTC and the maximum temperature was 20.9 °C at 1800 UTC. Wind direction was southeasterly early on and backed to northeasterly afterward due to the frontal passage. Wind speeds were less than 10 m s^{-1}.

- 25 October

The quasi-stationary front was located over southern Oklahoma at 0000 UTC and by 0600 UTC had strengthened into a cold front and moved southward into northern Texas as high pressure to the north strengthened and moved into Nebraska. By 2100 UTC the cold front was located near the Gulf Coast with high

pressure over north-central Kansas. A minimum temperature of 5.8 °C occurred at 1300 UTC while a maximum temperature of 15.2 °C occurred at 1800 UTC. Winds remained northeasterly and less than 10 m s⁻¹. Skies were either broken or scattered and cleared by 2200 UTC.

- 26 October

High pressure was located over central Kansas at 0000 UTC and persisted throughout the day. Light frost was reported at the Central Facility at 1300 UTC. The minimum temperature was 1.8 °C at 1100 UTC and the maximum temperature was 19.9 °C at 1800 UTC. Winds were initially northwesterly then backed to south-southwesterly as the high moved eastward into southern Missouri. Speeds were less than 6 m s⁻¹. Skies were either clear or scattered.

- 27 October

The high was located over northwestern Arkansas at 0000 UTC. It moved eastward into Kentucky while a trough moved into the Oklahoma panhandle by 1200 UTC. The trough was still over the Oklahoma panhandle at 2100 UTC while another high formed over central Arkansas. A minimum temperature of 3.6 °C occurred at 1200 UTC while a maximum temperature of 21.4 °C occurred at 1900 UTC. Winds were southerly never exceeding 7 m s⁻¹. Skies were scattered.

- 28 October

The 0000 UTC surface analysis showed the trough still over the Oklahoma panhandle while the high moved southeastward into northeastern Louisiana. By 2100 UTC the trough persisted over the Oklahoma panhandle and the surface

pressure gradient strengthened. Winds were southerly to southwesterly with a maximum speed of 9.8 m s^{-1} at 1800 UTC. The minimum temperature was 7.3 °C at 1200 UTC and the maximum temperature was 20.2 °C at 1800 UTC. Skies were either overcast or scattered.

• 29 October

The trough remained over the Oklahoma panhandle at 0000 UTC and a cold front extended westward through Colorado and Utah from a low in western Nebraska. By 0600 UTC the cold front moved southward into the Oklahoma panhandle and southwestern Kansas. A low was also located over the Oklahoma panhandle from which the trough extended southward into Texas. By 2100 UTC the cold front had moved into southwestern Oklahoma. Winds were generally southeasterly and did not exceed 7 m s^{-1}. A minimum temperature of 8.3 °C occurred at 1100 UTC while a maximum temperature of 17 °C occurred at 1900 UTC. Skies were clear during the first half of the 29th and overcast thereafter. Light drizzle was reported at the Central Facility at 2300 UTC due to the presence of the cold front.

• 30 October

The cold front extended across Oklahoma from northeast to southwest at 0000 UTC. Moderate drizzle was reported at the Central Facility from 0100-0500 UTC. By 0900 UTC the cold front became a quasi-stationary front which extended from southeastern Kansas to south-central Oklahoma. More drizzle was reported from 1000-1100 UTC. By 2100 UTC the front had moved northward and extended from southeastern Kansas to a low in western

Oklahoma. Winds were light and variable. The minimum temperature was 12.7°C at 1400 UTC and the maximum temperature was 18.1 °C at 2200 UTC. The minimum temperature was relatively warm because persistent overcast skies effectively trapped the outgoing longwave radiation.

• 31 October

The quasi-stationary front extended from southeastern Kansas across northern Oklahoma and into the Texas panhandle at 0000 UTC. Light to moderate rain was reported from 0000-0500 UTC. By 0600 UTC the front had strengthened into a cold front and heavy rain with thunder and lightning was reported from 0800-0900 UTC. At 1200 UTC the cold front was located over southeastern Oklahoma and by 2100 UTC had moved into Arkansas, Louisiana, and Texas. Winds were generally northerly with a maximum speed of 10.3 m s^{-1} at 1700 UTC. A minimum temperature of 8.3 °C occurred at 1400 UTC while a maximum temperature of 15.6 °C occurred at 0000 UTC. Skies were obscured for the first six hours, overcast for the next seven, broken for the next three, and scattered for the remaining eight hours.

• 1 November

High pressure was located over southwestern Oklahoma at 0000 UTC. By 0600 UTC the high had moved into central Texas and a trough had formed over the Oklahoma/Texas panhandle. The trough strengthened yet remained over the Oklahoma/Texas panhandle and the high moved eastward into central Arkansas by 1500 UTC. By 2100 UTC the trough had begun to move eastward as the high moved eastward into northeastern Arkansas. The minimum

temperature was 6.6 °C at 0600 and 1200 UTC and the maximum temperature was 19.2 °C from 2000-2100 UTC. Winds were generally southwesterly with a maximum of 10.3 m s⁻¹ at 1600 UTC. Skies were predominantly clear during the first 12 hours and broken during the remaining 12 hours.

- 2 November

The 0000 UTC surface analysis showed the trough located over the Oklahoma/Texas panhandle and a high located in eastern Mississippi. A southwesterly low-level jet (LLJ) of 18 m s⁻¹ at 850 hPa developed at Oklahoma City and advected in dry air from New Mexico. By 1200 UTC the trough had moved into western Oklahoma and a low pressure center was located in northeastern Colorado. The southwesterly LLJ increased to 21 m s⁻¹ at Oklahoma City and the dry-air advection resulted in a dew point depression of 27 °C at 850 hPa. The low moved into southwestern Kansas from which the trough extended through the Oklahoma/Texas panhandle. A minimum temperature of 11.6 °C occurred from 0500-0600 UTC and a maximum temperature of 21.4 °C occurred at 2100 UTC. Winds were generally southerly to southwesterly with a maximum speed of 12.1 m s⁻¹ at 1700 UTC. Skies were mainly broken or scattered.

- 3 November

At 0000 UTC there was a trough in western Oklahoma and a cold front extended across Kansas from the northeast to the southwest corners of the state. The southwesterly LLJ persisted at 21 m s⁻¹ but by 1200 UTC had increased to 26 m s⁻¹ and began advecting in moisture from the Gulf of Mexico. The cold front

95

moved into northwestern Oklahoma where it remained through 2100 UTC. The minimum temperature was 17.1 °C at 2300 UTC and the maximum temperature was 23.8 °C at 1800 UTC. Winds were initially southerly but veered to northwesterly by 1500 UTC as the front passed the Central Facility. Skies were generally broken or scattered.

- 4 November

The 0000 UTC surface analysis showed a cold front in northeastern Oklahoma transitioning to a quasi-stationary front across northwestern Oklahoma. The LLJ dissipated as the 850 hPa wind speed decreased to 13 m s^{-1}. By 0600 UTC the section of the front across northern Oklahoma was entirely quasi-stationary and thunderstorms had formed ahead of it, from which outflow boundaries moved southward into Arkansas and Texas. By 2100 UTC the front had strengthened into a cold front and extended from northeastern Oklahoma to south-central Oklahoma. A minimum temperature of 8 °C occurred from 1700-1900 UTC and a maximum temperature of 14.8 °C occurred at 0000 UTC. Winds were northerly and less than 9 m s^{-1}. Light fog was reported from 1400-2300 UTC. Skies were scattered during the first 12 hours and overcast thereafter.

- 5 November

The cold front extended from northeastern to south-central Oklahoma at 0000 UTC. Light drizzle was reported from 0000-0100 UTC and light rain from 0300-0500 UTC. By 0600 UTC the cold front had weakened and became quasi-stationary over southeastern Oklahoma. Rain was reported from 0900-1300 UTC and by 1500 UTC the quasi-stationary front had strengthened to a cold front and

moved into western Arkansas. By 2100 UTC a new low/trough had formed over the Oklahoma/Texas panhandle. The minimum temperature was 6 °C from 0700-1300 UTC and the maximum temperature was 11.3 °C at 2100 UTC. Winds were north-northeasterly to northwesterly and less than 10 m s^{-1}. Skies were generally overcast or scattered.

- 6 November

Low pressure was centered over southeastern New Mexico and the trough was located in northwestern Kansas at 0000 UTC. By 1200 UTC high pressure had formed over northeastern Oklahoma and the trough was located over the Oklahoma/Texas panhandle. The high strengthened, moved into central Missouri, and forced the trough westward into New Mexico and Colorado by 2100 UTC. A minimum temperature of 4 °C occurred from 1200-1300 UTC and a maximum temperature of 21 °C occurred from 1900-2100 UTC. Winds were light and variable. Skies were either clear or scattered.

- 7 November

A large anticyclone with a high pressure center over western Illinois was the dominant feature over Oklahoma at 0000 UTC. By 1200 UTC a lee-side trough approached the Oklahoma/Texas panhandle while the high moved into western Ohio. The trough remained just west of the Oklahoma/Texas panhandle at 2100 UTC. The minimum temperature was 6 °C at 1300 UTC and the maximum temperature was 21 °C from 1900-2000 UTC. Winds were southeasterly to southwesterly and less than 10 m s^{-1}. Skies were clear or scattered; however, they were broken from 1800-2200 UTC.

97

- 8 November

An associated low pressure center was located in southeastern Colorado with a trough extending southwestward into southwestern New Mexico at 0000 UTC. By 1200 UTC the low moved into southwestern Kansas from which a weak cold front extended across the Oklahoma/Texas panhandle. The low moved to south-central Kansas and the cold front strengthened and moved into the Texas panhandle. A minimum temperature of 14 °C occurred from 0200-0500 UTC and again at 0900 UTC and a maximum temperature of 24 °C occurred at 1900 UTC. Winds were southerly to southwesterly with a maximum speed of 10.7 m s^{-1} at 1400 UTC. Skies were generally scattered or broken.

- 9 November

The cold front extended from a low in northeastern Kansas southwestward across northwestern Oklahoma at 0000 UTC. By 0600 UTC the cold front had moved southeastward and thunderstorms were reported in north-central and southwestern Oklahoma. At 1200 UTC the cold front extended across extreme southeastern Oklahoma with thunderstorms reported in southeastern Oklahoma. High pressure formed in western Nebraska. By 2100 UTC the cold front had moved to near the Gulf Coast and the high previously in Nebraska moved southward into northwestern Kansas. The minimum temperature was 6 °C from 1300-1400 UTC and the maximum temperature was 21 °C at 2200 UTC. Winds were northwesterly to northeasterly and less than 10 m s^{-1}. Skies were generally scattered or broken.

- 10 November

High pressure was located over south-central Nebraska at 0000 UTC and by 1200 UTC had moved northeastward into the upper Mississippi Valley. At 2100 UTC Oklahoma remained under the influence of the anticyclone, which was located over Wisconsin. A minimum temperature of 3 °C occurred at 1100 UTC and a maximum temperature of 15 °C occurred from 1800-1900 UTC. Winds were light and variable. Skies were generally scattered or broken.

- 11 November

The 0900 UTC surface analysis showed high pressure centered in western Arkansas and a trough extending southward across eastern Colorado from a low pressure center in southeastern Wyoming. By 2100 UTC the low had moved southward into southeastern Colorado from which extended a trough southward across eastern New Mexico. The minimum temperature was 2.7 °C at 0800 UTC and the maximum temperature was 16 °C at 1800 and 2100 UTC. Winds were southeasterly to southwesterly and less than 7 m s^{-1}. Skies were predominantly scattered or clear.

- 12 November

The low remained over southeastern Colorado at 0000 UTC and by 2100 UTC a cold front had moved into the Rockies and extended from a low in north-central Colorado southward into New Mexico. Oklahoma remained under the influence of the western branch of a large anticyclone located in eastern North Carolina. A minimum temperature of 5 °C occurred from 1100-1200 UTC and a maximum temperature of 16 °C occurred at 2000 UTC. Winds were south-southeasterly and less than 8 m s^{-1}. Skies were generally scattered or overcast.

- 13 November

The cold front remained nearly stationary over eastern Colorado and New Mexico due to the strong blocking high located in eastern North Carolina at 0000 UTC. A 21 m s^{-1} south-southeasterly LLJ at Oklahoma City advected in moist air from the Gulf. Dew point depressions at Oklahoma City and Dallas were just 1 °C. At 1200 UTC the LLJ continued at 21 m s^{-1} and the cold front had moved into the Oklahoma/Texas panhandle. By 2100 UTC it was located in western Oklahoma. The minimum temperature was 12 °C from 0000-0400 UTC and the maximum temperature was 19 °C at 2200 UTC. Winds were southeasterly to southwesterly with a maximum speed of 11.2 m s^{-1}. Skies were mainly overcast. Light rain was reported from 1400-1500 UTC and again at 1700 and 1900 UTC.

- 14 November

The 0000 UTC surface analysis showed the cold front over western Oklahoma and by 1200 UTC the cold front had become quasi-stationary. By 2100 UTC the quasi-stationary front had moved into southeastern Oklahoma and high pressure formed behind it over the Rockies and Great Basin. A minimum temperature of 7 °C occurred at 1200 UTC and a maximum temperature of 17 °C occurred from 0100-0400 UTC. Winds were southwesterly through 0900 UTC and veered to north-northeasterly thereafter due to cold-air advection behind the front. Speeds were less than 7 m s^{-1}. Skies were scattered through 1200 UTC and broken thereafter. 0.2 inches of precipitation was reported at 0800 UTC.

Appendix B. Spring 1995 IOP Meteorology

The daily surface meteorological conditions at the Central Facility and adjacent areas were as follows:

- 17 April

Surface low pressure was centered over northeastern Kansas at 0000 UTC and an associated trough stretched into central Oklahoma. An area of strong radar echoes was located east of the Central Facility in northeastern Oklahoma and southeastern Kansas. By 1200 UTC the trough had transformed into a cold front extending across Oklahoma and was oriented northeast to southwest. Surface high pressure built in over the Great Plains behind the cold front. Winds were southerly ahead of the front at 0000 UTC and veered to northerly by 1200 UTC as cold air advected into the Central Facility area. There were showers and thunderstorms over the area during the day and a solid deck of low clouds dominated. Temperatures to the north of the front reached only to the 50s while south of the front some temperatures reached the mid-70s with dew point temperatures near 70 °F. A total of 11.4 mm (0.45 inches) of rain fell at the Central Facility. Severe convection and tornadoes were reported in southern Oklahoma.

- 18 April

At 0000 UTC a quasi-stationary front had formed from the cold front and was positioned within 100 km south of the Central Facility. A thunderstorm was reported at OKC. At 0300 UTC the quasi-stationary front had returned

northward and was located almost directly over the Central Facility. Another thunderstorm was reported to the north at ICT. By 1200 UTC the surface low was positioned over Iowa and an associated cold front extended southward through the Mississippi Valley. A trough trailed behind the cold front and was located over central Oklahoma. It exited the area by 1800 UTC. Skies cleared as dry air was advected in from the southwest. Morning lows were in the mid-40s and highs reached the low 60s. Additional rain totaling 8.4 mm (0.33 inches) fell at the Central Facility.

• 19 April

High pressure was centered over southern Oklahoma at 0000 UTC and two low pressure centers were located in southwestern Texas and New Mexico. Skies remained clear throughout most of the day but by 2100 UTC the low pressure area located to the southwest associated with a warm front across northern Texas moved northeastward into the Texas panhandle. The advection of warm, moist air by southerly flow originating from the Gulf south of the front and cyclonic flow around the low pressure area in the Texas panhandle triggered showers and thunderstorms across Oklahoma. Surface winds were moderately strong from the northeast during the day. Morning lows were in the mid-40s and high were in the low 60s.

• 20 April

The warm front persisted across northeastern Texas at 0000 UTC while a trough associated with a low in north-central Texas stretched northward across western Oklahoma. The trough moved eastward into eastern Oklahoma by 0300

UTC and the main area of thunderstorms was located in southeastern Kansas. During 0300-0600 UTC 0.76 mm (0.03 inches) of rain fell at the Central Facility. The surface low previously over north-central Texas occluded and moved northward into northeastern Kansas. The cold front associated with it extended southward across Arkansas. By 2100 UTC southwesterly flow dominated Oklahoma and a trough emanating from a low in northern Wyoming stretched southeastward into the Oklahoma/Texas panhandle. Significant low cloudiness persisted throughout the day. Morning lows were in the mid-40s and highs reached the 50s.

• 21 April

The trough moved quickly into central Oklahoma by 0000 UTC and was oriented from east to west. A low pressure center was located east of Amarillo, Texas, near the Oklahoma border. By 1200 UTC the trough had become a quasi-stationary front and moved southward into the Red River Valley where a low pressure center was also located. Another low was located in the Texas panhandle. The eastern portion of the front retreated back into Oklahoma due to stronger southeasterlies forced by a stronger surface pressure gradient. The front remained south of the Central Facility and northerly winds prevailed at the Central Facility. Skies were generally partly cloudy to clear while lows were in the upper 30s and highs were in the low 50s.

• 22 April

The quasi-stationary front continued to extend across southeastern Oklahoma and into northern Texas where a surface low was centered in the

Texas panhandle at 0000 UTC. A large area of high pressure began to build lee-side of the Rockies and into the Great Plains and by 0300 UTC was advecting enough cold air into Oklahoma to transform the quasi-stationary front into a cold front. The cold front exited Oklahoma by 0900 UTC while the surface high moved slowly into southern South Dakota by 1200 UTC. Thunderstorms developed in southwestern Oklahoma due to surface convergence and cyclonic flow behind the recently departed cold front. By 1500 UTC a trough oriented north to south bisected Oklahoma. It moved into eastern Oklahoma by 1800 UTC and spread thunderstorms and showers across Oklahoma. Winds remained northerly and skies were overcast with low clouds. Lows were in the low 30s and highs were in the mid-40s. A total of 10.41 mm (0.41 inches) of rain fell at the Central Facility.

- 23 April

At 0000 UTC surface high pressure was positioned over southeastern Colorado and a trough stretching across eastern Oklahoma produced rain and showers throughout most of the state. This regime persisted until 1200 UTC when the surface low over Mississippi associated with the trough began to move eastward. The high moved southward from Colorado into the Oklahoma panhandle by 2100 UTC at which time the precipitation terminated. A total of 14.24 mm (0.56 inches) of rain fell at the Central Facility. Northerly winds persisted throughout the day while low- to mid-level clouds became broken or scattered. Lows were near 40 and highs were near 60.

- 24 April

A cold front moved southward into southern South Dakota associated

with a low in northwestern Wisconsin. High pressure was located to the southwest in north-central Colorado. By 1800 UTC the high had moved southwestward into east-central Utah which allowed the cold front to move rapidly southward into northern Oklahoma, almost directly over the Central Facility. The 2100 UTC surface analysis showed the cold front had passed the Central Facility and a surface high had formed over northwestern Kansas. Shallow convection developed predominantly along the cold front in the late morning aided by a convectively unstable atmosphere and a weak trough aloft. Skies were partly cloudy in the morning and were generally broken thereafter with mainly low- and mid-level clouds. Morning lows reached the mid-30s and highs for the day hit the low-60s. Rain totaling 3.3 mm (0.13 inches) fell at the Central Facility.

• 25 April

The trailing edge of the cold front was located along the eastern Kansas/Oklahoma border, and, just to the south, a thunderstorm was reported in Tulsa at 0000 UTC. High pressure was centered to the south of Tulsa, probably as a response to the cold thunderstorm outflow. The front moved eastward into Arkansas and Missouri and by 1200 UTC another area of high pressure formed, this time over the four corners area. Another high was located over east-central Mississippi and was responsible for light southerlies across Oklahoma. This scenario continued and by 2100 UTC the surface pressure gradient increased resulting in surface winds up to 10 m s^{-1} over Oklahoma. A surface low over

southeastern Nebraska and associated warm and cold fronts developed lee-side of the Rockies. Skies were generally clear to scattered with mainly low- and mid-level clouds reported. Lows were in the upper 30s and highs reached the low 70s. Rain at the Central Facility amounted to 0.5 mm (0.02 inches).

• 26 April

The surface low remained over southeastern Nebraska at 0000 UTC but another low developed lee-side of the Rockies in southeastern Colorado. A trough extended southward from the low through the Oklahoma/Texas panhandle. A dry line formed across western Oklahoma by 0300 UTC. Dew point temperatures differed by as much as 18 °F in southwestern Oklahoma, the location of strongest dew point temperature gradient. By 1200 UTC the dryline vanished and a cold front stretched from a surface low in northwestern Oklahoma across Nebraska to another low in northeastern Kansas. By 2100 UTC the cold front weakened and was located across central Oklahoma. Winds were southerly ahead of the front in southeastern Oklahoma and north-northwesterly behind the front in northwestern Oklahoma. A significant LLJ formed over the southern Great Plains and transported low-level moisture into southeastern Oklahoma. The Central Facility radiosonde recorded maximum low-level winds of 29.4 m s^{-1} from 190° (654 m AGL), 34.4 m s^{-1} from 211° (804 m AGL), and 35.5 m s^{-1} from 209° (376 m AGL), at 0530 UTC, 0830 UTC, and 1130 UTC, respectively. Scattered showers and thundershowers developed over Oklahoma and at mid-day a line of strong thunderstorms formed along the front from northeastern Oklahoma into northern Texas. Morning lows were in the upper 40s and highs reached only the low 50s. No precipitation was measured at the

Central Facility.

- 27 April

The weak cold front moved into eastern Oklahoma by 0000 UTC and thunderstorms were reported in McAlester, Oklahoma and Joplin. High pressure moved in behind the front and was positioned over northeastern Wyoming. By 1200 UTC the cold front had moved eastward into Arkansas and the high had moved into northwestern Oklahoma. It moved slowly northeastward into southeastern Kansas by 2100 UTC. Surface winds were northerly in the morning and became easterly by evening as high pressure moved eastward. Skies were mostly clear with a few scattered low- and high-level clouds reported. Lows were near 30 and highs were in the low 60s.

- 28 April

High pressure was centered over southwestern Missouri and low pressure was located over the Great Basin at 0000 UTC. By 1200 UTC the high had moved eastward into southern Illinois and the low was positioned in northeastern Colorado. A weak quasi-stationary front stretched southward through eastern Colorado and New Mexico. The low moved southward to southeastern Colorado and the accompanying trough, oriented northwest to southeast, stretched from southeastern Colorado, across the Oklahoma/Texas panhandle, and into north-central Texas. Significant cloudiness returned from the southwest by morning and progressively lower cloud decks eventually shrouded the Central Facility with an overcast low-level cloud layer by late evening. Surface winds became moderately strong and southerly which advected in increasing

moisture. Significant showers and thunderstorms developed in late evening with an especially strong cluster of storms along the Kansas/Oklahoma border. Morning lows were in the mid-40s while highs reached the low 60s.

• 29 April

The trough became a warm front and was located over central Oklahoma at 0000 UTC. The low was centered over the Oklahoma panhandle. Six hours later at 0600 UTC the warm front had moved northward and extended from northwestern Oklahoma southeastward into northeast Texas. A thunderstorm was reported at Ponca City in north-central Oklahoma from which emanated a southward-moving outflow boundary. The warm front remained nearly stationary through 0900 UTC whereas the outflow boundary moved southward and away from thunderstorms reported at Ponca City, Witchita, and Joplin. At 1200 UTC the warm front moved northward into southeastern Oklahoma and its associated double lows moved southward into southern Oklahoma. Thunderstorms were reported in Ponca City and Tulsa, Oklahoma. By 1500 UTC a new low formed over northeastern Nebraska and an outflow boundary moved into southern Missouri and northwestern Arkansas in response to the thunderstorm in northeastern Oklahoma three hours earlier. A new thunderstorm was reported at Fort Smith. By 2100 UTC a low was located in the Red River Valley from which extended a warm front eastward into southern Arkansas and a cold front southwestward into Texas. A trough developed lee-side of the Rockies. Thunderstorm activity continued overnight and severe thunderstorms with heavy rain (up to 3-5 inches) created flooding problems in north-central Oklahoma. Thunderstorm activity decreased during the day and

exited the area by late-afternoon. Surface winds became northerly by evening. Skies in the afternoon ranged from scattered to overcast with mainly low- and mid-level clouds. Morning lows were in the low 50s and highs reached the low 60s. Precipitation totaling 17.78 mm (0.7 inches) was measured at the Central Facility.

• 30 April

The low was located in northeastern Texas at 0000 UTC while the trough remained lee-side of the Rockies. By 1200 UTC the trough moved into central Kansas and north-central Oklahoma causing showers at the Central Facility. Rain totaling 2.78 mm (0.11 inches) fell throughout the day. The trough exited the area and by 2100 UTC a quasi-stationary front had formed and stretched from the Oklahoma/Texas panhandle across northern Texas. Low-level cloudiness was reported and surface winds were northeasterly. Morning lows were in the mid-40s and highs were also in the mid-40s.

• 1 May

More thunderstorms developed by 0000 UTC, including ones reported at Ponca City and Joplin, with rain showers throughout northern Oklahoma and southern Kansas. There was cyclonic, convergent surface flow over Oklahoma and Kansas which continued until 1800 UTC, by which time the low had moved northeastward into western Kentucky. Skies were dominated by low-level clouds with generally broken to overcast coverage. Lows were in the upper 40s and highs reached the low 50s.

• 2 May

Winds were northerly due to high pressure over southeastern South

Dakota at 0000 UTC. By 1200 UTC the high had moved southward into northwestern Missouri. The high then moved northeastward into eastern Iowa as a cyclone located over the Rockies approached from the west. Surface winds over the Central Facility area became southeasterly ahead of the advancing frontal system in Colorado. Low-level warm-air advection established itself over the area. Morning lows were in the mid-30s and highs were in the upper 40s.

• 3 May

A low was located in southeastern Colorado and an associated weak warm front extended southward through eastern Colorado and New Mexico. A cold front trailed to the west. By 1200 UTC the low had moved into the Texas panhandle, the warm front stretched across northern Texas, and a trough extended northward across the Oklahoma panhandle and western Kansas. By 2100 UTC the low and warm front had moved farther south into Texas and the trough stretched northward across western Oklahoma and Kansas. Surface winds were east-southeasterly. Lows were in the upper 40s and highs were in the mid-40s. Rain totaling 1.78 mm (0.07 inches) was recorded at the Central Facility.

• 4 May

The trough was situated over western Oklahoma and central Kansas at 0000 UTC and by 1200 UTC had moved eastward into Arkansas and Missouri. Winds veered from east-southeasterly to northwesterly. High pressure built in behind the trough and by 2100 UTC was centered over southeastern Nebraska. Low clouds persisted over the area. Lows were in the upper 40s and highs were in the low 60s.

- 5 May

High pressure remained centered over southeastern Nebraska at 0000 UTC and by 1200 UTC had only moved into northwestern Missouri. An occluded front was located in the Great Basin. By 2100 UTC the high was still centered in northern Missouri while the occluded front advanced into the Rockies. Surface winds were easterly to northeasterly overnight and became southeasterly during the day. Significant cloudiness spread over the area during the day. Lows were near 40 and highs reached the mid-60s. One-hundredth of and inch of rain was measured at the Central Facility.

- 6 May

Thunderstorms developed in southwestern Oklahoma at 0000 UTC ahead of an advancing cold front that stretched across western Colorado and New Mexico. Surface winds were cyclonic and convergent over southern Oklahoma and northern Texas behind a quasi-stationary front in central Texas. This forcing resulted in showers in northern Oklahoma by 0300 UTC. High pressure remained over northern Missouri. By 0600 UTC the showers had ended but by 1200 UTC more thunderstorms developed in western Oklahoma. At 1500 UTC the quasi-stationary front in Texas and the cold front in eastern Colorado and New Mexico merged over southwestern Oklahoma producing more thunderstorms in southwestern Oklahoma and showers in northern Oklahoma. The thunderstorms spread across the state to the east and into southeastern Kansas. By 2100 UTC they dissipated and exited the area. Lows were in the low 50s and highs were in the upper 60s. Rain totaling 13.47 mm (0.53 inches) fell at the Central Facility.

111

- 7 May

    The front became quasi-stationary over northern Texas at 0000 UTC. At 0900 UTC the front began to move northward into southwestern Oklahoma and by 1200 UTC had become a warm front as warm, moist air was advected in from Texas. A thunderstorm was reported in Dodge City, Kansas ahead of an occlusion over southeastern Colorado and northeastern New Mexico. At 1500 UTC the warm front moved northward into northern Oklahoma. Dew point temperatures were in the mid- to upper 60s and thunderstorms developed in southwestern Oklahoma. By 1800 UTC a very intense squall line developed across central Kansas and Oklahoma and the warm front retreated southward into southern Oklahoma. By 2100 UTC the squall line had slowly progressed eastward and the warm front began to move northward again. Thunderstorms were reported in Ponca City and Tulsa. The atmosphere significantly de-stabilized over the southern Great Plains and thunderstorms affected the area early in the morning. Several rounds of thunderstorms occurred over the area during the day with reports of tornadoes concentrated to the south of the Central Facility. Precipitation began to clear from west to east in the evening with the passage of the squall line. Flooding was a problem to the south. Lows were in the upper 50s and highs reached the mid-60s. A total of 9.65 mm (0.38 inches) of rain was recorded at the Central Facility.

REFERENCES

Arakawa, A., and W. H. Schubert, 1974: The interaction of a cumulus cloud ensemble with the large-scale environment, Part I. *J. Atmos. Sci.* , 31, 674-701.

Arya, S. P., 1988: *Introduction to Micrometeorology* . Academic Press, Inc., San Diego, 307 pp.

Barnes, S. L., 1964: A technique for maximizing details in numerical weather maps analysis. *J. Appl. Meteor.* , 3, 396-409.

Caracena, F., 1987: Analytic approximation of discrete field samples with weighted sums and the gridless computation of field derivatives. *J. Atmos. Sci.* , 44, 3753-3768.

Cripe, D. G., 1994: Investigation of GCAPE quasi-equilibrium in the mid-latitudes. M. S. thesis, Colorado State University, 221 pp.

Crook, N. A., 1996: Sensitivity of moist convection forced by boundary layer processes to low-level thermodynamic fields. *Mon. Wea. Rev.* , 124, 1767-1785.

Emanuel, K. A., and D. J. Raymond, 1992: Report from a workshop on cumulus parameterization, Key-Biscayne, Florida, 3-5 May 1991. *Bull. Amer. Meteor. Soc.* , 73, 318-325.

Emanuel, K. A., 1994: *Atmospheric Convection* . Oxford University Press, Inc., New York, 580 pp.

Emanuel, K. A., J. D. Neelin, and C. S. Bretherton, 1994: On large-scale circulations in convecting atmospheres. *Quart. J. Roy. Meteor. Soc.* , 120, 1111-1143.

Holton, J. R., 1992: *An Introduction to Dynamic Meteorology* . Academic Press, Inc, San Diego, 511 pp.

Hong, X., M, J. Leach, and S. Raman, 1995: A sensitivity study of convective cloud formation by vegetation forcing with different atmospheric conditions. *J. Appl. Meteor.* , 34, 2008-2028.

Lorenz, E. N., 1955: Available potential energy and the maintenance of the general circulation. *Tellus* , 7, 157-167.

Lorenz, E. N., 1978: Available energy and the maintenance of a moist circulation. *Tellus*, **30**, 15-31.

Lorenz, E. N., 1979: Numerical evaluation of moist available energy. *Tellus*, **31**, 230-235.

Randall, D. A., and J, Wang, 1992: The moist available energy of a conditionally unstable atmosphere. *J. Atmos. Sci.*, **49**, 240-255.

Raymond, D. J., 1994: Cumulus convection and the Madden-Julian oscillation of the tropical troposphere. *Physica D*, **77**, 1-22.

Segal, M., R. W. Arritt, C. Clark, R. Rabin, and J. Brown, 1995: Scaling evaluation of the effect of surface characteristics on potential convection over uniform terrain. *Mon. Wea. Rev.*, **123**, 383-400.

Wang, J., and D. A. Randall, 1994: The moist available energy of a conditionally unstable atmosphere. Part II: Further analysis of GATE data. *J. Atmos. Sci.*, **51**, 703-710.

Wang, J., and D. A. Randall, 1996: A cumulus parameterization based on the generalized convective available potential energy. *J. Atmos. Sci.*, **53**, 716-727.

Weisman, M. L., and J. B. Klemp, 1986: Characteristics of isolated convective storms. In *Mesoscale Meteorology and Forecasting*. Peter S. Ray (Ed.), American Meteorological Society, Boston, MA, 390-413.